REPORT DOCUMENTATION PAGE

Form Approved
OMB No. 0704-0188

1. REPORT DATE *(DD-MM-YYYY)*	**2. REPORT TYPE**	**3. DATES COVERED** *(From - To)*
10-12-2009	Final Report	10 Sep 07 - 10 Sep 09

4. TITLE AND SUBTITLE

Phase-Sensitive Quantum Optical Sensor

5a. CONTRACT NUMBER
W911NF-07-1-0629

5b. GRANT NUMBER

5c. PROGRAM ELEMENT NUMBER

6. AUTHOR(S)

Prof. A. V. Sergienko

5d. PROJECT NUMBER

5e. TASK NUMBER

5f. WORK UNIT NUMBER

7. PERFORMING ORGANIZATION NAME(S) AND ADDRESS(ES)

Trustees of Boston University
881 Commonwealth Avenue
Boston, MA 02215

8. PERFORMING ORGANIZATION REPORT NUMBER

9. SPONSORING / MONITORING AGENCY NAME(S) AND ADDRESS(ES)

U. S. Army Research Office
P.O. Box 12211
Research Triangle Park, NC 27709-2211
ATTN: T. R. Govindan <tr.govindan@us.army.mil>

10. SPONSOR/MONITOR'S ACRONYM(S)

11. SPONSOR/MONITOR'S REPORT NUMBER(S)

12. DISTRIBUTION / AVAILABILITY STATEMENT

Approved for Public Release; Distribution Unlimited

13. SUPPLEMENTARY NOTES

The views, opinions and/or findings contained in this report are those of the author(s) and should not be construed as an official Department of the Army position, policy or decision, unless so designated by other documentation.

14. ABSTRACT

Our research program during this period has concentrated on investigating novel scientific and technological solutions for ultra-sensitive quantum-optical registration and sensing of phase shifts induced by external fields. The use of several types of nonclassical states of light and development of novel ultra-sensitive interferometric phase measurement configurations has been at the center of our research effort.

We have successfully completed the original research program. A new effect of "Ghost Imaging with Aberration Cancellation" has been discovered in the process, leading to the promise of significant enhancements in the fields of optical imaging and microscopy, as well as potential improvements to phase-sensitive optical sensors.

Our research has led to five research papers published in leading refereed physics journals, with one additional manuscript recently submitted for publication. Nine conference presentations have been given, including two Invited Talks. Four Invited Lectures have also been given at leading US and European research institutions, and several graduate and undergraduate students have been trained.

15. SUBJECT TERMS

Quantum interferometry, phase sensing, dispersion cancellation, correlated-photon aberration cancellation

16. SECURITY CLASSIFICATION OF:			**17. LIMITATION OF ABSTRACT**	**18. NUMBER OF PAGES**	**19a. NAME OF RESPONSIBLE PERSON**
a. REPORT	**b. ABSTRACT**	**c. THIS PAGE**			**19b. TELEPHONE NUMBER** *(include area code)*
UNCLASSIFIED	UNCLASSIFIED	UNCLASSIFIED			

REPORT OF INVENTIONS AND SUBCONTRACTS

(Pursuant to "Patent Rights" Contract Clause) (See Instructions on back)

Form Approved
OMB No. 9000-0095
Expires Aug 31, 2001

PLEASE DO NOT RETURN YOUR COMPLETED FORM TO THIS ADDRESS. RETURN COMPLETED FORM TO THE CONTRACTING OFFICER.

1.a. NAME OF CONTRACTOR/SUBCONTRACTOR	c. CONTRACT NUMBER	2.a. NAME OF GOVERNMENT PRIME CONTRACTOR	c. CONTRACT NUMBER	3. TYPE OF REPORT *(X one)*
Trustees of Boston University	W911NF-07-1-0629			☐ a. INTERIM ☒ b. FINAL

b. ADDRESS *(Include ZIP Code)*	d. AWARD DATE *(YYYYMMDD)*	b. ADDRESS *(Include ZIP Code)*	d. AWARD DATE *(YYYYMMDD)*	4. REPORTING PERIOD *(YYYYMMDD)*
881 Commonwealth Avenue Boston, MA 02215	20070910			a. FROM 20070910 b. TO 20090910

SECTION I - SUBJECT INVENTIONS

5. "SUBJECT INVENTIONS" REQUIRED TO BE REPORTED BY CONTRACTOR/SUBCONTRACTOR *(If "None," so state)*

NAME(S) OF INVENTOR(S) *(Last, First, Middle Initial)* a.	TITLE OF INVENTION(S) b.	DISCLOSURE NUMBER, PATENT APPLICATION SERIAL NUMBER OR PATENT NUMBER c.	ELECTION TO FILE PATENT APPLICATIONS *(X)* d.				CONFIRMATORY INSTRUMENT OR ASSIGNMENT FORWARDED TO CONTRACTING OFFICER *(X)* e.	
			(1) UNITED STATES		(2) FOREIGN			
			(a) YES	(b) NO	(a) YES	(b) NO	(a) YES	(b) NO
	none							

f. EMPLOYER OF INVENTOR(S) NOT EMPLOYED BY CONTRACTOR/SUBCONTRACTOR		g. ELECTED FOREIGN COUNTRIES IN WHICH A PATENT APPLICATION WILL BE FILED	
(1) (a) NAME OF INVENTOR *(Last, First, Middle Initial)*	(2) (a) NAME OF INVENTOR *(Last, First, Middle Initial)*	(1) TITLE OF INVENTION	(2) FOREIGN COUNTRIES OF PATENT APPLICATION
(b) NAME OF EMPLOYER	(b) NAME OF EMPLOYER		
(c) ADDRESS OF EMPLOYER *(Include ZIP Code)*	(c) ADDRESS OF EMPLOYER *(Include ZIP Code)*		

SECTION II - SUBCONTRACTS *(Containing a "Patent Rights" clause)*

6. SUBCONTRACTS AWARDED BY CONTRACTOR/SUBCONTRACTOR *(If "None," so state)*

NAME OF SUBCONTRACTOR(S) a.	ADDRESS *(Include ZIP Code)* b.	SUBCONTRACT NUMBER(S) c.	FAR "PATENT RIGHTS" d.		DESCRIPTION OF WORK TO BE PERFORMED UNDER SUBCONTRACT(S) e.	SUBCONTRACT DATES *(YYYYMMDD)* f.	
			(1) CLAUSE NUMBER	(2) DATE *(YYYYMM)*		(1) AWARD	(2) ESTIMATED COMPLETION

SECTION III - CERTIFICATION

7. CERTIFICATION OF REPORT BY CONTRACTOR/SUBCONTRACTOR *(Not required if: (X as appropriate))* ☐ **SMALL BUSINESS or** ☐ **NONPROFIT ORGANIZATION** X

I certify that the reporting party has procedures for prompt identification and timely disclosure of "Subject Inventions," that such procedures have been followed and that all "Subject Inventions" have been reported.

a. NAME OF AUTHORIZED CONTRACTOR/SUBCONTRACTOR OFFICIAL *(Last, First, Middle Initial)*	b. TITLE	c. SIGNATURE	d. DATE SIGNED

UNCLASSIFIED

Department of Electrical & Computer Engineering
Boston University

Professor Alexander Sergienko

Final Report

ARO grant No. W911NF-07-1-0629

Prepared for ARO Project Manager:

T. R. Govindan <tr.govindan@us.army.mil>

"Phase-Sensitive Quantum Optical Sensor"

Period of performance:

September 10, 2007 - September 10, 2009.

(2) SCIENTIFIC PROGRESS DURING REPORTING PERIOD

During this period we successfully executed all elements of our original statement of work. The work at Boston University has been carried out in collaboration with Dr. T. Bahder at AMRDEC in Huntsville, Alabama.

Our research program during this period has concentrated on investigating novel scientific and technological solutions for ultra-sensitive quantum-optical registration and sensing of phase shifts induced by external fields. The use of several types of nonclassical states of light and development of novel ultra-sensitive interferometric phase measurement configurations has been at the center of our research effort.

The major technical findings have been reported in several leading refereed journal papers and presented at several technical meetings.

The following results have been obtained during the period of performance:

1) We performed theoretical investigation of the limitations that a single-mode assumption carries when using Fock-state and NOON-state light in practical quantum interferometry. Optical dispersion is a significant contributor to a wave packet modulation in existing materials demonstrating good phase shifting capability in response to the action of an external field. This degrades the quality of observed interference pattern and the accuracy of phase evaluation.

We considered Mach-Zehnder and Hong-Ou-Mandel interferometers with nonclassical states of light as input, and studied the effect that dispersion inside the interferometer has on the sensitivity of phase measurements. We examined in detail a number of different one- and two-photon input states, including Fock, dual Fock, N00N states, and photon pairs from parametric down conversion. We computed the probabilities of the possible measurement outcomes as a function of the phase shift introduced between the arms of the interferometer, and then computed the Shannon mutual information between the phase shift value and the measurement outcomes. This provides a means of quantitatively comparing the utility of various input states and various interferometric arrangements for determining phase in the presence of dispersion. In addition, we considered a simplified model of parametric down conversion for which probabilities can be explicitly computed analytically, and which serves as a limiting case of the more realistic down conversion model.

The results obtained in this work have been summarized in a Physical Review A publication:

- D. S. Simon, A. V. Sergienko, and T. B. Bahder, ‘’Dispersion and Fidelity in Quantum Interferometry’’, Physical Review A **v. 78**, 053829 (2008).

2) We continued our quest to discover alternative quantum techniques for ultra-precise phase-shift measurement. A key component of this effort involved studying methods for controlling the dispersive effects that can degrade the sensor's effectiveness. We proposed a novel design for a phase-sensitive quantum interferometer that demonstrates an odd-order dispersion cancellation effect based on frequency-anticorrelated entangled photons. We used this special interferometer to demonstrate observation of both odd-order and even-order dispersion cancellation effects in one single experiment for the first time. In addition to demonstrating a peculiar quantum effect, this result carries strong promise for significantly enhancing resolution when evaluating phase shifts in dispersive optical materials.

These results provided the basis for a research paper recently published in Physical Review Letters:

- Olga Minaeva, Cristian Bonato, Bahaa E. A. Saleh, David S. Simon, and Alexander V. Sergienko, "Odd- and Even-Order Dispersion Cancellation in Quantum Interferometry", *Physical Review Letters*, **v. 102**, 100504 (2009).

Work is currently underway for the experimental investigation of this idea and its application to quantum phase sensing.

3) During the course of our detailed studies of quantum interference and phase sensitivity we were able to demonstrate a link between frequency dispersion and its spatial counterpart, aberration. We developed a theoretical framework for the effect and by means of quantum interferometry we produced the first experimental demonstration of even-order aberration cancellation. The effect is a spatial counterpart of spectral group velocity dispersion cancellation, which is associated with spectral entanglement. It is manifested in temporal interferometry by virtue of the multi-parameter spatial-spectral entanglement. Spatially-entangled photons generated by spontaneous parametric down conversion were subjected to spatial aberration introduced by a deformable adaptive mirror that modulates the wavefront. We showed that only odd-order spatial aberrations affect the quality of quantum interference.

Two manuscripts summarizing these findings have been published in Physical Review Letters and Physical Review A:

- Cristian Bonato, David S. Simon, Paolo Villoresi, and Alexander V. Sergienko, "Multiparameter Entangled-State Engineering Using Adaptive Optics", Physical Review A v. 79, 062304 (2009)
- Cristian Bonato, Alexander V. Sergienko, Bahaa E. A. Saleh, Stefano Bonora, and Paolo Villoresi, "Even-Order Aberration Cancellation in Quantum Interferometry'', *Physical Review Letters*, **v. 101**, 233603 (2008).

4) While investigating the physics of dispersion cancellation effects we have formulated specific conditions enabling total spatial dispersion cancellation to all orders. The following manuscript has been submitted for publication:

- D. S. Simon and A. V. Sergienko “Spatial-Dispersion Cancellation in Quantum Interferometry”, submitted to Physical Review A (2009)

As a final step in our research efforts on this project we’ve extended the notion of spatial dispersion (aberration) cancellation to the case of “ghost imaging”. This novel imaging configuration has been proposed and theoretically analyzed in a recent manuscript (D. S. Simon and A. V. Sergienko “Ghost Imaging with Aberration-Cancellation”) and could open the way for enhanced-quality aberration-free imaging. The paper been submitted for publication in Physical Review Letters.

Conclusion:

We have successfully completed the original research program. A new research effect “Ghost Imaging with Aberration-Cancellation” has been discovered in the process, leading to the promise of significant enhancements in the fields of optical imaging and microscopy, as well as potential improvements to phase-sensitive optical sensors.

Our research has led to five research papers published in leading refereed physics journals, with one additional manuscript recently submitted for publication. Nine conference presentations have been given, including two Invited Talks. Four Invited Lectures have also been given at leading US and European research institutions, and several graduate and undergraduate students have been trained.

ATTACHMENT

(1) Papers published in peer-reviewed journals

1. D.S. Simon and A.V. Sergienko, "Ghost Imaging with Aberration-Cancellation", submitted to *Physical Reviews Letters* **v.80**, 053813 (2009) [arXiv:0911.3056]
2. D. S. Simon and A. V. Sergienko "Spatial-Dispersion Cancellation in Quantum Interferometry", *Physical Review A* (2009)
3. Cristian Bonato, David S. Simon, Paolo Villoresi, and Alexander V. Sergienko, "Multiparameter Entangled-State Engineering Using Adaptive Optics", *Physical Review A* v. 79, 062304 (2009)
4. Olga Minaeva, Cristian Bonato, Bahaa E. A. Saleh, David S. Simon, and Alexander V.. Sergienko, "Odd- and Even-Order Dispersion Cancellation in Quantum Interferometry", *Physical Review Letters*, **v. 102**, 100504 (2009).
5. Cristian Bonato, Alexander V. Sergienko, Bahaa E. A. Saleh, Stefano Bonora, and Paolo Villoresi, "Even-Order Aberration Cancellation in Quantum Interferometry'', *Physical Review Letters*, **v. 101**, 233603 (2008).
6. D. S. Simon, A. V. Sergienko, and T. B. Bahder, ''Dispersion and Fidelity in Quantum Interferometry'', *Physical Review A* **v. 78**, 053829 (2008).

(b) Papers published in non-peer-reviewed journals: NONE

(c) Presentations

i) Presentations at meetings, but not published in Conference Proceedings:

A. V. Sergienko, O. Minaeva, D. Simon, B. E. A. Saleh, and C. Bonato, "Quantum Dispersion Cancellation in Frequency and in Space" CLEO/Europe-IQEC, 19th International Congress on Photonics in Europe, Munich, Germany, June 14-19, (2009).

Alexander Sergienko, Olga Minaeva, Cristian Bonato, Bahaa E. A. Saleh, Paolo Villoresi "Dispersion Cancellation and Manipulation in Quantum Interferometry" Frontiers in Optics 2008 OSA Annual Meeting, Rochester, NY, October 19-24 (2008). **(Invited)**

Olga Minaeva, Cristian Bonato, Bahaa E. A. Saleh, Alexander V.. Sergienko, "Odd- and Even-Order Dispersion Cancellation in Quantum Interferometry", Frontiers in Optics 2008 OSA Annual Meeting, Rochester, NY, October 19-24 (2008).

Alexander Sergienko, "Entanglement in Quantum Communication: Dispersion Cancellation and Decoherence-Free Subspaces", SECOQC Quantum Network Demonstartion Conference, Vienna, Austria, October 8-10 (2008).

Cristian Bonato, Olga Minaeva, Alexander V. Sergienko, Bahaa E. A. Saleh, Stefano Bonora, and Paolo Villoresi "Spatial and Spectral Phase Control in Quantum Interferometry", QCCQI 2008 Quantum/Classical Control in Quantum Information, Otranto, Italy, September 13-20 (2008).

T. B. Bahder, D. S. Simon, and A. V. Sergienko, "Effect of Dispersion on Fidelity of Quantum Interferometer", 3rd International conference of Quantum Information, ICQI 2008, Boston, Massachusetts, July 13-15 (2008).

A. V. Sergienko C. Bonato, B. E. A. Saleh, S. Bonora, P. Villoresi, "Aberration cancellation in quantum interferometry", 3rd International conference of Quantum Information, ICQI 2008, Boston, Massachusetts, July 13-15 (2008). **(Invited)**

C. Bonato, A. V. Sergienko, B. E. A. Saleh, S. Bonora, P. Villoresi, "Even-order aberration cancellation in quantum interferometry", 4th Internatinal Workshop "Advances in foundations of Quantum Mechanics and Quantum Information with Atoms and Photons", Turin, Italy, May 19-23 (2008).

A. V. Sergienko, C. Bonato, S. Bonora, P. Villoresi, "Engineering Multiparameter Entangled States With Adaptive Optics", 4th Internatinal Workshop "Advances in foundations of Quantum Mechanics and Quantum Information with Atoms and Photons", Turin, Italy, May 19-23 (2008). **(Invited).**

Invited lectures at Research Institutions:

1. "Quantum Measurement with Non-classical Light", Physics Department, Scuola Normale Superiore, Pisa, Italy, June 24 (2009).
2. "Quantum Communication and Measurement with Non-classical Light", Joint Colloquium Department of Physics and Fondazione Bruno Kessler, University of Trento, Trento, Italy May 21 (2009).
3. "Quantum Communication and Measurement with Non-classical Light", Dept. of Electrical Engineering and Dept. of Applied Physics, Yale University, New Haven, Connecticut, May 6 (2009).
4. "Principles and Applications of Quantum Dispersion Cancellation with Entangled Photons", Quantum Entanglement Workshop IEEE Photonics Society, Boston Photonics Society Chapter, MIT Lincoln Lab, Lexington, Massachusetts, April 22 (2009).

(f) Honors and Awards: NONE

(g) Titles of Patents Disclosed: NONE

(h) Patents / Inventions: NONE

(2) PERSONNEL DATA FOR THIS REPORTING PERIOD

(a) Name & FTE of Faculty supported by this agreement

Alexander V. Sergienko – 11%
Malvin C. Teich – 11%

(b) Name & FTE of Graduate Students supported by this agreement

David Simon – 50%
Olga Minaeva – 30 %
Cristian Bonato – 20%

(c) Name & FTE of Post Doctorates supported by this agreement
NONE

(d) Master's Degrees awarded

Joshua Spitzberg
David Simon

(e) Name & FTE of Undergraduate Students supported by this agreement

Andy Fraine

(f) Name & FTE of Other Staff supported by this agreement

NONE

(g) DEGREES AWARDED

(a) Master's
Joshua Spitzberg
David Simon

(a) Doctoral
Cristian Bonato
Olga Minaeva

(h) STUDENT METRICS FOR GRADUATING UNDERGRADUATES FUNDED BY THIS AGREEMENT DURING THIS REPORTING PERIOD

(a) Number of graduating undergraduate students = 0
(b) Number of undergraduate students graduating with degrees in science, mathematics, engineering, and technology fields = 0
(c) Number of graduating undergraduates who will continue to pursue graduate

degrees = 0

(d) Number of graduating undergraduates who intend to work for the Defense Department = 0

(e) Number of graduating undergraduates during this period who achieve a 3.5 to 4.0 GPA (Convert GPAs on any other scale to be an equivalent value on a 4.0 scale.) = 0

(f) Number of graduating undergraduates funded by a DoD funded Center of Excellence grant for Education, Research and Engineering = 0

(g) The number of undergraduates funded by your agreement who graduated during this period and will receive scholarships or fellowships for further studies in science, mathematics, engineering or technology fields = 0

Multiparameter entangled-state engineering using adaptive optics

Cristian Bonato,[1,2] David Simon,[1] Paolo Villoresi,[2] and Alexander V. Sergienko[1,3]
[1]*Department of Electrical and Computer Engineering, Boston University, Boston, Massachusetts 02215, USA*
[2]*Department of Information Engineering, CNR-INFM LUXOR, University of Padova, 35131 Padova, Italy*
[3]*Department of Physics, Boston University, Boston, Massachusetts, USA*
(Received 5 April 2009; published 5 June 2009)

We investigate how quantum coincidence interferometry is affected by a controllable manipulation of transverse wave vectors in type-II parametric down-conversion using adaptive optics techniques. In particular, we discuss the possibility of spatial walk-off compensation in quantum interferometry and an effect of even-order spatial aberration cancellation.

DOI: 10.1103/PhysRevA.79.062304 PACS number(s): 03.67.Bg, 42.50.St, 42.50.Dv, 42.30.Kq

I. INTRODUCTION

Quantum entanglement [1] is a valuable resource in many areas of quantum optics and quantum information processing. One of the most widespread techniques for generating entangled optical states is spontaneous parametric down-conversion (SPDC) [2–5]. SPDC is a second-order nonlinear optical process in which a pump photon is split into a pair of new photons with conservation of energy and momentum. The phase-matching relation establishes conditions to have efficient energy conversion between the pump and the down-converted waves, called signal and idler. This condition also sets a specific relation between the frequency and the emission angle of down-converted radiation. In other words, the quantum state emitted in the SPDC process cannot be factorized into separate frequency and wave-vector components. This leads to several interesting effects where the manipulation of a spatial variable affects the shape of the polarization-temporal interference pattern. For example, the dependence of polarization-temporal interference on the selection of collected wave vectors was studied in detail in [6].

Here we engineer the quantum state in the space of transverse momentum and we study how this spatial modulation is transferred to the polarization-spectral domain by means of quantum interferometry. We will focus on type-II SPDC using birefringent phase matching since the correlations between wave vectors and spectrum are stronger than those employing other phase-matching conditions.

Our aim is twofold. From one point of view, we study the effect of spatial modulations on temporal quantum interference. This could be useful, for example, in quantum optical coherence tomography (QOCT) [7,8]. When focusing light on a sample with nonplanar surface, the photons will acquire a spatial phase distribution in the far field, which may perturb the shape of the interference dip. Our results will provide a tool to understand this effect.

From a second point of view, we would like to study and characterize spatial modulation as a tool for quantum state engineering. This may find application in the field of quantum information processing, where it is important to gain a high degree of control over the production of quantum entangled states entangled in one or more degrees of freedom (hyperentanglement).

We start by introducing a theoretical model of a type-II quantum interferometer, comprising the polarization, spectral, and spatial degrees of freedom (Sec. II). A modulation in the wave-vector space is provided by an adaptive optical setup and equations for the polarization-temporal interference pattern in the coincidence rate are derived. In Sec. III, we introduce a numerical approach for practical evaluation of the results of the theoretical model, discussing a few examples for general spatial aberrations.

In Sec. IV we will highlight and discuss theoretically two interesting special cases. The first one is the possibility of restoring high visibility in type-II quantum interference with large collection apertures. In some situations, to collect a higher photon flux or a broader photon bandwidth, it can be useful to enlarge the collection apertures of the optical system. But when dealing with type-II SPDC in birefringent crystals, for large collection apertures the effect of spatial walkoff introduces distinguishability between the photons, leading to a reduced visibility of temporal and polarization quantum interference. We will show that high visibility can be restored with a linear phase shift along the vertical axis.

The second effect is the spatial counterpart of spectral dispersion cancellation [9,10]. In the limit of large detection apertures, the correlations between the photons' momenta will cancel out the effects of even-order aberrations, exactly as in the limit of slow detectors the frequency correlations cancel out the even-order terms of spectral dispersion. The experimental demonstration of this effect has been reported recently [11].

As we proceed from the general case of Secs. II and III into the specific examples of Sec. IV, we will gradually see that optical aberration is a subject with two very different faces. On one hand, aberrations in optical components are normally seen as undesirable, since they lead to distortions in imaging. We will see that these unwanted spatial modulations may to some extent be canceled. On the other hand, we will find that such spatial modulations may also be turned into a useful tool: by *deliberately* introducing spatial modulations (in effect, purposely adding aberrations in a controlled manner), we can produce useful effects such as the restoration of visibility mentioned above. The examples we provide in Sec. IV will illustrate these two aspects and will show that both can benefit from more detailed study of the interplay between spatial modulations and spectral correlations.

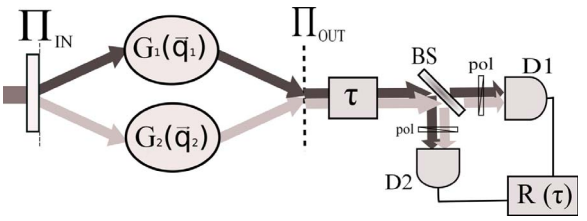

FIG. 1. (Color online) Scheme of the proposed setup. Horizontally polarized photons from type-II SPDC are assigned a phase dependent on the photon transverse momentum $\phi_o(q_o)$, while the vertically polarized ones are assigned a phase $\phi_e(q_e)$. The modulated photons enter a type-II quantum interferometer, which records the coincidence count rate as a function of the delay τ between the photons given by an appropriate delay line.

II. THEORETICAL MODEL

Consider the scheme in Fig. 1. A laser beam pumps a $\chi^{(2)}$ nonlinear material phase matched for type-II parametric down-conversion, creating a pair of entangled photons. Each of the generated photons passes through a Fourier-transform system, and then enters a modulation system which transforms transverse wave vectors for the horizontally (H) polarized photon according to the transfer function $G_1(\mathbf{q}_1)$ and for the vertically (V) polarized photon according to $G_2(\mathbf{q}_2)$. After being modulated in q space, the photons enter a type-II interferometer. A nonpolarizing beam splitter (BS) creates polarization entanglement from the polarization-correlated pair emitted by the source. The beams at the output ports of the beam splitter are directed toward two single-photon detectors. Two polarizers at 45° before the BS restore indistinguishability in the polarization degree of freedom. An adjustable delay line τ is scanned and the coincidence rate $R(\tau)$ between the detection events of the two detectors is recorded. An aperture is placed before the beam splitter to select an appropriate collection angle.

A. Notation

Consider a monochromatic plane wave of complex amplitude $E(\mathbf{r})=E_0e^{-i\mathbf{k}\cdot\mathbf{r}}$, with $\mathbf{r}=(x,y,z)$. For a given wavelength λ, corresponding to a frequency Ω, the wave vector can be split into a transverse component $\mathbf{q}=(q_x,q_y)$ and a longitudinal component $\beta(\mathbf{q};\Omega)$:

$$\mathbf{k}=[\mathbf{q},\beta(\mathbf{q};\Omega)]. \tag{1}$$

The wave number is

$$k(\Omega)=\frac{n(\Omega)\Omega}{c}. \tag{2}$$

The longitudinal component of the wave vector is

$$\beta(\mathbf{q},\Omega)=\sqrt{k^2(\Omega)-|\mathbf{q}|^2}. \tag{3}$$

Therefore the electric field at the position $\mathbf{r}$ and time t can be written as

$$E(\mathbf{r};t)=\int d\mathbf{q}\int d\Omega\tilde{E}(\mathbf{q},\Omega)e^{-i\mathbf{q}\cdot\boldsymbol{\rho}}e^{-i\beta(\mathbf{q};\Omega)z}e^{i\Omega t}, \tag{4}$$

where $\rho=(x,y)$.

In paraxial approximation $|\mathbf{q}|^2\ll k^2(\Omega)$, so that

$$\beta(\mathbf{q},\Omega)\approx k(\Omega)-\frac{|\mathbf{q}|^2}{2k(\Omega)}. \tag{5}$$

For a quasimonochromatic wave packet centered around the frequency Ω_0, one can write $\Omega=\Omega_0+\nu$, with $\nu\ll\Omega_0$. This expression can be approximated by

$$\beta(\mathbf{q},\Omega)\approx k_0+\frac{\nu}{u_0}-\frac{|\mathbf{q}|^2}{2k_0}, \tag{6}$$

where $k_0=k(\Omega_0)$ and $u_0=(\frac{dk(\Omega)}{d\Omega}|_{\Omega=\Omega_0})^{-1}$ is the group velocity for the propagation of the wave packet through the material.

B. State generation

Using first-order time-dependent perturbation theory, the two-photon state at the output of the nonlinear crystal can be calculated as

$$|\psi\rangle\sim-\frac{i}{\hbar}\int dtH_I(t)|0\rangle, \tag{7}$$

where the interaction Hamiltonian is

$$H_I(t)=\frac{1}{V}\int d\mathbf{r}\chi^{(2)}(\mathbf{r})E_p^{(+)}(\mathbf{r},t)E_s^{(-)}(\mathbf{r},t)E_i^{(-)}(\mathbf{r},t). \tag{8}$$

The strong, undepleted pump beam can be treated classically. Assuming a monochromatic plane wave propagating along the z direction,

$$E_p(\mathbf{r},t)=E_pe^{i(k_pz-\omega_pt)}. \tag{9}$$

The signal and idler photons are described by the following quantum field operators:

$$\hat{E}_j^{(-)}(\mathbf{r},t)=\int d\mathbf{q}_j\int d\omega_je^{i[\beta(\mathbf{q}_j,\omega_j)z+\mathbf{q}_j\cdot\boldsymbol{\rho}-\omega_jt]}\hat{a}(\mathbf{q}_j,\omega_j), \tag{10}$$

where $j=e,o$.

The biphoton quantum state at the output plane of the nonlinear crystal is [12]

$$|\psi\rangle=\int d\mathbf{q}\int d\nu\tilde{\Phi}(\mathbf{q},\nu)\hat{a}_o^\dagger(\mathbf{q},\Omega_0+\nu)\hat{a}_e^\dagger(-q,\Omega_0-\nu)|0\rangle. \tag{11}$$

Two photons are emitted from the nonlinear crystal, one horizontally polarized (ordinary photon) and the other vertically polarized (extraordinary photon), with anticorrelated frequencies and emission directions.

In the case of a single bulk crystal of thickness L and constant nonlinearity χ_o, the probability amplitude for having the signal photon in the mode $(\mathbf{q},\Omega_0+\nu)$ and the idler in the mode $(-\mathbf{q},\Omega_0-\nu)$ is

$$\tilde{\Phi}(\mathbf{q},\nu)=\mathrm{sinc}\left[\frac{L\Delta(\mathbf{q},\nu)}{2}\right]e^{i[\Delta(\mathbf{q},\nu)L/2]}. \tag{12}$$

For type-II collinear degenerate phase matching, the phase-mismatch function $\Delta(\mathbf{q},\nu)$ can be approximated to be

$$\Delta(\mathbf{q},\nu) = -\nu D + M\hat{\mathbf{e}}_2 \cdot \mathbf{q} + \frac{2|\mathbf{q}|^2}{k_p}, \tag{13}$$

where D is the difference between the inverse of the group velocities of the ordinary and extraordinary photons inside the birefringent crystal and the quadratic term in $\mathbf{q}$ is due to diffraction in paraxial approximation. The remaining term is the first-order approximation for the spatial walkoff.

C. Propagation

Consider a photon described by the operator $\hat{a}_j(\mathbf{q},\Omega)$ (polarization $j=e,o$, frequency Ω, and transverse momentum $\mathbf{q}$). Its propagation through an optical system to a point $\mathbf{x}_k$ on the output plane is described by the optical transfer function $H_j(\mathbf{x}_k,\mathbf{q};\Omega)$. In our setup, the field at the detector will be a superposition of contributions from the ordinary and extraordinary photons. The quantized electric fields at the detector planes are

$$\hat{E}_A^{(+)}(\mathbf{x}_A,t_A) = \int d\mathbf{q} \int d\omega e^{i\omega t_A}[H_e(\mathbf{x}_A,\mathbf{q};\omega)\hat{a}_e(\mathbf{q},\omega) + H_o(\mathbf{x}_A,\mathbf{q};\omega)\hat{a}_o(\mathbf{q},\omega)],$$

$$\hat{E}_B^{(+)}(\mathbf{x}_B,t_B) = \int d\mathbf{q} \int d\omega e^{i\omega t_B}[H_e(\mathbf{x}_B,\mathbf{q};\omega)\hat{a}_e(\mathbf{q},\omega) + H_o(\mathbf{x}_B,\mathbf{q};\omega)\hat{a}_o(\mathbf{q},\omega)]. \tag{14}$$

The probability amplitude for detecting a photon pair at the detector planes, with space-time coordinates $(\mathbf{x}_A,t_A)$ and $(\mathbf{x}_B,t_B)$, is

$$A(\mathbf{x}_A,\mathbf{x}_B;t_A,t_B) = \langle 0|\hat{E}_A^{(+)}(\mathbf{x}_A,t_A)\hat{E}_B^{(+)}(\mathbf{x}_B,t_B)|\psi\rangle. \tag{15}$$

For the biphoton probability amplitude we get

$$A(\mathbf{x}_A,\mathbf{x}_B;t_A,t_B) = \int d\mathbf{q}_o d\mathbf{q}_e d\omega_o d\omega_e \Phi(\mathbf{q}_o,\mathbf{q}_e;\omega_o,\omega_e) \times [H_e(\mathbf{x}_A,\mathbf{q}_e;\omega_e)H_o(\mathbf{x}_B,\mathbf{q}_o;\omega_o)e^{-i(\omega_e t_A+\omega_o t_B)} + H_o(\mathbf{x}_A,\mathbf{q}_o;\omega_o)H_e(\mathbf{x}_B,\mathbf{q}_e;\omega_e)e^{-i(\omega_o t_A+\omega_e t_B)}]. \tag{16}$$

This probability amplitude represents the superposition of two possible events leading to a coincidence count in the detectors:

(1) the V polarized photon with momentum $\mathbf{q}_e$ and frequency ω_e going through the lower branch to arrive at position x_A in detector A, while the H polarized photon with momentum $\mathbf{q}_o$ and frequency ω_o goes through the upper branch to arrive at position x_B in detector B; and

(2) the V polarized photon with momentum $\mathbf{q}_e$ and frequency ω_e going through the lower branch to arrive at position x_B in detector B, while the H polarized photon with momentum $\mathbf{q}_o$ and frequency ω_o goes through the upper branch to arrive at position x_A in detector A.

Since the superposition is coherent, there are quantum-interference effects between the two probability amplitudes.

1. State engineering section

In the state engineering section, each of the two branches consists of a pair of achromatic Fourier-transform systems coupled by a spatial light modulator or a deformable mirror. Each Fourier-transform system consists of a single lens of focal length f, separated from the optical elements before and after it by a distance f. The first Fourier system maps each incident transverse wave vector $\mathbf{q}$ on the plane Π_{in} to a point $\mathbf{x}(\mathbf{q})$ on the Fourier plane Π_F:

$$\mathbf{x}(\mathbf{q}) = \frac{f}{k_0}\mathbf{q}, \quad k_0 = \frac{\Omega_0}{c}, \tag{17}$$

where f is the focal length of the Fourier-transform system. Since we assume that the system is achromatic for a certain bandwidth around a central frequency Ω_0, the position $\mathbf{x}(\mathbf{q})$ depends only on $\mathbf{q}$ and not on ω.

The spatial modulator assigns a different amplitude and phase to the light incident on each point, as described by the function $G(\mathbf{x})=t(\mathbf{x})e^{i\varphi(\mathbf{x})}$. Each point is then mapped back to a wave vector on the plane Π_{out} by the second achromatic Fourier-transform system.

Using the formalism of Fourier optics [13], the transfer function between the planes Π_{in} and Π_{out} can be calculated to be

$$h_1(\mathbf{x_1},\mathbf{x_3}) = \int d\mathbf{x} G(\mathbf{x}) e^{-i(k_0/f)\mathbf{x}\cdot(\mathbf{x_1}+\mathbf{x_3})}. \tag{18}$$

The corresponding momentum-transfer function is

$$H_1(\mathbf{q_1},\mathbf{q_3}) = G\left[\frac{f}{k_0}\mathbf{q_1}\right]\delta(\mathbf{q_1}-\mathbf{q_3}). \tag{19}$$

2. Interferometer

After the plane Π_{out} the two photons enter a type-II quantum interferometer. Each propagates in free space to a birefringent delay line and a detection aperture $p(\mathbf{x})$ to be finally focused to the detection planes by means of lenses of focal length f_0. Following the derivation in [6] the transfer function is

$$H_2(\mathbf{x_i},\mathbf{q};\omega) = \int h(\mathbf{x_1},\mathbf{x_i};\omega)e^{i\mathbf{q}\cdot\mathbf{x_1}}d\mathbf{x}_1 = e^{i(\omega/c)(d_1+d_2+f_0)}\exp\left[-i\frac{\omega|\mathbf{x_i}|^2}{2cf_0}\left(\frac{d_2}{f_0}-1\right)\right] \times e^{-i(cd_1/2\omega)|\mathbf{q}|^2}\tilde{P}\left(\frac{\omega}{cf_0}\mathbf{x_i}-\mathbf{q}\right), \tag{20}$$

where $\tilde{P}(\mathbf{q})$ is the Fourier transform of $|p(\mathbf{x})|^2$.

A combination of the two different stages is described by the transfer function

$$H_\alpha(\mathbf{x_j},\mathbf{q}_\alpha;\omega_\alpha) = G_\alpha\left[\frac{f}{k_0}\mathbf{q}_\alpha\right]H_2(\mathbf{x_j},\mathbf{q}_\alpha;\omega), \tag{21}$$

where the two functions $G_1(\mathbf{q})$ and $G_2(\mathbf{q})$ are the momentum-transfer functions which describe the modulation

imparted, respectively, on the ordinary and the extraordinary photons.

D. Detection

Since the single-photon detectors used in quantum optics experiments are slow with respect to the temporal coherence of the photons and their area is larger than the spot onto which the photons are focused by the collection lens, we integrate over the spatial and temporal coordinates. Therefore the coincidence count rate expressed in terms of the biphoton probability amplitude is

$$R(\tau) = \int d\mathbf{x}_A \int d\mathbf{x}_B \int dt_A \int dt_B |A(\mathbf{x}_A, \mathbf{x}_B; t_A, t_B)|^2. \quad (22)$$

Following the derivation described in Appendix A, one gets

$$R(\tau) = R_0 \left[1 - \Lambda\left(1 - \frac{2\tau}{DL} \right) W_M(\tau) \right], \quad (23)$$

where $\Lambda(x)$ is the triangular function

$$\Lambda(x) = \begin{cases} 1 - |x|, & |x| \le 1 \\ 0, & |x| > 1. \end{cases} \quad (24)$$

Therefore, the coincidence count rate $R(\tau)$ is given by the summation of a background level R_0 and an interference pattern given by the triangular dip $\Lambda(1-\frac{2\tau}{DL})$ that one gets when working with narrow apertures, modulated by the function $W_M(\tau)$ which depends on the details of the adaptive optical system.

The expressions for R_0 and $W_M(\tau)$ are

$$\begin{aligned} R_0 = & \int d\mathbf{q} \int d\mathbf{q}' \ \mathrm{sinc}[ML\hat{\mathbf{e}}_2 \cdot (\mathbf{q} - \mathbf{q}')] \\ & \times G_1^*\left(\frac{f}{k_0}\mathbf{q} \right) G_1\left(\frac{f}{k_0}\mathbf{q}' \right) G_2^*\left(-\frac{f}{k_0}\mathbf{q} \right) \\ & \times G_2\left(-\frac{f}{k_0}\mathbf{q}' \right) e^{-i(ML/2)\hat{\mathbf{e}}_2 \cdot (\mathbf{q} - \mathbf{q}')} e^{i(2d_1/k_p)[|\mathbf{q}|^2 - |\mathbf{q}'|^2]} \\ & \times \tilde{P}_A(\mathbf{q} - \mathbf{q}') \tilde{P}_B(-\mathbf{q} + \mathbf{q}') \end{aligned} \quad (25)$$

and

$$\begin{aligned} W_M(\tau) = & \frac{1}{R_0} \int d\mathbf{q} \int d\mathbf{q}' \ \mathrm{sinc}\left[ML\hat{\mathbf{e}}_2 \cdot (\mathbf{q} + \mathbf{q}') \Lambda \right. \\ & \left. \times \left(1 - \frac{2\tau}{DL} \right) \right] G_1^*\left(\frac{f}{k_0}\mathbf{q} \right) G_1\left(\frac{f}{k_0}\mathbf{q}' \right) G_2^*\left(-\frac{f}{k_0}\mathbf{q} \right) \\ & \times G_2\left(-\frac{f}{k_0}\mathbf{q}' \right) e^{-i(M/D)\tau\hat{\mathbf{e}}_2 \cdot (\mathbf{q} - \mathbf{q}')} e^{i(2d_1/k_p)[|\mathbf{q}|^2 - |\mathbf{q}'|^2]} \\ & \times \tilde{P}_A[\mathbf{q} + \mathbf{q}'] \tilde{P}_B[-(\mathbf{q} + \mathbf{q}')]. \end{aligned} \quad (26)$$

In the following we will assume there is spatial modulation only on one of the photons; therefore we set $G_2(\mathbf{q}) \equiv 1$.

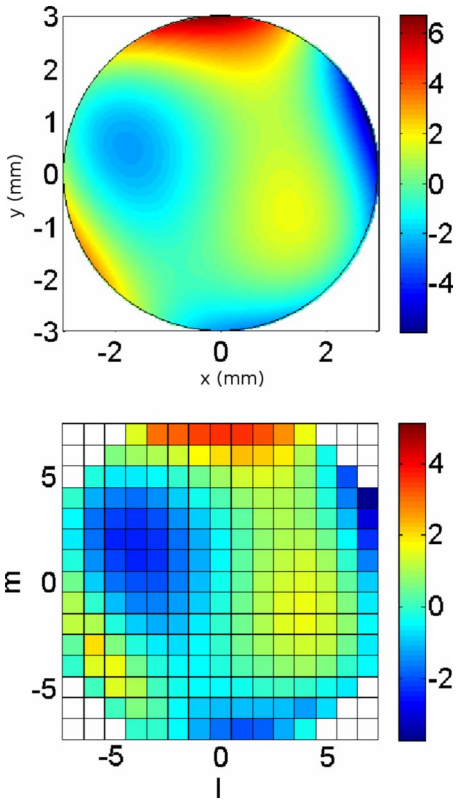

FIG. 2. (Color online) Example of the numerical approach adopted to evaluate Eqs. (25) and (26). The spatial modulation surface is discretized in sufficiently small squares over which the phase is averaged.

III. NUMERICAL SOLUTIONS FOR A GENERAL PHASE SHIFT

Numerically solving for the quantities in Eqs. (25) and (26) in the case of a general aberration may be computationally demanding. Here, we propose an approximation, valid in the case where the function $G(\mathbf{x})$ changes smoothly over the mirror surface, as it is the case in experimentally relevant situations. This model is also interesting from the practical point of view, since in many cases adaptive optical systems are implemented using spatial light modulators or segmented deformable mirrors, where the modulation surface is partitioned into small pixels.

Suppose we partition the Fourier plane Π_F into small squares (pixels) of side d (Fig. 2). Let us define the rectangular function

$$\Pi(\mathbf{x}) = \begin{cases} 0 & \text{if } |\mathbf{x}| > \frac{1}{2} \\ 1 & \text{if } |\mathbf{x}| < \frac{1}{2}. \end{cases} \quad (27)$$

The pixel (l,m) is identified by

$$\sigma_{l,m}(x,y) = \Pi\left[\frac{x}{d} + l \right] \Pi\left[\frac{y}{d} + m \right], \quad (28)$$

selecting the area

$$\left(l - \tfrac{1}{2} \right) d < x < \left(l + \tfrac{1}{2} \right) d,$$

$$\left(m-\tfrac{1}{2}\right)d < y < \left(m+\tfrac{1}{2}\right)d. \tag{29}$$

We approximate the value of the phase in each square by the mean value of the actual phase within the square:

$$\varphi_{lm} = \frac{1}{d^2}\int dxdy\varphi(x,y)\Pi\left[\frac{x}{d}+l\right]\Pi\left[\frac{y}{d}+m\right]. \tag{30}$$

That is,

$$e^{i\varphi(x,y)} \approx \sum_{l,m} e^{i\varphi_{l,m}\Pi[(x/d)+l]\Pi[(y/d)+m]}. \tag{31}$$

In this case (see Appendix B for a justification)

$$\sum_{l,m} e^{i\phi_{l,m}\Pi[(x/d)+l]\Pi[(y/d)+m]} = \sum_{l,m} e^{i\phi_{l,m}}\Pi\left[\frac{x}{d}+l\right]\Pi\left[\frac{y}{d}+m\right]. \tag{32}$$

Substituting this expression into Eq. (23) and collecting the integrations, one finds

$$R(\tau) \approx \sum_{l,m}\sum_{\lambda,\mu} e^{-i\phi_{lm}-\phi_{\lambda,\mu}}\alpha_{l\lambda}I_{m\mu}(\tau), \tag{33}$$

where

$$\alpha_{l\lambda} = \int dq_x \int dQ_x \Pi\left[\frac{f}{kd}q_x - l\right]\Pi\left[\frac{f}{kd}Q_x - \lambda\right]e^{j(2d_1/k_p)(q_x^2-Q_x^2)P[q_x+Q_x]P[-(q_x+Q_x)]} \tag{34}$$

and

$$I_{m,\mu}(\tau) = \int dq_y \int dQ_y \Pi\left[\frac{f}{kd}q_y - m\right]\Pi\left[\frac{f}{kd}Q_y - \mu\right]e^{j(2d_1/k_p)(q_y^2-Q_y^2)}e^{-j(M/D)\tau(q_y-Q_y)}$$
$$\times \mathrm{Sinc}\left[ML(q_y+Q_y)\Lambda\left(1-\frac{2\tau}{DL}\right)\right]P[q_y+Q_y]P[-(q_y+Q_y)]. \tag{35}$$

Performing the integrations one gets

$$\alpha_{l\lambda} = \int dx\tilde{P}(x)\Lambda\left[\frac{fx}{kd}-(l+\lambda)\right]\mathrm{sinc}\left\{\frac{2dd_1}{f}x\Lambda\left[\frac{fx}{kd}-(l+\lambda)\right]\right\}e^{i(dd_1/f)(l-\lambda)x} \tag{36}$$

and

$$I_{m\mu}(\tau) = \int dx\tilde{P}(x)\Lambda\left[\frac{fx}{kd}-(m+\mu)\right]\mathrm{sinc}\left\{MLx\Lambda\left[1-\frac{2\tau}{DL}\right]\right\}$$
$$\times \mathrm{sinc}\left\{\frac{2kd}{f}\left(\frac{2d_1}{k_p}x-\frac{M}{D}\tau\right)\Lambda\left[\frac{fx}{kd}-(m+\mu)\right]\right\}e^{i(kd/f)[(2d_1/k_p)x-(M/D)\tau](m-\mu)}. \tag{37}$$

A similar expression can be found for the background coincidence rate:

$$R_0 \approx \sum_{l,m}\sum_{\lambda,\mu} e^{-i(\phi_{lm}-\phi_{\lambda,\mu})}R_{l\lambda}^{(x)}R_{m\mu}^{(y)}, \tag{38}$$

where

$$R_{l\lambda}^{(x)} = \int dx\tilde{P}(x)\Lambda\left[\frac{fx}{kd}-(l-\lambda)\right]\mathrm{sinc}\left\{\frac{2dd_1}{f}x\Lambda\left[\frac{fx}{kd}-(l-\lambda)\right]\right\}e^{i(dd_1/f)(l+\lambda)x} \tag{39}$$

and

$$R_{m\mu}^{(y)} = \int dx\tilde{P}(x)\Lambda\left[\frac{fx}{kd}-(m-\mu)\right]\mathrm{sinc}(MLx)\mathrm{sinc}\left\{\frac{2dd_1}{f}x\Lambda\left[\frac{fx}{kd}-(m-\mu)\right]\right\}e^{i[(dd_1/f)(m+\mu)-ML/2]x}. \tag{40}$$

The advantage of our numerical approach is that one can calculate and tabulate the functions $R_{l\lambda}^{(x)}$, $R_{m\mu}^{(y)}$, $\alpha_{l\lambda}$, and $I_{m\mu}(\tau)$ for a given configuration, determined by the focal length f, the shape of the detection apertures, the width of the deformable optics, and the distance between the crystal and the detectors. Then, to calculate the shape of the interference pattern for a certain phase distribution on the adaptive optics, one just needs to change the coefficient of a linear combination of the tabulated functions. This can be a helpful tool for studying the effect of specific aberrations on the temporal

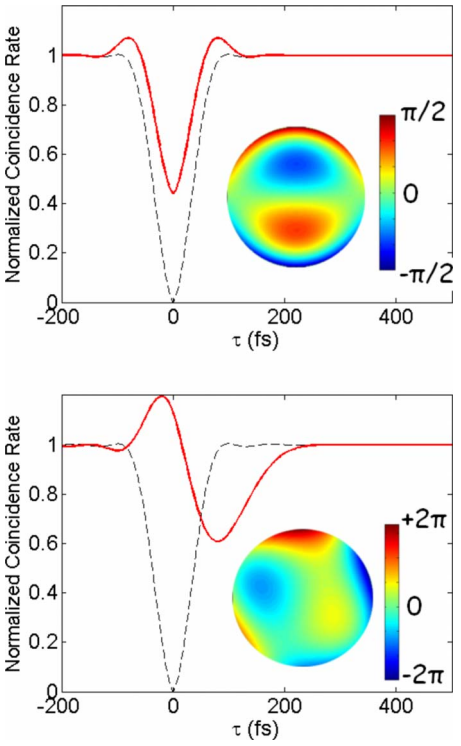

FIG. 3. (Color online) Examples of the shape of the polarization quantum-interference dip with two different spatial phase modulations (in black the unperturbed dip, in red the modulated one). In the upper figure the effect of a small amount of coma along the vertical axis is shown. In the lower figure a more complicated superposition of aberrations affects dramatically the shape of the dip.

interference or to engineer the shape of the Hong-Ou-Mandel (HOM) dip.

Some examples of how the temporal quantum-interference dip is modulated by a generic spatial phase shift are reported in Fig. 3, for coma (upper plot) and a superposition of several different aberrations (lower plot). The interference visibility clearly degrades in presence of wave-front aberrations.

IV. PARTICULAR CASES

In this section we will discuss the quantum-interference pattern, described by Eq. (23), for a few simple cases. First we will consider the case when no spatial modulation is assigned to the photons and Eq. (23) will reduce to the results already described in the literature for quantum interferometry with multiparametric entangled states from type-II down-conversion [6]. Then we will examine the effect of a linear phase, describing its implications for the compensation of the spatial walkoff between the two photons. Finally we will describe what happens in the approximation of sufficiently large detection apertures, introducing the effect of even-order aberration cancellation.

A. No phase modulation

Applying no phase modulation, our equations reduce to the ones derived in [6]. Particularly we find

$$R_0 = \tilde{P}_A(\mathbf{0})\tilde{P}_B(\mathbf{0}) \tag{41}$$

and

$$W_G(\tau) = \mathrm{Sinc}\left[\frac{M^2 L k_p}{2d_1 D}\tau\Lambda\left(1-\frac{2\tau}{DL}\right)\right]\tilde{P}_A \times\left[\frac{Mk_p}{2d_1 D}\tau\hat{\mathbf{e}}_2\right]\tilde{P}_B\left[-\frac{Mk_p}{2d_1 D}\tau\hat{\mathbf{e}}_2\right]. \tag{42}$$

The shape of the interference pattern is essentially given by the product of the triangular function by the Fourier transform of the aperture function, centered at $\tau=0$. For physically relevant parameters the sinc function is almost flat in the region where the triangular function is not zero.

To get an analytic result one may assume Gaussian detection apertures of radius R_G centered along the system's optical axis:

$$p(\mathbf{x}) = e^{-|\mathbf{x}|^2/2R_G^2}. \tag{43}$$

In this case the solution is quite simple:

$$R(\tau) = R_0\left[1-\Lambda\left(1-\frac{2\tau}{DL}\right)e^{-\tau^2/2\tau_1^2}\right], \tag{44}$$

with

$$\tau_1 = \frac{2d_1 D}{k_p M R_G}. \tag{45}$$

Typically, sharp circular apertures are used in experiments. In this case, the function $\tilde{P}[\mathbf{q}]$ is described in terms of the Bessel function $J_1(x)$. For a circular aperture of radius R,

$$\tilde{P}[\mathbf{q}] = \frac{J_1(2R|\mathbf{q}|)}{R|\mathbf{q}|}. \tag{46}$$

However the Gaussian approximation is still a good one if the width R_G of the Gaussian is taken to roughly fit the Bessel function (of width R): in our case we take $R_G = R/(2\sqrt{2})$.

Therefore Eq. (44) is still approximately valid in the case of sharp circular apertures, just taking

$$\tau_1 = \frac{4\sqrt{2}d_1 D}{k_p M R_B}. \tag{47}$$

Mathematically, in Eq. (44) the interference pattern is given by the multiplication of a triangular function centered at $\tau=DL/2$ by a Gaussian function centered at $\tau=0$. The width of the Gaussian function τ_1 decreases with increasing radius of the aperture R_B. Therefore, in the small-aperture approximation, the width of the Gaussian is so large that it is approximately constant between $\tau=0$ and $\tau=DL/2$, giving the typical triangular dip found in quantum-interference experiments. On the other hand, increasing the aperture size, the width of the Gaussian function decreases, reducing the dip visibility (see Fig. 4). Physically, this can be explained by the fact that by increasing the aperture size we let more wave vectors into the system, and so the spatial walkoff in type-II interferometry introduces distinguishability, reducing

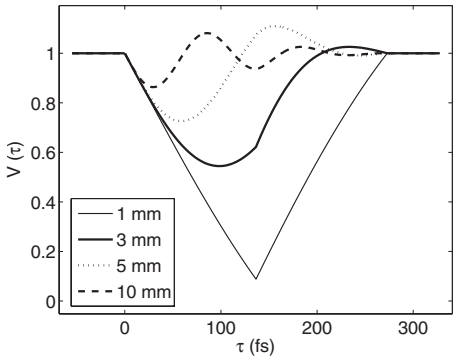

FIG. 4. On the right side we can see the interference patterns with three different detector aperture sizes: the corresponding aperture functions are shown on the left side.

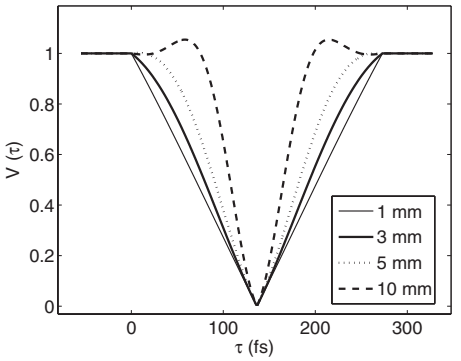

FIG. 5. Quantum-interference pattern for different detector aperture sizes, introducing a linear modulation of the deformable mirror, in order to restore the indistinguishability between the photons, decreased by the spatial walkoff in the generation process.

the interference visibility. Enlarging the aperture sizes is often useful in practice, for example, to get a higher photon flux. Moreover, since in the SPDC process different frequency bands are emitted at different angles, it may be necessary to open the detection aperture in applications where a broader bandwidth is needed. This is clearly a problem when using type-II phase matching in birefringent crystals, since the visibility of temporal and polarization interference gets drastically reduced.

B. Linear phase shift

Suppose now we introduce a linear phase function with the spatial light modulator, along the direction $\mathbf{s}_1$,

$$\varphi(\mathbf{x}) = \mathbf{s_1} \cdot \mathbf{x}, \tag{48}$$

we get

$$W_M(\tau) = \mathrm{Sinc}\left[\frac{M^2 L k_p}{2d_1 D}\tau\Lambda\left(1-\frac{2\tau}{DL}\right)\right]\tilde{P}_A \times\left[\frac{Mk_p}{2d_1 D}\tau\hat{\mathbf{e}}_2 + 2f\mathbf{s_1}\right]\tilde{P}_B\left[-\frac{Mk_p}{2d_1 D}\tau\hat{\mathbf{e}}_2 - 2f\mathbf{s_1}\right]. \tag{49}$$

If we compare Eq. (49) with Eq. (44) we can see that the structure is the same. We again have a triangular function centered at $\tau = DL/2$, along with two aperture functions. But this time, instead of being centered at $\tau = 0$, the aperture functions can be shifted at will along the τ axis. Suppose we now apply a tilt along the y axis ($s_{1x} = 0$). The modulation function is then shifted to

$$\tau_{center} = \frac{fD}{k_0 M} s_{1y}. \tag{50}$$

To get the highest possible visibility, the center of the modulation function must be matched to the center of the triangular dip,

$$\tau_{center} = \frac{DL}{2}, \tag{51}$$

so that

$$s_{1y} = \frac{k_0 ML}{2f}. \tag{52}$$

In the case of a reflective system, in which the phase modulation is implemented by means of a deformable mirror (Fig. 5), tilted by an angle θ,

$$\varphi(\mathbf{x}) = 2k_0 \tan\theta y = s_{1y} y. \tag{53}$$

Therefore, the amount of tilt necessary to restore high visibility is

$$\tan\theta = \frac{ML}{4f}. \tag{54}$$

In the case of a 1.5 mm crystal, with $M = 0.0723$ (pump at 405 nm, SPDC at 810 nm) and lenses with focal length of 20 cm in the $4f$ system, we get

$$\theta = 0.14 \text{ mrad}. \tag{55}$$

C. Large-aperture approximation

If the detection apertures are large enough for the $\tilde{P}_i$ function to be successfully approximated by a delta function, we get

$$W_M(\tau) = \int d\mathbf{q} G_1^*\left(\frac{f}{k_0}\mathbf{q}\right) G_1\left(-\frac{f}{k_0}\mathbf{q}\right) e^{-i(2M/D)\tau\hat{\mathbf{e}}_2\cdot\mathbf{q}}. \tag{56}$$

Suppose that the spatial modulator is a circular aperture with radius r, with unit transmission and phase modulation described by the function $\varphi(\mathbf{x})$,

$$G_1(\mathbf{x}) = \begin{cases} 0 & \text{if } |\mathbf{x}| > r \\ e^{i\varphi(\mathbf{x})} & \text{if } |\mathbf{x}| < r. \end{cases} \tag{57}$$

In this case the function $\varphi(\mathbf{x})$ can be expanded on a set of polynomials which are orthogonal on the unit circle, such as the Zernicke polynomials:

$$\varphi(\mathbf{q}) = \sum_n \sum_m \varphi_{nm} R_n^m(\rho)\cos(m\theta),$$

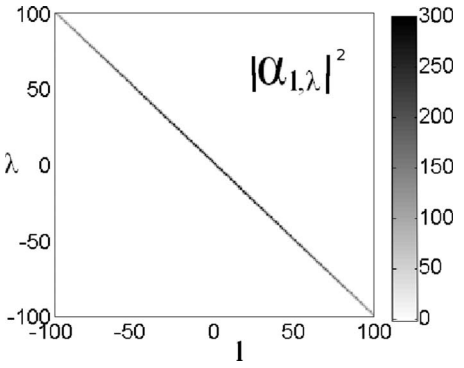

FIG. 6. Plot of the values of $|\alpha_{l,\lambda}|^2$, for $l,\lambda=-100,\ldots,+100$. The radius of the detection apertures is $R=5$ mm, the distance between the exit plane of the modulation section and the detection apertures is $d-1=1$ m, and the size of the modulation pixels is $d=25$ μm. Clearly only the diagonal elements are nonzero, i.e., the ones for which $\lambda=-l$. In this situation the effect of even-order aberration cancellation is present.

$$m=-n,-n+2,-n+4,\ldots,n, \tag{58}$$

where $\mathbf{q}=(\rho\cos\theta,\rho\sin\theta)$. To calculate $\varphi(-\mathbf{q})$ we note that $-\mathbf{q}=[\rho\cos(\theta+\pi),\rho\sin(\theta+\pi)]$, so

$$\varphi(-\mathbf{q})=\sum_n\sum_m R_n^m(\rho)\cos[m(\theta+\pi)]. \tag{59}$$

If m is even then $\cos[m(\theta+\pi)]=\cos(m\theta)$; otherwise if m is odd $\cos[m(\theta+\pi)]=-\cos m\theta$. Therefore

$$\varphi(\mathbf{q})-\varphi(-\mathbf{q})=2\sum_n\sum_{\mathrm{m\ odd}}\varphi_{nm}R_n^m(\rho)\cos(m\theta). \tag{60}$$

So, only the Zernicke polynomials with m odd contribute to the shape of the interference pattern. This effect is the spatial counterpart of the dispersion cancellation effect, in which only the odd-order terms in the Taylor expansion of the spectral phase survive. The experimental demonstration of this effect was recently reported in [11].

An interesting question is how large the detection apertures should effectively be, in order to obtain the even-order aberration cancellation effect. According to the numerical approach proposed in Sec. IV, the even-order aberration cancellation effect manifests itself in the limit where $\tilde{P}(x)\approx\delta(x)$, so that

$$\alpha_{l,\lambda}\to\delta(l+\lambda). \tag{61}$$

In Fig. 6, a plot of the value for $\alpha_{l,\lambda}$ is shown for typical values of the relevant experimental parameters (detection aperture radius $R=5$ mm, detection distance $d_1=1$ m, and size $d=0.1$ mm of each pixel in the Fourier plane of the adaptive optical system). Clearly, only the diagonal elements (the ones for which $l=-\lambda$) are significant, suggesting that the effect of even-order aberration cancellation may be observable for most typical experimental parameters.

To get an idea of what happens for different experimental conditions, we can compute the ratio between the intensities

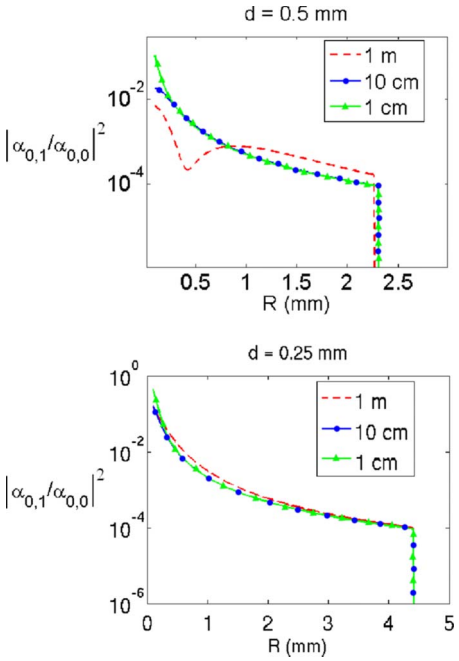

FIG. 7. (Color online) Plot of the ratio ρ_0 between the intensities of the nondiagonal coefficient α_{01} and the diagonal coefficient α_{00} as a function of the radius of Gaussian detection apertures, R, for different values of the distance between the exit plane of the modulation section and the detection apertures ($d_1=1,10,100$ cm). On the upper plot the size of the modulation pixel d is $d=0.5$ mm, while in the second case it is $d=0.25$ mm. Clearly, for experimentally interesting cases, the off-diagonal coefficient is at least 3 orders of magnitude smaller than the diagonal one, leading to even-order aberration cancellation.

of the nondiagonal coefficient α_{01} and the diagonal coefficient α_{00}:

$$\rho_0=\frac{|\alpha_{01}|^2}{|\alpha_{00}|^2}. \tag{62}$$

The lower the value for ρ_0 is, the less significant the coefficients for $\lambda\neq-l$ are: the even-order aberration cancellation effect will therefore manifest itself more clearly.

Values for ρ_0 are shown in Fig. 7 for two different cases. In both pictures, the value of ρ_0 is shown as a function of the Gaussian detection aperture radius R, for three different values of the distance between the plane Π_3 and the detection lenses d_1. In the upper panel, the size of each small square in which the spatial phase is assumed to be constant is $d=0.5$ mm, while in the second case it is $d=0.25$ mm. In both cases ρ_0 is significantly smaller than 1, and it becomes smaller and smaller, increasing the value of the detection aperture radius. However, ρ_0 is smaller for larger values of d, implying that the spatial variability of the modulation phase plays a role in the degree of even-order cancellation of the modulation itself.

It turns out that for the aberration cancellation effect to appear, it is in fact only necessary for one aperture to be large and for one detector to be integrated over. This is sufficient to produce the transverse-momentum delta functions that lead to even-order cancellation. To demonstrate this, we

can, for example, consider the case where the aperture at B is large, and the detector at B is integrated over, while the aperture at A is taken to be finite, with detector A treated as pointlike. The location of the pointlike detector will henceforth simply be denoted as x, and we continue to work within the quasimonochromatic approximation. If we integrate only over x_B, leaving x unintegrated, then it is straightforward to show that the analogs of Eqs. (A3) and (A4) are

$$W^{(0)}(\mathbf{x},\mathbf{q},\mathbf{q}',\nu) = e^{-(icd/\Omega_0)(q^2-q'^2)}\left\{\tilde{Q}\left(q+\frac{\Omega_0 x}{cf_0}\right)\tilde{Q}'\left(-q'-\frac{\Omega_0 x}{cf_0}\right)\tilde{P}_B(q'-q)+\tilde{Q}\left(-q+\frac{\Omega_0 x}{cf_0}\right)\tilde{Q}'\left(q'-\frac{\Omega_0 x}{cf_0}\right)\tilde{P}_B(q-q')\right\}, \tag{63}$$

$$W(\mathbf{x},\mathbf{q},\mathbf{q}',\nu) = e^{-(icd/\Omega_0)(q^2-q'^2)}\left\{\tilde{Q}\left(q+\frac{\Omega_0 x}{cf_0}\right)\tilde{Q}'\left(-q'+\frac{\Omega_0 x}{cf_0}\right)\tilde{P}_B(-q'-q)+\tilde{Q}\left(-q+\frac{\Omega_0 x}{cf_0}\right)\tilde{Q}'\left(+q'+\frac{\Omega_0 x}{cf_0}\right)\tilde{P}_B(q-q')\right\}. \tag{64}$$

We have defined $\tilde{Q}$ and $\tilde{Q}'$ to be the Fourier transforms, respectively, of p_A and p_A^*. $\tilde{P}_B$ is, as before, the Fourier transform of $|p_B|^2$. We now let aperture B become large, so that the function $\tilde{P}_B$ goes over to a delta function. For $G_1(x)=e^{i\phi(x)}$ and $G_2(x)=1$, we can substitute these results into the coincidence rate (which will now be a function of both τ and the position x of detector A), and carry out the q' and ν integrals. For the modulation term, we find

$$R_M(x,\tau) = R(x,\tau) - R_0(x) \tag{65}$$

$$\begin{aligned} &= \int dq e^{i[\phi(q)-\phi(-q)]} e^{(2iM\pi/D)\mathbf{e_2}\cdot\mathbf{q}} e^{(2iq^2/k_p)[(2\pi/D)+L]} \\ &\times \mathrm{Sinc}\left(\frac{2q^2L}{k_p}\right)\left[\tilde{Q}\left(q+\frac{\Omega_0 x}{cf_0}\right)\tilde{Q}^*\left(-q-\frac{\Omega_0 x}{cf_0}\right)\right. \\ &\left.+\tilde{Q}\left(-q+\frac{\Omega_0 x}{cf_0}\right)\tilde{Q}^*\left(q-\frac{\Omega_0 x}{cf_0}\right)\right]. \end{aligned} \tag{66}$$

Here, we have used the fact that the Fourier transform of $p_A^*(x)$ equals the complex conjugate of the Fourier transform of $p_A(-x)$, in order to write $\tilde{Q}'$ in terms of $\tilde{Q}$. We see from the presence of the factor $e^{i[\phi(q)-\phi(-q)]}$ that even-order aberration cancellation occurs even though one aperture is finite and the corresponding detector is pointlike. This point may be of importance in future attempts to produce aberration-canceled imaging.

V. CONCLUSIONS

Summarizing, in this paper we have carried out a theoretical study of the relation between the wave-front modulation of the entangled SPDC photons and the shape of the resulting temporal quantum-interference pattern. Due to the multiparametric nature of the generated entangled states, the modulation on the spatial degree of freedom can affect the shape of the polarization-temporal interference pattern in the coincidence rate. Our aim is twofold: from one side we want to study the effect of wave-front aberration on quantum interferometry, and from the other we want to discuss a way to engineer multiparametrically entangled states.

We have introduced a theoretical model for calculation of the shape of the polarization-temporal interference pattern given a certain general phase modulation in the crystal far field, assuming as a free parameter the shape and the dimension of the collection apertures. Using a numerical method to study the resulting equation has shown that for typical experimental cases the hypothesis of large apertures can be assumed to be valid. In such an approximation, only the odd part of the assigned phase modulation affects the shape of the interference pattern. This effect has recently been demonstrated experimentally [11].

Moreover, it is often useful in experiments to enlarge the collection aperture in order to collect a higher photon flux and larger optical bandwidth. But when working with type-II birefringently phase-matched down-conversion, spatial walkoff between the emitted photons introduces distinguishability between the two possible events that can lead to coincidence detection, reducing the visibility of quantum interference. Such walkoff can be compensated for with a linear phase shift in the vertical direction, restoring high visibility.

ACKNOWLEDGMENTS

This work was supported by a U.S. Army Research Office (USARO) Multidisciplinary University Research Initiative (MURI) grant; by the Bernard M. Gordon Center for Subsurface Sensing and Imaging Systems (CenSSIS), an NSF Engineering Research Center; by the Intelligence Advanced Research Projects Activity (IARPA) and USARO through Grant No. W911NF-07-1-0629; and by the strategic project QUINTET of the Department of Information Engineering of the University of Padova. C.B. also acknowledges financial support from Fondazione Cassa di Risparmio di Padova e Rovigo.

APPENDIX A: SKETCH OF DERIVATION OF EQ. (23)

In this appendix we sketch the major steps for the derivation of Eq. (23). Substituting Eq. (21) into Eq. (16) and the result into Eq. (22), one finds the following expressions for R_0 and $W_G(\tau)$:

$$R_0 = \int d\mathbf{q}d\mathbf{q}'d\nu\Phi^*(\mathbf{q},\nu)\Phi(\mathbf{q}',\nu)G_1^*\left(\frac{f}{k}\mathbf{q}\right)G_1\left(\frac{f}{k}\mathbf{q}'\right)G_2^*\left(-\frac{f}{k}\mathbf{q}\right)G_2\left(-\frac{f}{k}\mathbf{q}'\right)W^{(0)}(\mathbf{q},\mathbf{q}',\nu), \tag{A1}$$

$$W_M(\tau) = \frac{1}{R_0}\int d\mathbf{q}d\mathbf{q}'d\nu\Phi^*(\mathbf{q},\nu)\Phi(\mathbf{q}',-\nu)G_1^*\left(\frac{f}{k}\mathbf{q}\right)G_1\left(\frac{f}{k}\mathbf{q}'\right)G_2^*\left(-\frac{f}{k}\mathbf{q}\right)G_2\left(-\frac{f}{k}\mathbf{q}'\right)W(\mathbf{q},\mathbf{q}',\nu), \tag{A2}$$

where

$$W^{(0)}(\mathbf{q},\mathbf{q}',\nu) = \int d\mathbf{x}_A d\mathbf{x}_B H^*(\mathbf{x}_A,\mathbf{q},\nu)H^*(\mathbf{x}_B,-\mathbf{q},-\nu)H(\mathbf{x}_A,\mathbf{q}',\nu)H(\mathbf{x}_B,-\mathbf{q}',-\nu)$$
$$+ H^*(\mathbf{x}_A,-\mathbf{q},-\nu)H^*(\mathbf{x}_B,\mathbf{q},\nu)H(\mathbf{x}_A,-\mathbf{q}',-\nu)H(\mathbf{x}_B,\mathbf{q}',\nu) \tag{A3}$$

and

$$W(\mathbf{q},\mathbf{q}',\nu) = \int d\mathbf{x}_A d\mathbf{x}_B H^*(\mathbf{x}_A,\mathbf{q},\nu)H^*(\mathbf{x}_B,-\mathbf{q},-\nu)H(\mathbf{x}_A,-\mathbf{q}',\nu)H(\mathbf{x}_B,\mathbf{q}',-\nu)$$
$$+ H^*(\mathbf{x}_A,-\mathbf{q},-\nu)H^*(\mathbf{x}_B,\mathbf{q},\nu)H(\mathbf{x}_A,\mathbf{q}',-\nu)H(\mathbf{x}_B,-\mathbf{q}',\nu). \tag{A4}$$

The angular and spectral emission function $\Phi(\mathbf{q},\nu)$ is given by

$$\Phi(\mathbf{q},\nu) = \int dz\Pi\left[\frac{z}{L}+\frac{1}{2}\right]e^{-i\Delta(\mathbf{q},\nu)z}. \tag{A5}$$

Performing the integrals over the spatial coordinates $d\mathbf{x}_A$ and $\mathbf{x}_B$, one gets

$$W^{(0)}(\mathbf{q},\mathbf{q}',\nu) = e^{i(2d_1/k_p)[|\mathbf{q}|^2-|\mathbf{q}'|^2]}\{\tilde{P}_A[(\mathbf{q}-\mathbf{q}')]\tilde{P}_B[-(\mathbf{q}-\mathbf{q}')] + \tilde{P}_A[-(\mathbf{q}-\mathbf{q}')]\tilde{P}_B[(\mathbf{q}-\mathbf{q}')]\} \tag{A6}$$

and

$$W(\mathbf{q},\mathbf{q}',\nu) = e^{i(2d_1/k_p)[|\mathbf{q}|^2-|\mathbf{q}'|^2]}\{\tilde{P}_A[(\mathbf{q}+\mathbf{q}')]\tilde{P}_B[-(\mathbf{q}+\mathbf{q}')] + \tilde{P}_A[-(\mathbf{q}+\mathbf{q}')]\tilde{P}_B[(\mathbf{q}+\mathbf{q}')]\}. \tag{A7}$$

Finally, use of the integral representation for the sinc function [Eq. (A5)] allows the ν integration to be carried out, but at the expense of introducing two integrations over a pair of new parameters (say, z and z'). Note the following relation, which can easily be verified by sketching the functions on the left-hand side:

$$\Pi[x]\Pi[x-\alpha] = \begin{cases} 1 & \text{if } -1 \le \alpha \le 0, \quad -\frac{1}{2} \le x \le \frac{1}{2}+\alpha \\ 1 & \text{if } 0 \le \alpha \le 1, \quad -\frac{1}{2}+\alpha \le x \le \frac{1}{2} \\ 0 & \text{otherwise.} \end{cases} \tag{A8}$$

From this, it follows that

$$\int \Pi[x]\Pi[x-\alpha]dx = \Lambda(\alpha), \tag{A9}$$

where $\Lambda(\alpha)$ is the triangle function. These facts allow us to carry out the two z integrations that arise from the sinc function, leading to the result shown in Eq. (23).

APPENDIX B: JUSTIFICATION OF EQ. (32)

Suppose we have a set A, which can be partitioned into a collection of disjoint subsets A_k, with $k=1,2,\ldots$:

$$\bigcup_k A_k = A, \quad A_k \cap A_l = \phi \quad \text{if } k \neq l. \tag{B1}$$

To each set we can associate a characteristic function,

$$\chi_k(x) = \begin{cases} 1, & x \in A_k \\ 0, & x \notin A_k, \end{cases} \tag{B2}$$

such that

$$\sum_k \chi_k(x) = \chi_A(x), \quad \chi_k(x)\chi_l(x) = \delta_{kl}\chi_k(x), \tag{B3}$$

where χ_A is the characteristic function for the full set,

$$\chi_A(x) = \begin{cases} 1, & x \in A \\ 0, & x \notin A. \end{cases} \tag{B4}$$

The term $e^{i\phi_k\chi_k(x)}$ assumes the value of $e^{i\phi_k}$ for $\chi_k(x)=1$ and the value of 1 for $\chi_k(x)=0$ $[1-\chi_k(x)=1]$, so

$$\exp\left[i\sum_k \phi_k\chi_k(x)\right] = \prod_k e^{i\phi_k\chi_k(x)} = \prod_k \{1[1-\chi_k(x)] + e^{i\phi_k}\chi_k(x)\} = \prod_k [1 + (e^{i\phi_k} - 1)\chi_k]. \tag{B5}$$

If we express the first few terms we get

$$\begin{aligned}\prod_k [1 + (e^{i\phi_k} - 1)\chi_k] &= [1 + (e^{i\phi_1} - 1)\chi_1][1 + (e^{i\phi_2} - 1)\chi_2]\cdots \\ &= 1 + (e^{i\phi_1} - 1)\chi_1 + (e^{i\phi_2} - 1)\chi_2 + \cdots + (e^{i\phi_1} - 1)(e^{i\phi_2} - 1)\chi_1\chi_2 + (e^{i\phi_1} - 1)(e^{i\phi_3} - 1)\chi_1\chi_3 \\ &\quad + \cdots + (e^{i\phi_1} - 1)(e^{i\phi_1} - 1)(e^{i\phi_1} - 1)\chi_1\chi_2\chi_3 + (e^{i\phi_1} - 1)(e^{i\phi_2} - 1)(e^{i\phi_4} - 1)\chi_1\chi_2\chi_4 + \cdots .\end{aligned} \tag{B6}$$

So that in the end

$$\exp\left[i\sum_k \phi_k\chi_k(x)\right] = 1 + \sum_k [(e^{i\phi_k} - 1)\chi_k] = 1 + \sum_k e^{i\phi_k}\chi_k - \sum_k \chi_k = \sum_k e^{i\phi_k}\chi_k. \tag{B7}$$

Since the square sets we have used in Sec. IV satisfy Eq. (B1), then the result expressed in Eq. (B5) is valid for our case.

[1] E. Schrödinger, Naturwiss. **23**, 807 (1935).
[2] D. N. Klyshko, JETP Lett. **6**, 23 (1967).
[3] S. E. Harris, M. K. Osham, and R. L. Byer, Phys. Rev. Lett. **18**, 732 (1967).
[4] T. G. Giallorenzi and C. L. Tang, Phys. Rev. **166**, 225 (1968).
[5] D. A. Kleinman, Phys. Rev. **174**, 1027 (1968).
[6] M. Atature, G. Di Giuseppe, M. D. Shaw, A. V. Sergienko, B. E. A. Saleh, and M. C. Teich, Phys. Rev. A **66**, 023822 (2002).
[7] A. F. Abouraddy, M. B. Nasr, B. E. A. Saleh, A. V. Sergienko, and M. C. Teich, Phys. Rev. A **65**, 053817 (2002).
[8] M. B. Nasr, B. E. A. Saleh, A. V. Sergienko, and M. C. Teich, Phys. Rev. Lett. **91**, 083601 (2003).
[9] J. D. Franson, Phys. Rev. A **45**, 3126 (1992).
[10] A. M. Steinberg, P. G. Kwiat, and R. Y. Chiao, Phys. Rev. A **45**, 6659 (1992).
[11] C. Bonato, A. V. Sergienko, B. E. A. Saleh, S. Bonora, and P. Villoresi, Phys. Rev. Lett. **101**, 233603 (2008).
[12] M. H. Rubin, Phys. Rev. A **54**, 5349 (1996).
[13] J. W. Goodman, *Introduction to Fourier Optics*, 2nd ed. (McGraw-Hill, New York, 1996).

Even-Order Aberration Cancellation in Quantum Interferometry

Cristian Bonato,[1,2] Alexander V. Sergienko,[1,3] Bahaa E. A. Saleh,[1] Stefano Bonora,[2] and Paolo Villoresi[2]
[1]*Department of Electrical & Computer Engineering, Boston University, Boston, Massachusetts 02215, USA*
[2]*CNR-INFM LUXOR, Department of Information Engineering, University of Padova, Padova, Italy*
[3]*Department of Physics, Boston University, Boston, Massachusetts 02215, USA*
(Received 18 July 2008; published 2 December 2008)

We report the first experimental demonstration of even-order aberration cancellation in quantum interferometry. The effect is a spatial counterpart of the spectral group velocity dispersion cancellation, which is associated with spectral entanglement. It is manifested in temporal interferometry by virtue of the multiparameter spatial-spectral entanglement. Spatially entangled photons, generated by spontaneous parametric down-conversion, were subjected to spatial aberrations introduced by a deformable mirror that modulates the wave front. We show that only odd-order spatial aberrations affect the quality of quantum interference.

DOI: 10.1103/PhysRevLett.101.233603 PACS numbers: 42.50.Dv, 03.67.Bg, 42.30.Kq, 42.50.St

The nonlinear optical effect of spontaneous parametric down-conversion (SPDC) has been a reliable source of entangled-photon states for the last 30 years. A photon of the pump radiation has a random chance to be converted into two photons with lower energy while traveling though the nonlinear material. Conservation of energy and momentum governs the spatial and spectral state of the down converted light. In the case of a monochromatic pump beam, energy conservation leads to strong anticorrelation between the frequency components of signal and idler wave packets. This symmetric superposition of all possible anticorrelated frequencies with respect to the degenerate frequency of signal and idler waves gives rise to frequency entanglement.

Even-order dispersion cancellation is among the most interesting consequences of frequency entanglement [1,2]. If one of the two photons of an entangled pair travels through a dispersive material and both photons are combined on a beam splitter in a Hong-Ou-Mandel configuration [3], then the rate of coincidences between the counts of two single-photon detectors placed at the output ports depends on the odd-order dispersion terms only when observed as a function of the path difference between the two arms before the beam splitter. The detrimental effect of even-order dispersion (such as group velocity dispersion), which leads to the wave packet broadening, is canceled. This has been exploited in several applications such as the measurement of photon traveling time trough a material [4], and improving the accuracy of remote clock synchronization [5]. Optical coherence tomography [6,7] has also benefited from this nonclassical effect. This quantum effect has inspired recent developments of classical nonlinear optical systems mimicking dispersion cancellation [8,9].

The wave vector of a monochromatic wave at a given frequency Ω has a bidimensional transverse wave vector $\mathbf{q}$ (in the plane orthogonal to the propagation direction) and a longitudinal component $\kappa(\mathbf{q},\Omega)=\sqrt{[n^2(\Omega)\Omega^2/c^2]-|\mathbf{q}|^2}$. In parametric down-conversion with a plane-wave pump, momentum conservation leads to anticorrelation of the transverse wave vector components [10]. This analogy with frequency anticorrelation [11] suggests the existence of a spatial counterpart to dispersion cancellation. However, no experimental observation of a spatial dispersion-cancellation effect has been reported so far.

The longitudinal component of the wave vector, on the other hand, sets up the phase-matching relation that establishes conditions for an effective energy conversion between three interacting waves, pump, signal, and idler. Since the longitudinal wave vector depends both on frequency and on transverse momentum, this condition sets a specific relation between the frequency and the emission angle of down-converted radiation. In other words, the frequency and transverse momentum degrees of freedom cannot be factorized and the overall quantum state is concurrently entangled in both ω and $\mathbf{q}$ (multiparameter entanglement). This leads to several interesting effects where the manipulation of a spatial variable affects the shape of the temporal interference pattern and also polarization interference pattern [12] .

In this Letter, we exploit the multiparameter entangled states generated by SPDC to demonstrate the effect of even-order spatial aberration cancellation. We use an SPDC source to produce momentum-anticorrelated photons and we modulate their wave fronts by a transfer function $H(\mathbf{q})$. Because of the correlations between $\mathbf{q}$ and ω, the manipulation in the $\mathbf{q}$ space will introduce changes in the ω space. Therefore the spatial wave front modulation will affect the temporal interference pattern, which can be observed using a polarization two-photon interferometer [12,13]. With this technique we show that, due to the anticorrelation of the transverse momenta, the even-order aberrations are canceled out, and only the odd-order contributions influence the resulting interference pattern. We believe this effect may lead to interesting applications in the field of quantum imaging.

The setup of our experiment is sketched in Fig. 1. A laser diode with a single longitudinal-mode selection (405 nm, 35 mW) pumps a 1.5-mm thick BBO (BaB_2O_4) crystal that is cut for a collinear degenerate type-II phase matching. Approximating the pump beam with a plane wave, the two orthogonally polarized photons emitted by the crystal can be described by the quantum state [10]:

$$|\psi\rangle = \int d\mathbf{q} \int d\omega \xi(\mathbf{q}, \omega) \hat{a}_H^\dagger(\mathbf{q}, \Omega_0 + \omega) \times \hat{a}_V^\dagger(-\mathbf{q}, \Omega_0 - \omega)|0\rangle, \quad (1)$$

where

$$\xi(\mathbf{q}, \omega) = \mathrm{sinc}\left[\frac{L\Delta(\mathbf{q}, \omega)}{2}\right] e^{i(L\Delta(\mathbf{q},\omega)/2)}. \quad (2)$$

The phase-mismatch function $\Delta(\mathbf{q}, \omega)$ in the paraxial approximation takes the form

$$\Delta(\mathbf{q}, \omega) = -\omega D + M\hat{\mathbf{e}}_2 \cdot \mathbf{q} + \frac{2|\mathbf{q}|^2}{k_p}, \quad (3)$$

where D is the difference between the inverse of the group velocities of the ordinary and the extraordinary waves inside the birefringent crystal and M is their spatial walk-off in the vertical direction $\hat{\mathbf{e}}_2$. The term $\frac{2|q|^2}{k_p}$ is due to diffraction during the propagation of photons through the crystal. In case of a BBO crystal, phase-matched for a degenerate ($\lambda_0 = 810$ nm) collinear type-II down-conversion, $D = 182$ ps/mm and $M = 0.0723$.

A polarizing beam splitter (PBS) separates the horizontally polarized photon and the vertically polarized one into two distinct paths, one towards a flat mirror (FM) and the other towards a deformable mirror (DM). Each photon passes through a 4-f system comprising a lens (L1) of focal length $f = 200$ mm positioned at a distance f from the output plane of the crystal, and the same distance f from the mirror. On the way from the crystal to the mirror, the lens maps each wave vector component to a different point $\mathbf{x}(\mathbf{q}, \omega)$ on the mirror surface. The limited down-conversion bandwidth (about 30 nm for a collection angle of 25 mrad) allows us to neglect the frequency dependence of the 4-f system; assuming that the lens is achromatic:

$$\mathbf{x}(\mathbf{q}, \omega) = \frac{f}{k(\omega)}\mathbf{q} \approx \frac{f}{k_o}\mathbf{q}. \quad (4)$$

The deformation of the mirror surface at point $\mathbf{x}$ can be described by the function $\zeta(\mathbf{x})$. A photon focused to the point $\mathbf{x}$ by the lens will travel a distance $\zeta(\mathbf{x})$ to the mirror surface, will be reflected and will travel a distance $\zeta(\mathbf{x})$ back to the lens focal plane. Therefore it will acquire a phase shift:

$$\varphi(\mathbf{x}) \approx 2k_o\zeta(\mathbf{x}). \quad (5)$$

After reflection from the mirror, the same lens maps every point back to a wave vector. Mathematically, the transformation induced by the 4-f system can be described by the transfer function:

$$H(\mathbf{q}) = p\left(\frac{f}{k}\mathbf{q}\right) e^{i\varphi[(f/k_o)\mathbf{q}]}, \quad (6)$$

where the pupil function $p(\mathbf{x})$ describes the circular aperture of the mirror.

The deformable mirror [14] consists of a thin nitrocellulose silver-coated membrane (12 mm diameter, 5 μm thick, initial flatness less than 20 nm rms) that is deformed by electrostatic forces created when a voltage drop (maximum 270 V) is applied to 37 electrodes. The action produced by each actuator was mapped by measuring the induced deformation with a Zygo interferometer, creating an influence function matrix.

In addition, each photon, traveling from the PBS to the mirror and back passes twice through a quarter-wave-plate oriented at 45° and flips its polarization state. This way the photon that has been transmitted is now reflected at the polarizing beam splitter (PBS) and vice versa, resulting in both photons leaving the modulation section together towards the polarization interferometer.

The polarization interferometer [13,15] consists of a birefringent delay line (DL, made of two sliding quartz wedges) providing a variable delay τ and a nonpolarizing beam splitter (BS) that splits the photons in two paths directed to two single-photon detectors D_1 and D_2. A polarizer oriented at 45° is placed in front of each detector in order to erase information about the polarization of the incoming photon. Photons were collected by a lens in each arm and focused onto the detector's active area. To maximize the spatial collection capability we used two open-

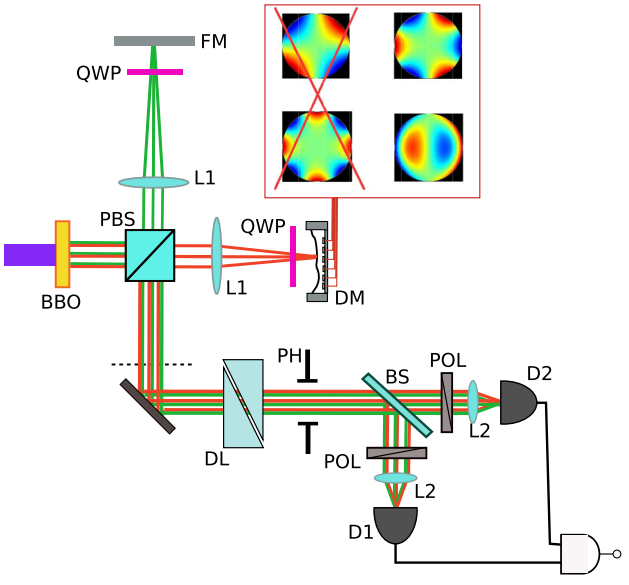

FIG. 1 (color online). Schematic of the experimental setup. Examples of aberrations induced by the deformable mirror are illustrated in the inset: the even-parity aberrations on the left are canceled, while the odd-parity ones on the right alter the shape of the interference pattern.

face (180 μm diameter) single-photon silicon avalanche photodiodes. Using a fiber coupler would limit the number of collected spatial modes. All experiments have been performed with an 8-mm diameter pinhole placed at 330 mm from the output plane of the 4-f system, therefore collecting photons from an angle of about 25 mrad. A dichroic mirror and a pair of interference bandpass filters with a bandwidth that is greater than that of down-conversion have been used to reject the residual pump radiation and the background light. The number of coincidences acquired as a function of optical polarization delay τ shows a high-visibility quantum interference pattern in the form of a dip [12].

Since the photon-counting detectors are slow, compared with the coherence time of down-converted photons, and since their surface is larger than the spot size, the expression for the coincidence rate, in the paraxial approximation, is [16]

$$R_C(\tau) = R_0\left[1 - \Lambda\left(1 - \frac{2\tau}{DL}\right)W_M(\tau)\right], \tag{7}$$

where R_0 is the background coincidence rate, $\Lambda(\alpha)$ is a triangular function [$\Lambda(\alpha) = 1 - |\alpha|$ if $|\alpha| < 1$, and $\Lambda(\alpha) = 0$, otherwise], and

$$W_M(\tau) = \int d\mathbf{q}d\mathbf{q}' e^{i(2d_1/k_p)[|\mathbf{q}|^2 - |\mathbf{q}'|^2]}\tilde{P}_A[\mathbf{q} + \mathbf{q}']\mathrm{sinc}\left[ML\hat{\mathbf{e}}_2 \cdot (\mathbf{q} + \mathbf{q}')\Lambda\left(1 - \frac{2\tau}{DL}\right)\right] \times H\left(\frac{f}{k}\mathbf{q}\right)H^*\left(\frac{f}{k}\mathbf{q}'\right)e^{-i(M/D)\tau\hat{\mathbf{e}}_2\cdot(\mathbf{q}-\mathbf{q}')}. \tag{8}$$

The function $\Lambda(1 - \frac{2\tau}{DL})$ represents a usual triangular dip one obtains in type-II quantum interferometry when working in the single spatial-mode approximation (using narrow pinholes). The function $W_M(\tau)$ takes into account the deformation of the triangular dip induced by the modulation of the transverse wave vectors and the Fourier transform of the shape of the detection apertures $\tilde{P}_A[\mathbf{q}]$. In particular, the function $W_M(\tau)$ describes how manipulation in the $\mathbf{q}$ space by a filter $H(\mathbf{q})$ is converted into a modification of the temporal interference pattern, by means of the coupling between wave vectors and frequencies set by the phase-matching conditions.

If the detection apertures are sufficiently large, the function $\tilde{P}_A[\mathbf{q} + \mathbf{q}']$ can be well approximated by a delta function, so that Eq. (8) can be simplified to

$$W_M^{R\to\infty}(\tau) = \int d\mathbf{q}H^*\left(\frac{f}{k_0}\mathbf{q}\right)H\left(-\frac{f}{k_0}\mathbf{q}\right)e^{i(2Mk_0/fD)\tau\hat{\mathbf{e}}_2\cdot\mathbf{q}}. \tag{9}$$

If the function $H(\mathbf{q})$ has a circular symmetry, its phase $\varphi(\mathbf{q}) = \arg\{H(\mathbf{q})\}$ can be expanded using a set of Zernike polynomials, which are orthogonal on the unit circle [17],

$$\varphi(\mathbf{q}) = \sum_n \sum_m \varphi_{nm} R_n^m(\rho)\cos(m\theta), \tag{10}$$

where $\mathbf{q} = (\rho\cos\theta, \rho\sin\theta)$ and $m = -n, -n+2, -n+4, \ldots, n$. Using the fact that $-\mathbf{q} = [\rho\cos(\theta + \pi), \rho\sin(\theta + \pi)]$, and that if m is even, then $\cos[m(\theta + \pi)] = \cos(m\theta)$, while if m is odd, then $\cos[m(\theta + \pi)] = -\cos(m\theta)$, one gets

$$\varphi(\mathbf{q}) - \varphi(-\mathbf{q}) = 2\sum_n \sum_{m\ odd} \varphi_{nm} R_n^m(\rho)\cos(m\theta). \tag{11}$$

This means that only Zernike polynomials with m odd (and consequently n odd) will contribute to the shape of the interference pattern. For example, contributions from astigmatism ($n = 2$, $m = \pm 2$), defocus ($n = 2$, $m = 0$), and spherical aberration ($n = 4$, $m = 0$) will all be canceled. On the contrary, coma ($n = 3$, $m = \pm 1$) and trefoil ($n = 3$, $m = \pm 3$) will be present.

We studied different types of aberrations: coma along the x axis ($n = 3$, $m = +1$), coma along the y axis ($n = 3$, $m = -1$), astigmatism ($n = 2$, $m = 2$), and the aberration corresponding to $n = 4$ and $m = 4$. The experimental data for coma oriented along the x and y (parallel to the vertical-polarization) directions are presented in Fig. 2. Because of the multiparameter entanglement of the two-photon state, the wave front distortion induced by the deformable mirror modulates the spectral degree of freedom, resulting in a modification of the temporal interference pattern. We increased the maximum amplitude of the mirror deformation from 0.2 μm ($\sim 0.25\lambda_0$) to 0.75 μm ($\sim\lambda_0$) (peak-to valley deformation) for coma along x and from 0.2 μm to 0.4 μm ($\sim 0.5\lambda_0$) for coma along y axis. The shape of the interference pattern is changed dramatically when the intensity of the coma aberration increases. Theoretical predictions (solid lines) based on the experimental parame-

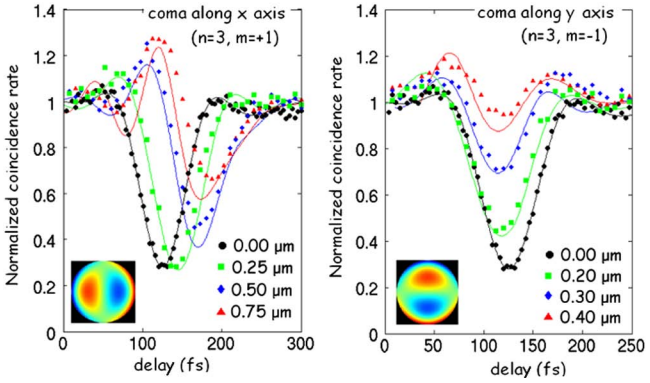

FIG. 2 (color online). Coincidence-rate interference patterns when coma ($n = 3$, $m = \pm 1$) along the x axis (on the left) and along the y axis (on the right) is imposed on the deformable mirror. Solid lines illustrate theoretical fitting with experimental parameters. The initial relative tilt between the deformable mirror (DM) and the flat mirror (FM) is used as an adjustable parameter to account for the imperfectness of experimental alignment between two arms. The shapes of adaptive mirror deformation producing selected aberrations are illustrated in the insets.

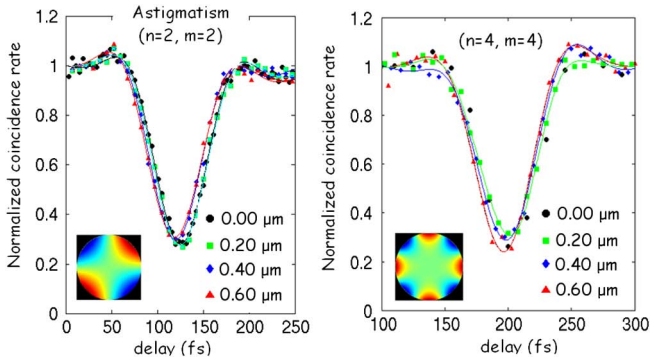

FIG. 3 (color online). Interference patterns in the coincidence rate when astigmatism at 45° (left picture) and the aberration described by $n = 4$, $m = 4$ are dialed on the mirror. The intensity of the aberrations has been scanned from 0.2 to 0.8 μm peak-to-valley deformation. The interference pattern is insensitive to the aberrations within experimental errors.

ters are superposed to experimental data in Fig. 2: the matching between the two curves is pretty good.

Experimentally obtained data for astigmatism (with symmetry axes oriented at 45° with respect to the x-y axes) and for the aberration identified by $n = 4$ and $m = 4$ are shown in Fig. 3. The effect of these even-order aberrations is effectively canceled out due to the spatial correlations between the photons in parametric down-conversion. Therefore, such type of spatial aberrations do not affect the shape of the dip so that the known quantum interference pattern is retained.

This effect has a clear analogy with even-order frequency dispersion cancellation due to frequency entanglement in SPDC. In case of spectral dispersion, the use of a nonmonochromatic pump reduces the degree of correlation between spectral components of entangled photons and degrades the dispersion cancellation effect. In our case of even-order aberration cancellation, sharp spatial correlations can be obtained only in the approximation of a plane-wave pump beam. Therefore, wave vector correlations get weaker for focused pump beams and the aberration cancellation effect also degrades when the pump beam is focused tightly on the crystal. Furthermore, the spectral dispersion cancellation effect works in the limit of slow detectors because it requires integration over the temporal degree of freedom. Similarly, the even-order aberration cancellation works well only in the situation when the collection apertures used in experiment are sufficiently large to enable effective integration over the spatial degrees of freedom [16].

The question remains whether the effect we have reported is purely quantum, or some classical counterpart can be envisioned, as in the case of spectral dispersion cancellation. We believe that a classical optical configuration mimicking even-order aberration cancellation could potentially be discovered by exploiting a light source with strong degree of spatial intensity correlation similar to optical speckles.

In conclusion, we have demonstrated experimentally the effect of cancelling even-order spatial aberration in quantum interferometry using entangled-photon states generated in a type-II spontaneous parametric down-conversion process. This effect may prove helpful in enhancing the spatial resolution in quantum imaging.

This work was supported by a U.S. Army Research Office (ARO) Multidisciplinary University Research Initiative (MURI) Grant; by the Bernard M. Gordon Center for Subsurface Sensing and Imaging Systems (CenSSIS), an NSF Engineering Research Center; by the Intelligence Advanced Research Projects Activity (IARPA), ARO through Grant No. W911NF-07-1-0629 and DEI-UniPD QUINTET project. C. B. also acknowledges financial support from Fondazione CARIPARO.

[1] J. D. Franson, Phys. Rev. A **45**, 3126 (1992).
[2] A. M. Steinberg, P. G. Kwiat, and R. Y. Chiao, Phys. Rev. A **45**, 6659 (1992).
[3] C. K. Hong, Z. Y. Ou, and L. Mandel, Phys. Rev. Lett. **59**, 2044 (1987).
[4] A. M. Steinberg, P. G. Kwiat, and R. Y. Chiao, Phys. Rev. Lett. **68**, 2421 (1992).
[5] V. Giovannetti, S. Lloyd, L. Maccone, and F. N. C. Wong, Phys. Rev. Lett. **87**, 117902 (2001).
[6] A. F. Abouraddy, M. B. Nasr, B. E. A. Saleh, A. V. Sergienko, and M. C. Teich, Phys. Rev. A **65**, 053817 (2002).
[7] M. B. Nasr, B. E. A. Saleh, A. V. Sergienko, and M. C. Teich, Phys. Rev. Lett. **91**, 083601 (2003).
[8] K. J. Resch, P. Puvanathasan, J. S. Lunden, M. W. Mitchell, and K. Bizheva, Opt. Express **15**, 8797 (2007).
[9] B. I. Erkmen and J. H. Shapiro, Phys. Rev. A **74**, 041601 (R) (2006).
[10] M. H. Rubin, Phys. Rev. A **54**, 5349 (1996).
[11] B. E. A. Saleh, A. F. Abouraddy, A. V. Sergienko, and M. C. Teich, Phys. Rev. A **62**, 043816 (2000).
[12] M. Atature, G. DiGiuseppe, M. D. Shaw, A. V. Sergienko, B. E. A. Saleh, and M. C. Teich, Phys. Rev. A **66**, 023822 (2002).
[13] Y. H. Shih, A. V. Sergienko, M. H. Rubin, T. E. Kiess, and C. O. Alley, Phys. Rev. A **50**, 23 (1994).
[14] S. Bonora, I. Capraro, L. Poletto, M. Romanin, C. Trestino, and P. Villoresi, Rev. Sci. Instrum. **77**, 093102 (2006).
[15] M. H. Rubin, D. N. Klyshko, Y. H. Shih, and A. V. Sergienko, Phys. Rev. A **50**, 5122 (1994).
[16] C. Bonato, A. V. Sergienko, and P. Villoresi, arXiv:0810.0932.
[17] M. Born and E. Wolf, *Principles of Optics* (Cambridge University Press, Cambridge, U.K., 1999).

Multiparameter entangled-state engineering using adaptive optics

Cristian Bonato,[1,2] David Simon,[1] Paolo Villoresi,[2] and Alexander V. Sergienko[1,3]
[1]*Department of Electrical and Computer Engineering, Boston University, Boston, Massachusetts 02215, USA*
[2]*Department of Information Engineering, CNR-INFM LUXOR, University of Padova, 35131 Padova, Italy*
[3]*Department of Physics, Boston University, Boston, Massachusetts, USA*
(Received 5 April 2009; published 5 June 2009)

We investigate how quantum coincidence interferometry is affected by a controllable manipulation of transverse wave vectors in type-II parametric down-conversion using adaptive optics techniques. In particular, we discuss the possibility of spatial walk-off compensation in quantum interferometry and an effect of even-order spatial aberration cancellation.

DOI: 10.1103/PhysRevA.79.062304 PACS number(s): 03.67.Bg, 42.50.St, 42.50.Dv, 42.30.Kq

I. INTRODUCTION

Quantum entanglement [1] is a valuable resource in many areas of quantum optics and quantum information processing. One of the most widespread techniques for generating entangled optical states is spontaneous parametric down-conversion (SPDC) [2–5]. SPDC is a second-order nonlinear optical process in which a pump photon is split into a pair of new photons with conservation of energy and momentum. The phase-matching relation establishes conditions to have efficient energy conversion between the pump and the down-converted waves, called signal and idler. This condition also sets a specific relation between the frequency and the emission angle of down-converted radiation. In other words, the quantum state emitted in the SPDC process cannot be factorized into separate frequency and wave-vector components. This leads to several interesting effects where the manipulation of a spatial variable affects the shape of the polarization-temporal interference pattern. For example, the dependence of polarization-temporal interference on the selection of collected wave vectors was studied in detail in [6].

Here we engineer the quantum state in the space of transverse momentum and we study how this spatial modulation is transferred to the polarization-spectral domain by means of quantum interferometry. We will focus on type-II SPDC using birefringent phase matching since the correlations between wave vectors and spectrum are stronger than those employing other phase-matching conditions.

Our aim is twofold. From one point of view, we study the effect of spatial modulations on temporal quantum interference. This could be useful, for example, in quantum optical coherence tomography (QOCT) [7,8]. When focusing light on a sample with nonplanar surface, the photons will acquire a spatial phase distribution in the far field, which may perturb the shape of the interference dip. Our results will provide a tool to understand this effect.

From a second point of view, we would like to study and characterize spatial modulation as a tool for quantum state engineering. This may find application in the field of quantum information processing, where it is important to gain a high degree of control over the production of quantum entangled states entangled in one or more degrees of freedom (hyperentanglement).

We start by introducing a theoretical model of a type-II quantum interferometer, comprising the polarization, spectral, and spatial degrees of freedom (Sec. II). A modulation in the wave-vector space is provided by an adaptive optical setup and equations for the polarization-temporal interference pattern in the coincidence rate are derived. In Sec. III, we introduce a numerical approach for practical evaluation of the results of the theoretical model, discussing a few examples for general spatial aberrations.

In Sec. IV we will highlight and discuss theoretically two interesting special cases. The first one is the possibility of restoring high visibility in type-II quantum interference with large collection apertures. In some situations, to collect a higher photon flux or a broader photon bandwidth, it can be useful to enlarge the collection apertures of the optical system. But when dealing with type-II SPDC in birefringent crystals, for large collection apertures the effect of spatial walkoff introduces distinguishability between the photons, leading to a reduced visibility of temporal and polarization quantum interference. We will show that high visibility can be restored with a linear phase shift along the vertical axis.

The second effect is the spatial counterpart of spectral dispersion cancellation [9,10]. In the limit of large detection apertures, the correlations between the photons' momenta will cancel out the effects of even-order aberrations, exactly as in the limit of slow detectors the frequency correlations cancel out the even-order terms of spectral dispersion. The experimental demonstration of this effect has been reported recently [11].

As we proceed from the general case of Secs. II and III into the specific examples of Sec. IV, we will gradually see that optical aberration is a subject with two very different faces. On one hand, aberrations in optical components are normally seen as undesirable, since they lead to distortions in imaging. We will see that these unwanted spatial modulations may to some extent be canceled. On the other hand, we will find that such spatial modulations may also be turned into a useful tool: by *deliberately* introducing spatial modulations (in effect, purposely adding aberrations in a controlled manner), we can produce useful effects such as the restoration of visibility mentioned above. The examples we provide in Sec. IV will illustrate these two aspects and will show that both can benefit from more detailed study of the interplay between spatial modulations and spectral correlations.

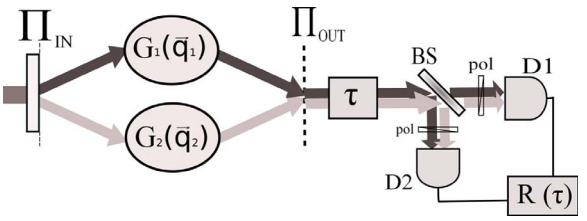

FIG. 1. (Color online) Scheme of the proposed setup. Horizontally polarized photons from type-II SPDC are assigned a phase dependent on the photon transverse momentum $\phi_o(q_o)$, while the vertically polarized ones are assigned a phase $\phi_e(q_e)$. The modulated photons enter a type-II quantum interferometer, which records the coincidence count rate as a function of the delay τ between the photons given by an appropriate delay line.

II. THEORETICAL MODEL

Consider the scheme in Fig. 1. A laser beam pumps a $\chi^{(2)}$ nonlinear material phase matched for type-II parametric down-conversion, creating a pair of entangled photons. Each of the generated photons passes through a Fourier-transform system, and then enters a modulation system which transforms transverse wave vectors for the horizontally (H) polarized photon according to the transfer function $G_1(\mathbf{q}_1)$ and for the vertically (V) polarized photon according to $G_2(\mathbf{q}_2)$. After being modulated in q space, the photons enter a type-II interferometer. A nonpolarizing beam splitter (BS) creates polarization entanglement from the polarization-correlated pair emitted by the source. The beams at the output ports of the beam splitter are directed toward two single-photon detectors. Two polarizers at 45° before the BS restore indistinguishability in the polarization degree of freedom. An adjustable delay line τ is scanned and the coincidence rate $R(\tau)$ between the detection events of the two detectors is recorded. An aperture is placed before the beam splitter to select an appropriate collection angle.

A. Notation

Consider a monochromatic plane wave of complex amplitude $E(\mathbf{r})=E_0e^{-i\mathbf{k}\cdot\mathbf{r}}$, with $\mathbf{r}=(x,y,z)$. For a given wavelength λ, corresponding to a frequency Ω, the wave vector can be split into a transverse component $\mathbf{q}=(q_x,q_y)$ and a longitudinal component $\beta(\mathbf{q};\Omega)$:

$$\mathbf{k}=[\mathbf{q},\beta(\mathbf{q};\Omega)]. \tag{1}$$

The wave number is

$$k(\Omega)=\frac{n(\Omega)\Omega}{c}. \tag{2}$$

The longitudinal component of the wave vector is

$$\beta(\mathbf{q},\Omega)=\sqrt{k^2(\Omega)-|\mathbf{q}|^2}. \tag{3}$$

Therefore the electric field at the position $\mathbf{r}$ and time t can be written as

$$E(\mathbf{r};t)=\int d\mathbf{q}\int d\Omega\tilde{E}(\mathbf{q},\Omega)e^{-i\mathbf{q}\cdot\boldsymbol{\rho}}e^{-i\beta(\mathbf{q};\Omega)z}e^{i\Omega t}, \tag{4}$$

where $\rho=(x,y)$.

In paraxial approximation $|\mathbf{q}|^2\ll k^2(\Omega)$, so that

$$\beta(\mathbf{q},\Omega)\approx k(\Omega)-\frac{|\mathbf{q}|^2}{2k(\Omega)}. \tag{5}$$

For a quasimonochromatic wave packet centered around the frequency Ω_0, one can write $\Omega=\Omega_0+\nu$, with $\nu\ll\Omega_0$. This expression can be approximated by

$$\beta(\mathbf{q},\Omega)\approx k_0+\frac{\nu}{u_0}-\frac{|\mathbf{q}|^2}{2k_0}, \tag{6}$$

where $k_0=k(\Omega_0)$ and $u_0=(\frac{dk(\Omega)}{d\Omega}|_{\Omega=\Omega_0})^{-1}$ is the group velocity for the propagation of the wave packet through the material.

B. State generation

Using first-order time-dependent perturbation theory, the two-photon state at the output of the nonlinear crystal can be calculated as

$$|\psi\rangle\sim-\frac{i}{\hbar}\int dtH_I(t)|0\rangle, \tag{7}$$

where the interaction Hamiltonian is

$$H_I(t)=\frac{1}{V}\int d\mathbf{r}\chi^{(2)}(\mathbf{r})E_p^{(+)}(\mathbf{r},t)E_s^{(-)}(\mathbf{r},t)E_i^{(-)}(\mathbf{r},t). \tag{8}$$

The strong, undepleted pump beam can be treated classically. Assuming a monochromatic plane wave propagating along the z direction,

$$E_p(\mathbf{r},t)=E_pe^{i(k_pz-\omega_pt)}. \tag{9}$$

The signal and idler photons are described by the following quantum field operators:

$$\hat{E}_j^{(-)}(\mathbf{r},t)=\int d\mathbf{q}_j\int d\omega_je^{i[\beta(\mathbf{q}_j,\omega_j)z+\mathbf{q}_j\cdot\boldsymbol{\rho}-\omega_jt]}\hat{a}(\mathbf{q}_j,\omega_j), \tag{10}$$

where $j=e,o$.

The biphoton quantum state at the output plane of the nonlinear crystal is [12]

$$|\psi\rangle=\int d\mathbf{q}\int d\nu\tilde{\Phi}(\mathbf{q},\nu)\hat{a}_o^\dagger(\mathbf{q},\Omega_0+\nu)\hat{a}_e^\dagger(-q,\Omega_0-\nu)|0\rangle. \tag{11}$$

Two photons are emitted from the nonlinear crystal, one horizontally polarized (ordinary photon) and the other vertically polarized (extraordinary photon), with anticorrelated frequencies and emission directions.

In the case of a single bulk crystal of thickness L and constant nonlinearity χ_o, the probability amplitude for having the signal photon in the mode $(\mathbf{q},\Omega_0+\nu)$ and the idler in the mode $(-\mathbf{q},\Omega_0-\nu)$ is

$$\tilde{\Phi}(\mathbf{q},\nu)=\mathrm{sinc}\left[\frac{L\Delta(\mathbf{q},\nu)}{2}\right]e^{i[\Delta(\mathbf{q},\nu)L/2]}. \tag{12}$$

For type-II collinear degenerate phase matching, the phase-mismatch function $\Delta(\mathbf{q},\nu)$ can be approximated to be

$$\Delta(\mathbf{q},\nu) = -\nu D + M\hat{\mathbf{e}}_2 \cdot \mathbf{q} + \frac{2|\mathbf{q}|^2}{k_p}, \tag{13}$$

where D is the difference between the inverse of the group velocities of the ordinary and extraordinary photons inside the birefringent crystal and the quadratic term in $\mathbf{q}$ is due to diffraction in paraxial approximation. The remaining term is the first-order approximation for the spatial walkoff.

C. Propagation

Consider a photon described by the operator $\hat{a}_j(\mathbf{q},\Omega)$ (polarization $j=e,o$, frequency Ω, and transverse momentum $\mathbf{q}$). Its propagation through an optical system to a point $\mathbf{x}_k$ on the output plane is described by the optical transfer function $H_j(\mathbf{x}_k,\mathbf{q};\Omega)$. In our setup, the field at the detector will be a superposition of contributions from the ordinary and extraordinary photons. The quantized electric fields at the detector planes are

$$\hat{E}_A^{(+)}(\mathbf{x}_A,t_A) = \int d\mathbf{q} \int d\omega e^{i\omega t_A}[H_e(\mathbf{x}_A,\mathbf{q};\omega)\hat{a}_e(\mathbf{q},\omega) + H_o(\mathbf{x}_A,\mathbf{q};\omega)\hat{a}_o(\mathbf{q},\omega)],$$

$$\hat{E}_B^{(+)}(\mathbf{x}_B,t_B) = \int d\mathbf{q} \int d\omega e^{i\omega t_B}[H_e(\mathbf{x}_B,\mathbf{q};\omega)\hat{a}_e(\mathbf{q},\omega) + H_o(\mathbf{x}_B,\mathbf{q};\omega)\hat{a}_o(\mathbf{q},\omega)]. \tag{14}$$

The probability amplitude for detecting a photon pair at the detector planes, with space-time coordinates $(\mathbf{x}_A,t_A)$ and $(\mathbf{x}_B,t_B)$, is

$$A(\mathbf{x}_A,\mathbf{x}_B;t_A,t_B) = \langle 0|\hat{E}_A^{(+)}(\mathbf{x}_A,t_A)\hat{E}_B^{(+)}(\mathbf{x}_B,t_B)|\psi\rangle. \tag{15}$$

For the biphoton probability amplitude we get

$$A(\mathbf{x}_A,\mathbf{x}_B;t_A,t_B) = \int d\mathbf{q}_o d\mathbf{q}_e d\omega_o d\omega_e \Phi(\mathbf{q}_o,\mathbf{q}_e;\omega_o,\omega_e) \times [H_e(\mathbf{x}_A,\mathbf{q}_e;\omega_e)H_o(\mathbf{x}_B,\mathbf{q}_o;\omega_o)e^{-i(\omega_e t_A+\omega_o t_B)} + H_o(\mathbf{x}_A,\mathbf{q}_o;\omega_o)H_e(\mathbf{x}_B,\mathbf{q}_e;\omega_e)e^{-i(\omega_o t_A+\omega_e t_B)}]. \tag{16}$$

This probability amplitude represents the superposition of two possible events leading to a coincidence count in the detectors:

(1) the V polarized photon with momentum $\mathbf{q}_e$ and frequency ω_e going through the lower branch to arrive at position x_A in detector A, while the H polarized photon with momentum $\mathbf{q}_o$ and frequency ω_o goes through the upper branch to arrive at position x_B in detector B; and

(2) the V polarized photon with momentum $\mathbf{q}_e$ and frequency ω_e going through the lower branch to arrive at position x_B in detector B, while the H polarized photon with momentum $\mathbf{q}_o$ and frequency ω_o goes through the upper branch to arrive at position x_A in detector A.

Since the superposition is coherent, there are quantum-interference effects between the two probability amplitudes.

1. State engineering section

In the state engineering section, each of the two branches consists of a pair of achromatic Fourier-transform systems coupled by a spatial light modulator or a deformable mirror. Each Fourier-transform system consists of a single lens of focal length f, separated from the optical elements before and after it by a distance f. The first Fourier system maps each incident transverse wave vector $\mathbf{q}$ on the plane Π_{in} to a point $\mathbf{x}(\mathbf{q})$ on the Fourier plane Π_F:

$$\mathbf{x}(\mathbf{q}) = \frac{f}{k_0}\mathbf{q}, \quad k_0 = \frac{\Omega_0}{c}, \tag{17}$$

where f is the focal length of the Fourier-transform system. Since we assume that the system is achromatic for a certain bandwidth around a central frequency Ω_0, the position $\mathbf{x}(\mathbf{q})$ depends only on $\mathbf{q}$ and not on ω.

The spatial modulator assigns a different amplitude and phase to the light incident on each point, as described by the function $G(\mathbf{x})=t(\mathbf{x})e^{i\varphi(\mathbf{x})}$. Each point is then mapped back to a wave vector on the plane Π_{out} by the second achromatic Fourier-transform system.

Using the formalism of Fourier optics [13], the transfer function between the planes Π_{in} and Π_{out} can be calculated to be

$$h_1(\mathbf{x_1},\mathbf{x_3}) = \int d\mathbf{x} G(\mathbf{x}) e^{-i(k_0/f)\mathbf{x}\cdot(\mathbf{x_1}+\mathbf{x_3})}. \tag{18}$$

The corresponding momentum-transfer function is

$$H_1(\mathbf{q_1},\mathbf{q_3}) = G\left[\frac{f}{k_0}\mathbf{q_1}\right]\delta(\mathbf{q_1}-\mathbf{q_3}). \tag{19}$$

2. Interferometer

After the plane Π_{out} the two photons enter a type-II quantum interferometer. Each propagates in free space to a birefringent delay line and a detection aperture $p(\mathbf{x})$ to be finally focused to the detection planes by means of lenses of focal length f_0. Following the derivation in [6] the transfer function is

$$H_2(\mathbf{x_i},\mathbf{q};\omega) = \int h(\mathbf{x_1},\mathbf{x_i};\omega)e^{i\mathbf{q}\cdot\mathbf{x_1}}d\mathbf{x}_1 = e^{i(\omega/c)(d_1+d_2+f_0)}\exp\left[-i\frac{\omega|\mathbf{x_i}|^2}{2cf_0}\left(\frac{d_2}{f_0}-1\right)\right] \times e^{-i(cd_1/2\omega)|\mathbf{q}|^2}\tilde{P}\left(\frac{\omega}{cf_0}\mathbf{x_i}-\mathbf{q}\right), \tag{20}$$

where $\tilde{P}(\mathbf{q})$ is the Fourier transform of $|p(\mathbf{x})|^2$.

A combination of the two different stages is described by the transfer function

$$H_\alpha(\mathbf{x_j},\mathbf{q}_\alpha;\omega_\alpha) = G_\alpha\left[\frac{f}{k_0}\mathbf{q}_\alpha\right]H_2(\mathbf{x_j},\mathbf{q}_\alpha;\omega), \tag{21}$$

where the two functions $G_1(\mathbf{q})$ and $G_2(\mathbf{q})$ are the momentum-transfer functions which describe the modulation

imparted, respectively, on the ordinary and the extraordinary photons.

D. Detection

Since the single-photon detectors used in quantum optics experiments are slow with respect to the temporal coherence of the photons and their area is larger than the spot onto which the photons are focused by the collection lens, we integrate over the spatial and temporal coordinates. Therefore the coincidence count rate expressed in terms of the biphoton probability amplitude is

$$R(\tau) = \int d\mathbf{x}_A \int d\mathbf{x}_B \int dt_A \int dt_B |A(\mathbf{x}_A, \mathbf{x}_B; t_A, t_B)|^2. \quad (22)$$

Following the derivation described in Appendix A, one gets

$$R(\tau) = R_0 \left[1 - \Lambda\left(1 - \frac{2\tau}{DL} \right) W_M(\tau) \right], \quad (23)$$

where $\Lambda(x)$ is the triangular function

$$\Lambda(x) = \begin{cases} 1 - |x|, & |x| \le 1 \\ 0, & |x| > 1. \end{cases} \quad (24)$$

Therefore, the coincidence count rate $R(\tau)$ is given by the summation of a background level R_0 and an interference pattern given by the triangular dip $\Lambda(1-\frac{2\tau}{DL})$ that one gets when working with narrow apertures, modulated by the function $W_M(\tau)$ which depends on the details of the adaptive optical system.

The expressions for R_0 and $W_M(\tau)$ are

$$\begin{aligned} R_0 = \int d\mathbf{q} \int d\mathbf{q}' \ & \mathrm{sinc}[ML\hat{\mathbf{e}}_2 \cdot (\mathbf{q} - \mathbf{q}')] \\ & \times G_1^*\left(\frac{f}{k_0}\mathbf{q} \right) G_1\left(\frac{f}{k_0}\mathbf{q}' \right) G_2^*\left(-\frac{f}{k_0}\mathbf{q} \right) \\ & \times G_2\left(-\frac{f}{k_0}\mathbf{q}' \right) e^{-i(ML/2)\hat{\mathbf{e}}_2 \cdot (\mathbf{q}-\mathbf{q}')} e^{i(2d_1/k_p)[|\mathbf{q}|^2 - |\mathbf{q}'|^2]} \\ & \times \tilde{P}_A(\mathbf{q} - \mathbf{q}') \tilde{P}_B(-\mathbf{q} + \mathbf{q}') \end{aligned} \quad (25)$$

and

$$\begin{aligned} W_M(\tau) = \frac{1}{R_0} \int d\mathbf{q} \int d\mathbf{q}' \ & \mathrm{sinc}\left[ML\hat{\mathbf{e}}_2 \cdot (\mathbf{q} + \mathbf{q}') \Lambda \right. \\ & \left. \times \left(1 - \frac{2\tau}{DL} \right) \right] G_1^*\left(\frac{f}{k_0}\mathbf{q} \right) G_1\left(\frac{f}{k_0}\mathbf{q}' \right) G_2^*\left(-\frac{f}{k_0}\mathbf{q} \right) \\ & \times G_2\left(-\frac{f}{k_0}\mathbf{q}' \right) e^{-i(M/D)\tau\hat{\mathbf{e}}_2 \cdot (\mathbf{q}-\mathbf{q}')} e^{i(2d_1/k_p)[|\mathbf{q}|^2 - |\mathbf{q}'|^2]} \\ & \times \tilde{P}_A[\mathbf{q} + \mathbf{q}'] \tilde{P}_B[-(\mathbf{q} + \mathbf{q}')]. \end{aligned} \quad (26)$$

In the following we will assume there is spatial modulation only on one of the photons; therefore we set $G_2(\mathbf{q}) \equiv 1$.

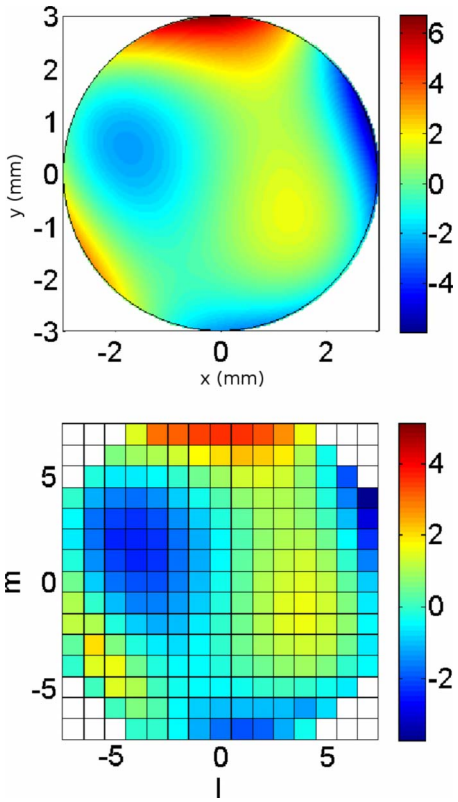

FIG. 2. (Color online) Example of the numerical approach adopted to evaluate Eqs. (25) and (26). The spatial modulation surface is discretized in sufficiently small squares over which the phase is averaged.

III. NUMERICAL SOLUTIONS FOR A GENERAL PHASE SHIFT

Numerically solving for the quantities in Eqs. (25) and (26) in the case of a general aberration may be computationally demanding. Here, we propose an approximation, valid in the case where the function $G(\mathbf{x})$ changes smoothly over the mirror surface, as it is the case in experimentally relevant situations. This model is also interesting from the practical point of view, since in many cases adaptive optical systems are implemented using spatial light modulators or segmented deformable mirrors, where the modulation surface is partitioned into small pixels.

Suppose we partition the Fourier plane Π_F into small squares (pixels) of side d (Fig. 2). Let us define the rectangular function

$$\Pi(\mathbf{x}) = \begin{cases} 0 & \text{if } |\mathbf{x}| > \frac{1}{2} \\ 1 & \text{if } |\mathbf{x}| < \frac{1}{2}. \end{cases} \quad (27)$$

The pixel (l,m) is identified by

$$\sigma_{l,m}(x,y) = \Pi\left[\frac{x}{d} + l \right] \Pi\left[\frac{y}{d} + m \right], \quad (28)$$

selecting the area

$$\left(l - \tfrac{1}{2}\right)d < x < \left(l + \tfrac{1}{2}\right)d,$$

$$\left(m-\tfrac{1}{2}\right)d < y < \left(m+\tfrac{1}{2}\right)d. \tag{29}$$

We approximate the value of the phase in each square by the mean value of the actual phase within the square:

$$\varphi_{lm} = \frac{1}{d^2}\int dxdy\varphi(x,y)\Pi\left[\frac{x}{d}+l\right]\Pi\left[\frac{y}{d}+m\right]. \tag{30}$$

That is,

$$e^{i\varphi(x,y)} \approx \sum_{l,m} e^{i\varphi_{l,m}\Pi[(x/d)+l]\Pi[(y/d)+m]}. \tag{31}$$

In this case (see Appendix B for a justification)

$$\sum_{l,m} e^{i\phi_{l,m}\Pi[(x/d)+l]\Pi[(y/d)+m]} = \sum_{l,m} e^{i\phi_{l,m}}\Pi\left[\frac{x}{d}+l\right]\Pi\left[\frac{y}{d}+m\right]. \tag{32}$$

Substituting this expression into Eq. (23) and collecting the integrations, one finds

$$R(\tau) \approx \sum_{l,m}\sum_{\lambda,\mu} e^{-i\phi_{lm}-\phi_{\lambda,\mu}}\alpha_{l\lambda}I_{m\mu}(\tau), \tag{33}$$

where

$$\alpha_{l\lambda} = \int dq_x \int dQ_x \Pi\left[\frac{f}{kd}q_x - l\right]\Pi\left[\frac{f}{kd}Q_x - \lambda\right]e^{j(2d_1/k_p)(q_x^2-Q_x^2)P[q_x+Q_x]P[-(q_x+Q_x)]} \tag{34}$$

and

$$I_{m,\mu}(\tau) = \int dq_y \int dQ_y \Pi\left[\frac{f}{kd}q_y - m\right]\Pi\left[\frac{f}{kd}Q_y - \mu\right]e^{j(2d_1/k_p)(q_y^2-Q_y^2)}e^{-j(M/D)\tau(q_y-Q_y)}$$
$$\times \mathrm{Sinc}\left[ML(q_y+Q_y)\Lambda\left(1-\frac{2\tau}{DL}\right)\right]P[q_y+Q_y]P[-(q_y+Q_y)]. \tag{35}$$

Performing the integrations one gets

$$\alpha_{l\lambda} = \int dx\tilde{P}(x)\Lambda\left[\frac{fx}{kd}-(l+\lambda)\right]\mathrm{sinc}\left\{\frac{2dd_1}{f}x\Lambda\left[\frac{fx}{kd}-(l+\lambda)\right]\right\}e^{i(dd_1/f)(l-\lambda)x} \tag{36}$$

and

$$I_{m\mu}(\tau) = \int dx\tilde{P}(x)\Lambda\left[\frac{fx}{kd}-(m+\mu)\right]\mathrm{sinc}\left\{MLx\Lambda\left[1-\frac{2\tau}{DL}\right]\right\}$$
$$\times \mathrm{sinc}\left\{\frac{2kd}{f}\left(\frac{2d_1}{k_p}x-\frac{M}{D}\tau\right)\Lambda\left[\frac{fx}{kd}-(m+\mu)\right]\right\}e^{i(kd/f)[(2d_1/k_p)x-(M/D)\tau](m-\mu)}. \tag{37}$$

A similar expression can be found for the background coincidence rate:

$$R_0 \approx \sum_{l,m}\sum_{\lambda,\mu} e^{-i(\phi_{lm}-\phi_{\lambda,\mu})}R_{l\lambda}^{(x)}R_{m\mu}^{(y)}, \tag{38}$$

where

$$R_{l\lambda}^{(x)} = \int dx\tilde{P}(x)\Lambda\left[\frac{fx}{kd}-(l-\lambda)\right]\mathrm{sinc}\left\{\frac{2dd_1}{f}x\Lambda\left[\frac{fx}{kd}-(l-\lambda)\right]\right\}e^{i(dd_1/f)(l+\lambda)x} \tag{39}$$

and

$$R_{m\mu}^{(y)} = \int dx\tilde{P}(x)\Lambda\left[\frac{fx}{kd}-(m-\mu)\right]\mathrm{sinc}(MLx)\mathrm{sinc}\left\{\frac{2dd_1}{f}x\Lambda\left[\frac{fx}{kd}-(m-\mu)\right]\right\}e^{i[(dd_1/f)(m+\mu)-ML/2]x}. \tag{40}$$

The advantage of our numerical approach is that one can calculate and tabulate the functions $R_{l\lambda}^{(x)}$, $R_{m\mu}^{(y)}$, $\alpha_{l\lambda}$, and $I_{m\mu}(\tau)$ for a given configuration, determined by the focal length f, the shape of the detection apertures, the width of the deformable optics, and the distance between the crystal and the detectors. Then, to calculate the shape of the interference pattern for a certain phase distribution on the adaptive optics, one just needs to change the coefficient of a linear combination of the tabulated functions. This can be a helpful tool for studying the effect of specific aberrations on the temporal

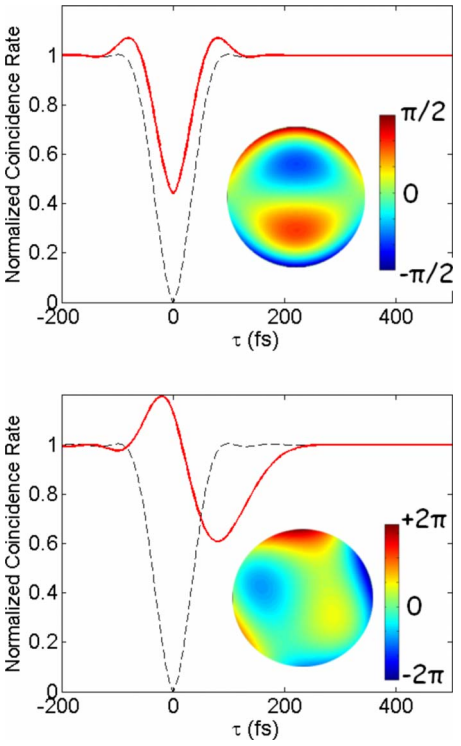

FIG. 3. (Color online) Examples of the shape of the polarization quantum-interference dip with two different spatial phase modulations (in black the unperturbed dip, in red the modulated one). In the upper figure the effect of a small amount of coma along the vertical axis is shown. In the lower figure a more complicated superposition of aberrations affects dramatically the shape of the dip.

interference or to engineer the shape of the Hong-Ou-Mandel (HOM) dip.

Some examples of how the temporal quantum-interference dip is modulated by a generic spatial phase shift are reported in Fig. 3, for coma (upper plot) and a superposition of several different aberrations (lower plot). The interference visibility clearly degrades in presence of wave-front aberrations.

IV. PARTICULAR CASES

In this section we will discuss the quantum-interference pattern, described by Eq. (23), for a few simple cases. First we will consider the case when no spatial modulation is assigned to the photons and Eq. (23) will reduce to the results already described in the literature for quantum interferometry with multiparametric entangled states from type-II down-conversion [6]. Then we will examine the effect of a linear phase, describing its implications for the compensation of the spatial walkoff between the two photons. Finally we will describe what happens in the approximation of sufficiently large detection apertures, introducing the effect of even-order aberration cancellation.

A. No phase modulation

Applying no phase modulation, our equations reduce to the ones derived in [6]. Particularly we find

$$R_0 = \tilde{P}_A(\mathbf{0})\tilde{P}_B(\mathbf{0}) \tag{41}$$

and

$$W_G(\tau) = \mathrm{Sinc}\left[\frac{M^2 L k_p}{2d_1 D}\tau\Lambda\left(1-\frac{2\tau}{DL}\right)\right]\tilde{P}_A \times\left[\frac{Mk_p}{2d_1 D}\tau\hat{\mathbf{e}}_2\right]\tilde{P}_B\left[-\frac{Mk_p}{2d_1 D}\tau\hat{\mathbf{e}}_2\right]. \tag{42}$$

The shape of the interference pattern is essentially given by the product of the triangular function by the Fourier transform of the aperture function, centered at $\tau=0$. For physically relevant parameters the sinc function is almost flat in the region where the triangular function is not zero.

To get an analytic result one may assume Gaussian detection apertures of radius R_G centered along the system's optical axis:

$$p(\mathbf{x}) = e^{-|\mathbf{x}|^2/2R_G^2}. \tag{43}$$

In this case the solution is quite simple:

$$R(\tau) = R_0\left[1-\Lambda\left(1-\frac{2\tau}{DL}\right)e^{-\tau^2/2\tau_1^2}\right], \tag{44}$$

with

$$\tau_1 = \frac{2d_1 D}{k_p M R_G}. \tag{45}$$

Typically, sharp circular apertures are used in experiments. In this case, the function $\tilde{P}[\mathbf{q}]$ is described in terms of the Bessel function $J_1(x)$. For a circular aperture of radius R,

$$\tilde{P}[\mathbf{q}] = \frac{J_1(2R|\mathbf{q}|)}{R|\mathbf{q}|}. \tag{46}$$

However the Gaussian approximation is still a good one if the width R_G of the Gaussian is taken to roughly fit the Bessel function (of width R): in our case we take $R_G = R/(2\sqrt{2})$.

Therefore Eq. (44) is still approximately valid in the case of sharp circular apertures, just taking

$$\tau_1 = \frac{4\sqrt{2}d_1 D}{k_p M R_B}. \tag{47}$$

Mathematically, in Eq. (44) the interference pattern is given by the multiplication of a triangular function centered at $\tau=DL/2$ by a Gaussian function centered at $\tau=0$. The width of the Gaussian function τ_1 decreases with increasing radius of the aperture R_B. Therefore, in the small-aperture approximation, the width of the Gaussian is so large that it is approximately constant between $\tau=0$ and $\tau=DL/2$, giving the typical triangular dip found in quantum-interference experiments. On the other hand, increasing the aperture size, the width of the Gaussian function decreases, reducing the dip visibility (see Fig. 4). Physically, this can be explained by the fact that by increasing the aperture size we let more wave vectors into the system, and so the spatial walkoff in type-II interferometry introduces distinguishability, reducing

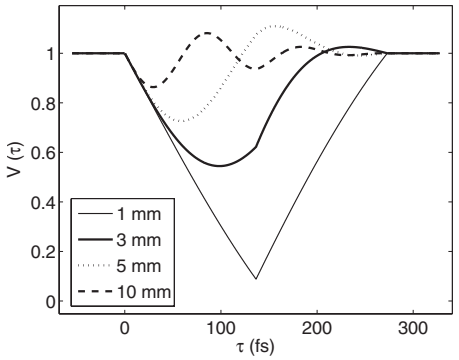

FIG. 4. On the right side we can see the interference patterns with three different detector aperture sizes: the corresponding aperture functions are shown on the left side.

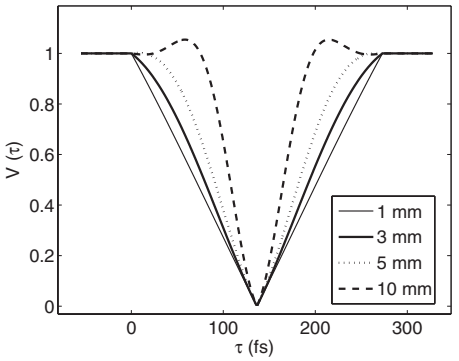

FIG. 5. Quantum-interference pattern for different detector aperture sizes, introducing a linear modulation of the deformable mirror, in order to restore the indistinguishability between the photons, decreased by the spatial walkoff in the generation process.

the interference visibility. Enlarging the aperture sizes is often useful in practice, for example, to get a higher photon flux. Moreover, since in the SPDC process different frequency bands are emitted at different angles, it may be necessary to open the detection aperture in applications where a broader bandwidth is needed. This is clearly a problem when using type-II phase matching in birefringent crystals, since the visibility of temporal and polarization interference gets drastically reduced.

B. Linear phase shift

Suppose now we introduce a linear phase function with the spatial light modulator, along the direction $\mathbf{s}_1$,

$$\varphi(\mathbf{x}) = \mathbf{s_1} \cdot \mathbf{x}, \tag{48}$$

we get

$$W_M(\tau) = \mathrm{Sinc}\left[\frac{M^2 L k_p}{2d_1 D}\tau\Lambda\left(1-\frac{2\tau}{DL}\right)\right]\tilde{P}_A \times\left[\frac{Mk_p}{2d_1 D}\tau\hat{\mathbf{e}}_\mathbf{2}+2f\mathbf{s_1}\right]\tilde{P}_B\left[-\frac{Mk_p}{2d_1 D}\tau\hat{\mathbf{e}}_\mathbf{2}-2f\mathbf{s_1}\right]. \tag{49}$$

If we compare Eq. (49) with Eq. (44) we can see that the structure is the same. We again have a triangular function centered at $\tau = DL/2$, along with two aperture functions. But this time, instead of being centered at $\tau = 0$, the aperture functions can be shifted at will along the τ axis. Suppose we now apply a tilt along the y axis ($s_{1x} = 0$). The modulation function is then shifted to

$$\tau_{center} = \frac{fD}{k_0 M} s_{1y}. \tag{50}$$

To get the highest possible visibility, the center of the modulation function must be matched to the center of the triangular dip,

$$\tau_{center} = \frac{DL}{2}, \tag{51}$$

so that

$$s_{1y} = \frac{k_0 ML}{2f}. \tag{52}$$

In the case of a reflective system, in which the phase modulation is implemented by means of a deformable mirror (Fig. 5), tilted by an angle θ,

$$\varphi(\mathbf{x}) = 2k_0 \tan\theta y = s_{1y} y. \tag{53}$$

Therefore, the amount of tilt necessary to restore high visibility is

$$\tan\theta = \frac{ML}{4f}. \tag{54}$$

In the case of a 1.5 mm crystal, with $M = 0.0723$ (pump at 405 nm, SPDC at 810 nm) and lenses with focal length of 20 cm in the $4f$ system, we get

$$\theta = 0.14 \text{ mrad}. \tag{55}$$

C. Large-aperture approximation

If the detection apertures are large enough for the $\tilde{P}_i$ function to be successfully approximated by a delta function, we get

$$W_M(\tau) = \int d\mathbf{q} G_1^*\left(\frac{f}{k_0}\mathbf{q}\right) G_1\left(-\frac{f}{k_0}\mathbf{q}\right) e^{-i(2M/D)\tau\hat{\mathbf{e}}_\mathbf{2}\cdot\mathbf{q}}. \tag{56}$$

Suppose that the spatial modulator is a circular aperture with radius r, with unit transmission and phase modulation described by the function $\varphi(\mathbf{x})$,

$$G_1(\mathbf{x}) = \begin{cases} 0 & \text{if } |\mathbf{x}| > r \\ e^{i\varphi(\mathbf{x})} & \text{if } |\mathbf{x}| < r. \end{cases} \tag{57}$$

In this case the function $\varphi(\mathbf{x})$ can be expanded on a set of polynomials which are orthogonal on the unit circle, such as the Zernicke polynomials:

$$\varphi(\mathbf{q}) = \sum_n \sum_m \varphi_{nm} R_n^m(\rho)\cos(m\theta),$$

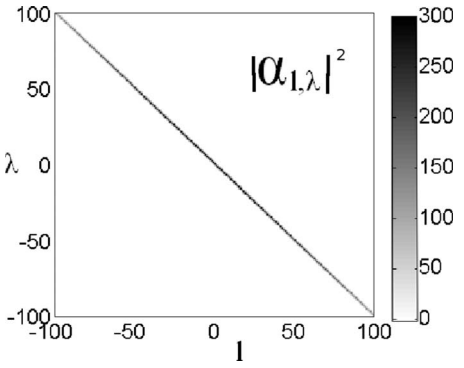

FIG. 6. Plot of the values of $|\alpha_{l,\lambda}|^2$, for $l,\lambda=-100,\ldots,+100$. The radius of the detection apertures is $R=5$ mm, the distance between the exit plane of the modulation section and the detection apertures is $d-1=1$ m, and the size of the modulation pixels is $d=25$ μm. Clearly only the diagonal elements are nonzero, i.e., the ones for which $\lambda=-l$. In this situation the effect of even-order aberration cancellation is present.

$$m=-n,-n+2,-n+4,\ldots,n, \tag{58}$$

where $\mathbf{q}=(\rho\cos\theta,\rho\sin\theta)$. To calculate $\varphi(-\mathbf{q})$ we note that $-\mathbf{q}=[\rho\cos(\theta+\pi),\rho\sin(\theta+\pi)]$, so

$$\varphi(-\mathbf{q})=\sum_n\sum_m R_n^m(\rho)\cos[m(\theta+\pi)]. \tag{59}$$

If m is even then $\cos[m(\theta+\pi)]=\cos(m\theta)$; otherwise if m is odd $\cos[m(\theta+\pi)]=-\cos m\theta$. Therefore

$$\varphi(\mathbf{q})-\varphi(-\mathbf{q})=2\sum_n\sum_{\mathrm{m\ odd}}\varphi_{nm}R_n^m(\rho)\cos(m\theta). \tag{60}$$

So, only the Zernicke polynomials with m odd contribute to the shape of the interference pattern. This effect is the spatial counterpart of the dispersion cancellation effect, in which only the odd-order terms in the Taylor expansion of the spectral phase survive. The experimental demonstration of this effect was recently reported in [11].

An interesting question is how large the detection apertures should effectively be, in order to obtain the even-order aberration cancellation effect. According to the numerical approach proposed in Sec. IV, the even-order aberration cancellation effect manifests itself in the limit where $\tilde{P}(x)\approx\delta(x)$, so that

$$\alpha_{l,\lambda}\to\delta(l+\lambda). \tag{61}$$

In Fig. 6, a plot of the value for $\alpha_{l,\lambda}$ is shown for typical values of the relevant experimental parameters (detection aperture radius $R=5$ mm, detection distance $d_1=1$ m, and size $d=0.1$ mm of each pixel in the Fourier plane of the adaptive optical system). Clearly, only the diagonal elements (the ones for which $l=-\lambda$) are significant, suggesting that the effect of even-order aberration cancellation may be observable for most typical experimental parameters.

To get an idea of what happens for different experimental conditions, we can compute the ratio between the intensities

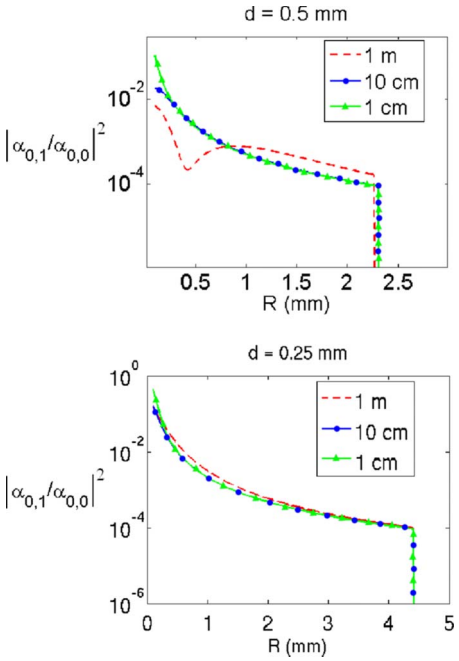

FIG. 7. (Color online) Plot of the ratio ρ_0 between the intensities of the nondiagonal coefficient α_{01} and the diagonal coefficient α_{00} as a function of the radius of Gaussian detection apertures, R, for different values of the distance between the exit plane of the modulation section and the detection apertures ($d_1=1,10,100$ cm). On the upper plot the size of the modulation pixel d is $d=0.5$ mm, while in the second case it is $d=0.25$ mm. Clearly, for experimentally interesting cases, the off-diagonal coefficient is at least 3 orders of magnitude smaller than the diagonal one, leading to even-order aberration cancellation.

of the nondiagonal coefficient α_{01} and the diagonal coefficient α_{00}:

$$\rho_0=\frac{|\alpha_{01}|^2}{|\alpha_{00}|^2}. \tag{62}$$

The lower the value for ρ_0 is, the less significant the coefficients for $\lambda\neq-l$ are: the even-order aberration cancellation effect will therefore manifest itself more clearly.

Values for ρ_0 are shown in Fig. 7 for two different cases. In both pictures, the value of ρ_0 is shown as a function of the Gaussian detection aperture radius R, for three different values of the distance between the plane Π_3 and the detection lenses d_1. In the upper panel, the size of each small square in which the spatial phase is assumed to be constant is $d=0.5$ mm, while in the second case it is $d=0.25$ mm. In both cases ρ_0 is significantly smaller than 1, and it becomes smaller and smaller, increasing the value of the detection aperture radius. However, ρ_0 is smaller for larger values of d, implying that the spatial variability of the modulation phase plays a role in the degree of even-order cancellation of the modulation itself.

It turns out that for the aberration cancellation effect to appear, it is in fact only necessary for one aperture to be large and for one detector to be integrated over. This is sufficient to produce the transverse-momentum delta functions that lead to even-order cancellation. To demonstrate this, we

can, for example, consider the case where the aperture at B is large, and the detector at B is integrated over, while the aperture at A is taken to be finite, with detector A treated as pointlike. The location of the pointlike detector will henceforth simply be denoted as x, and we continue to work within the quasimonochromatic approximation. If we integrate only over x_B, leaving x unintegrated, then it is straightforward to show that the analogs of Eqs. (A3) and (A4) are

$$W^{(0)}(\mathbf{x},\mathbf{q},\mathbf{q}',\nu)=e^{-(icd/\Omega_0)(q^2-q'^2)}\left\{\tilde{Q}\left(q+\frac{\Omega_0 x}{cf_0}\right)\tilde{Q}'\left(-q'-\frac{\Omega_0 x}{cf_0}\right)\tilde{P}_B(q'-q)+\tilde{Q}\left(-q+\frac{\Omega_0 x}{cf_0}\right)\tilde{Q}'\left(q'-\frac{\Omega_0 x}{cf_0}\right)\tilde{P}_B(q-q')\right\}, \tag{63}$$

$$W(\mathbf{x},\mathbf{q},\mathbf{q}',\nu)=e^{-(icd/\Omega_0)(q^2-q'^2)}\left\{\tilde{Q}\left(q+\frac{\Omega_0 x}{cf_0}\right)\tilde{Q}'\left(-q'+\frac{\Omega_0 x}{cf_0}\right)\tilde{P}_B(-q'-q)+\tilde{Q}\left(-q+\frac{\Omega_0 x}{cf_0}\right)\tilde{Q}'\left(+q'+\frac{\Omega_0 x}{cf_0}\right)\tilde{P}_B(q-q')\right\}. \tag{64}$$

We have defined $\tilde{Q}$ and $\tilde{Q}'$ to be the Fourier transforms, respectively, of p_A and p_A^*. $\tilde{P}_B$ is, as before, the Fourier transform of $|p_B|^2$. We now let aperture B become large, so that the function $\tilde{P}_B$ goes over to a delta function. For $G_1(x)=e^{i\phi(x)}$ and $G_2(x)=1$, we can substitute these results into the coincidence rate (which will now be a function of both τ and the position x of detector A), and carry out the q' and ν integrals. For the modulation term, we find

$$R_M(x,\tau)=R(x,\tau)-R_0(x) \tag{65}$$

$$\begin{aligned}&=\int dq e^{i[\phi(q)-\phi(-q)]}e^{(2iM\pi/D)\mathbf{e_2}\cdot\mathbf{q}}e^{(2iq^2/k_p)[(2\pi/D)+L]}\\&\times\mathrm{Sinc}\left(\frac{2q^2L}{k_p}\right)\left[\tilde{Q}\left(q+\frac{\Omega_0 x}{cf_0}\right)\tilde{Q}^*\left(-q-\frac{\Omega_0 x}{cf_0}\right)\right.\\&\left.+\tilde{Q}\left(-q+\frac{\Omega_0 x}{cf_0}\right)\tilde{Q}^*\left(q-\frac{\Omega_0 x}{cf_0}\right)\right].\end{aligned} \tag{66}$$

Here, we have used the fact that the Fourier transform of $p_A^*(x)$ equals the complex conjugate of the Fourier transform of $p_A(-x)$, in order to write $\tilde{Q}'$ in terms of $\tilde{Q}$. We see from the presence of the factor $e^{i[\phi(q)-\phi(-q)]}$ that even-order aberration cancellation occurs even though one aperture is finite and the corresponding detector is pointlike. This point may be of importance in future attempts to produce aberration-canceled imaging.

V. CONCLUSIONS

Summarizing, in this paper we have carried out a theoretical study of the relation between the wave-front modulation of the entangled SPDC photons and the shape of the resulting temporal quantum-interference pattern. Due to the multiparametric nature of the generated entangled states, the modulation on the spatial degree of freedom can affect the shape of the polarization-temporal interference pattern in the coincidence rate. Our aim is twofold: from one side we want to study the effect of wave-front aberration on quantum interferometry, and from the other we want to discuss a way to engineer multiparametrically entangled states.

We have introduced a theoretical model for calculation of the shape of the polarization-temporal interference pattern given a certain general phase modulation in the crystal far field, assuming as a free parameter the shape and the dimension of the collection apertures. Using a numerical method to study the resulting equation has shown that for typical experimental cases the hypothesis of large apertures can be assumed to be valid. In such an approximation, only the odd part of the assigned phase modulation affects the shape of the interference pattern. This effect has recently been demonstrated experimentally [11].

Moreover, it is often useful in experiments to enlarge the collection aperture in order to collect a higher photon flux and larger optical bandwidth. But when working with type-II birefringently phase-matched down-conversion, spatial walkoff between the emitted photons introduces distinguishability between the two possible events that can lead to coincidence detection, reducing the visibility of quantum interference. Such walkoff can be compensated for with a linear phase shift in the vertical direction, restoring high visibility.

ACKNOWLEDGMENTS

This work was supported by a U.S. Army Research Office (USARO) Multidisciplinary University Research Initiative (MURI) grant; by the Bernard M. Gordon Center for Subsurface Sensing and Imaging Systems (CenSSIS), an NSF Engineering Research Center; by the Intelligence Advanced Research Projects Activity (IARPA) and USARO through Grant No. W911NF-07-1-0629; and by the strategic project QUINTET of the Department of Information Engineering of the University of Padova. C.B. also acknowledges financial support from Fondazione Cassa di Risparmio di Padova e Rovigo.

APPENDIX A: SKETCH OF DERIVATION OF EQ. (23)

In this appendix we sketch the major steps for the derivation of Eq. (23). Substituting Eq. (21) into Eq. (16) and the result into Eq. (22), one finds the following expressions for R_0 and $W_G(\tau)$:

$$R_0 = \int d\mathbf{q}d\mathbf{q}'d\nu\Phi^*(\mathbf{q},\nu)\Phi(\mathbf{q}',\nu)G_1^*\left(\frac{f}{k}\mathbf{q}\right)G_1\left(\frac{f}{k}\mathbf{q}'\right)G_2^*\left(-\frac{f}{k}\mathbf{q}\right)G_2\left(-\frac{f}{k}\mathbf{q}'\right)W^{(0)}(\mathbf{q},\mathbf{q}',\nu), \tag{A1}$$

$$W_M(\tau) = \frac{1}{R_0}\int d\mathbf{q}d\mathbf{q}'d\nu\Phi^*(\mathbf{q},\nu)\Phi(\mathbf{q}',-\nu)G_1^*\left(\frac{f}{k}\mathbf{q}\right)G_1\left(\frac{f}{k}\mathbf{q}'\right)G_2^*\left(-\frac{f}{k}\mathbf{q}\right)G_2\left(-\frac{f}{k}\mathbf{q}'\right)W(\mathbf{q},\mathbf{q}',\nu), \tag{A2}$$

where

$$W^{(0)}(\mathbf{q},\mathbf{q}',\nu) = \int d\mathbf{x}_A d\mathbf{x}_B H^*(\mathbf{x}_A,\mathbf{q},\nu)H^*(\mathbf{x}_B,-\mathbf{q},-\nu)H(\mathbf{x}_A,\mathbf{q}',\nu)H(\mathbf{x}_B,-\mathbf{q}',-\nu)$$
$$+ H^*(\mathbf{x}_A,-\mathbf{q},-\nu)H^*(\mathbf{x}_B,\mathbf{q},\nu)H(\mathbf{x}_A,-\mathbf{q}',-\nu)H(\mathbf{x}_B,\mathbf{q}',\nu) \tag{A3}$$

and

$$W(\mathbf{q},\mathbf{q}',\nu) = \int d\mathbf{x}_A d\mathbf{x}_B H^*(\mathbf{x}_A,\mathbf{q},\nu)H^*(\mathbf{x}_B,-\mathbf{q},-\nu)H(\mathbf{x}_A,-\mathbf{q}',\nu)H(\mathbf{x}_B,\mathbf{q}',-\nu)$$
$$+ H^*(\mathbf{x}_A,-\mathbf{q},-\nu)H^*(\mathbf{x}_B,\mathbf{q},\nu)H(\mathbf{x}_A,\mathbf{q}',-\nu)H(\mathbf{x}_B,-\mathbf{q}',\nu). \tag{A4}$$

The angular and spectral emission function $\Phi(\mathbf{q},\nu)$ is given by

$$\Phi(\mathbf{q},\nu) = \int dz\Pi\left[\frac{z}{L}+\frac{1}{2}\right]e^{-i\Delta(\mathbf{q},\nu)z}. \tag{A5}$$

Performing the integrals over the spatial coordinates $d\mathbf{x}_A$ and $\mathbf{x}_B$, one gets

$$W^{(0)}(\mathbf{q},\mathbf{q}',\nu) = e^{i(2d_1/k_p)[|\mathbf{q}|^2-|\mathbf{q}'|^2]}\{\tilde{P}_A[(\mathbf{q}-\mathbf{q}')]\tilde{P}_B[-(\mathbf{q}-\mathbf{q}')] + \tilde{P}_A[-(\mathbf{q}-\mathbf{q}')]\tilde{P}_B[(\mathbf{q}-\mathbf{q}')]\} \tag{A6}$$

and

$$W(\mathbf{q},\mathbf{q}',\nu) = e^{i(2d_1/k_p)[|\mathbf{q}|^2-|\mathbf{q}'|^2]}\{\tilde{P}_A[(\mathbf{q}+\mathbf{q}')]\tilde{P}_B[-(\mathbf{q}+\mathbf{q}')] + \tilde{P}_A[-(\mathbf{q}+\mathbf{q}')]\tilde{P}_B[(\mathbf{q}+\mathbf{q}')]\}. \tag{A7}$$

Finally, use of the integral representation for the sinc function [Eq. (A5)] allows the ν integration to be carried out, but at the expense of introducing two integrations over a pair of new parameters (say, z and z'). Note the following relation, which can easily be verified by sketching the functions on the left-hand side:

$$\Pi[x]\Pi[x-\alpha] = \begin{cases} 1 & \text{if } -1 \le \alpha \le 0, \quad -\frac{1}{2} \le x \le \frac{1}{2}+\alpha \\ 1 & \text{if } 0 \le \alpha \le 1, \quad -\frac{1}{2}+\alpha \le x \le \frac{1}{2} \\ 0 & \text{otherwise.} \end{cases} \tag{A8}$$

From this, it follows that

$$\int \Pi[x]\Pi[x-\alpha]dx = \Lambda(\alpha), \tag{A9}$$

where $\Lambda(\alpha)$ is the triangle function. These facts allow us to carry out the two z integrations that arise from the sinc function, leading to the result shown in Eq. (23).

APPENDIX B: JUSTIFICATION OF EQ. (32)

Suppose we have a set A, which can be partitioned into a collection of disjoint subsets A_k, with $k=1,2,\ldots$:

$$\bigcup_k A_k = A, \quad A_k \cap A_l = \phi \quad \text{if } k \neq l. \tag{B1}$$

To each set we can associate a characteristic function,

$$\chi_k(x) = \begin{cases} 1, & x \in A_k \\ 0, & x \notin A_k, \end{cases} \tag{B2}$$

such that

$$\sum_k \chi_k(x) = \chi_A(x), \quad \chi_k(x)\chi_l(x) = \delta_{kl}\chi_k(x), \tag{B3}$$

where χ_A is the characteristic function for the full set,

$$\chi_A(x) = \begin{cases} 1, & x \in A \\ 0, & x \notin A. \end{cases} \tag{B4}$$

The term $e^{i\phi_k\chi_k(x)}$ assumes the value of $e^{i\phi_k}$ for $\chi_k(x)=1$ and the value of 1 for $\chi_k(x)=0$ $[1-\chi_k(x)=1]$, so

$$\exp\left[i\sum_k \phi_k\chi_k(x)\right] = \prod_k e^{i\phi_k\chi_k(x)} = \prod_k \{1[1-\chi_k(x)] + e^{i\phi_k}\chi_k(x)\} = \prod_k [1 + (e^{i\phi_k} - 1)\chi_k]. \tag{B5}$$

If we express the first few terms we get

$$\begin{aligned}\prod_k [1 + (e^{i\phi_k} - 1)\chi_k] &= [1 + (e^{i\phi_1} - 1)\chi_1][1 + (e^{i\phi_2} - 1)\chi_2]\cdots \\ &= 1 + (e^{i\phi_1} - 1)\chi_1 + (e^{i\phi_2} - 1)\chi_2 + \cdots + (e^{i\phi_1} - 1)(e^{i\phi_2} - 1)\chi_1\chi_2 + (e^{i\phi_1} - 1)(e^{i\phi_3} - 1)\chi_1\chi_3 \\ &\quad + \cdots + (e^{i\phi_1} - 1)(e^{i\phi_1} - 1)(e^{i\phi_1} - 1)\chi_1\chi_2\chi_3 + (e^{i\phi_1} - 1)(e^{i\phi_2} - 1)(e^{i\phi_4} - 1)\chi_1\chi_2\chi_4 + \cdots .\end{aligned} \tag{B6}$$

So that in the end

$$\exp\left[i\sum_k \phi_k\chi_k(x)\right] = 1 + \sum_k [(e^{i\phi_k} - 1)\chi_k] = 1 + \sum_k e^{i\phi_k}\chi_k - \sum_k \chi_k = \sum_k e^{i\phi_k}\chi_k. \tag{B7}$$

Since the square sets we have used in Sec. IV satisfy Eq. (B1), then the result expressed in Eq. (B5) is valid for our case.

[1] E. Schrödinger, Naturwiss. **23**, 807 (1935).
[2] D. N. Klyshko, JETP Lett. **6**, 23 (1967).
[3] S. E. Harris, M. K. Osham, and R. L. Byer, Phys. Rev. Lett. **18**, 732 (1967).
[4] T. G. Giallorenzi and C. L. Tang, Phys. Rev. **166**, 225 (1968).
[5] D. A. Kleinman, Phys. Rev. **174**, 1027 (1968).
[6] M. Atature, G. Di Giuseppe, M. D. Shaw, A. V. Sergienko, B. E. A. Saleh, and M. C. Teich, Phys. Rev. A **66**, 023822 (2002).
[7] A. F. Abouraddy, M. B. Nasr, B. E. A. Saleh, A. V. Sergienko, and M. C. Teich, Phys. Rev. A **65**, 053817 (2002).
[8] M. B. Nasr, B. E. A. Saleh, A. V. Sergienko, and M. C. Teich, Phys. Rev. Lett. **91**, 083601 (2003).
[9] J. D. Franson, Phys. Rev. A **45**, 3126 (1992).
[10] A. M. Steinberg, P. G. Kwiat, and R. Y. Chiao, Phys. Rev. A **45**, 6659 (1992).
[11] C. Bonato, A. V. Sergienko, B. E. A. Saleh, S. Bonora, and P. Villoresi, Phys. Rev. Lett. **101**, 233603 (2008).
[12] M. H. Rubin, Phys. Rev. A **54**, 5349 (1996).
[13] J. W. Goodman, *Introduction to Fourier Optics*, 2nd ed. (McGraw-Hill, New York, 1996).

Odd- and Even-Order Dispersion Cancellation in Quantum Interferometry

Olga Minaeva,[1,2] Cristian Bonato,[1,3] Bahaa E. A. Saleh,[1] David S. Simon,[1] and Alexander V. Sergienko[1,4,*]

[1]*Department of Electrical & Computer Engineering, Boston University, Boston, Massachusetts 02215, USA*
[2]*Department of Physics, Moscow State Pedagogical University, 119992 Moscow, Russia*
[3]*CNR-INFM LUXOR, Department of Information Engineering, University of Padova, Padova, Italy*
[4]*Department of Physics, Boston University, Boston, Massachusetts 02215, USA*

(Received 16 October 2008; published 12 March 2009)

We describe a novel effect involving odd-order dispersion cancellation. We demonstrate that odd- and even-order dispersion cancellation may be obtained in different regions of a single quantum interferogram using frequency-anticorrelated entangled photons and a new type of quantum interferometer. This offers new opportunities for quantum communication and metrology in dispersive media.

DOI: 10.1103/PhysRevLett.102.100504 PACS numbers: 03.67.Bg, 42.30.Kq, 42.50.Dv, 42.50.St

Introduction.—The even-order dispersion cancellation effect based on nonclassical frequency-anticorrelated entangled photons has been known in quantum optics for some time [1,2]. The nonlinear optical process of spontaneous parametric down conversion (SPDC) traditionally provides a reliable source of frequency-entangled photon pairs with anticorrelated spectral components, as a consequence of energy conservation. If the frequency of the signal photon is ω_s, then the frequency of its twin idler photon must be $\omega_i = \Omega_p - \omega_s$, where Ω_p is the frequency of the pump beam. A quantum interferometer records the modulation in the rate of coincidence between pulses from two photon-counting detectors at the output ports of a beam splitter in response to a temporal delay between two spectrally correlated photons entering its input ports symmetrically. This type of quantum optics intensity correlation measurement, exhibited in the Hong-Ou-Mandel (HOM) interferometer [3], is manifested by an observed dip in the rate of coincidences. In previous demonstrations of dispersion cancellation, one photon of the down-converted pair travels through a dispersive material in one arm of the HOM interferometer while its twin travels only through air. The final coincidence interference dip is not broadened in this case, demonstrating insensitivity to even-order dispersion coefficients [2,4].

Even-order dispersion cancellation has been used in quantum-information processing, quantum communication, and in quantum optical metrology. For example, it enhances the precision of measuring photon tunneling time through a potential barrier [5] and improves the accuracy of remote clock synchronization [6]. The same effect provides superior resolution in quantum optical coherence tomography [7] by eliminating the broadening of the interference envelope resulting from group velocity dispersion. The potential of quantum even-order dispersion cancellation has recently stimulated efforts to mimic this effect by use of classical nonlinear optical analogues [8–10].

In this Letter, we introduce a novel type of quantum interferometer that enables the demonstration of the odd-order dispersion cancellation as a part of a new dispersion management technique. In our design, both even-order and odd-order dispersion cancellation effects can be recorded as parts of a single quantum interference pattern.

HOM interferometers are commonly used to produce either $|\Psi\rangle \sim |2,0\rangle$-$|0,2\rangle$ state, when the delay τ_1 is set to balance the two paths, ensuring destructive interference in the middle of the interference dip, or a superposition of $|1,1\rangle$, $|0,2\rangle$, and $|2,0\rangle$ states, when the delay τ_1 significantly unbalances two paths and shifts coincidences to the shoulder of HOM interference pattern. Mach-Zehnder (MZ) interferometers fed by a particular quantum state have also been studied in detail [11].

In the new design, two interferometers work together: one output port of a HOM interferometer provides input to a MZ interferometer. The state of light introduced into the MZ interferometer is continuously modified when the delay τ_1 in the HOM interferometer is scanned. A signal from one of the HOM output ports is fed into a MZ interferometer with a dispersive sample providing a phase shift ϕ in one arm, as shown in Fig. 1. The delay τ_2 inside the MZ interferometer is kept at a fixed value. A peculiar quantum interference pattern is observed in the rate of

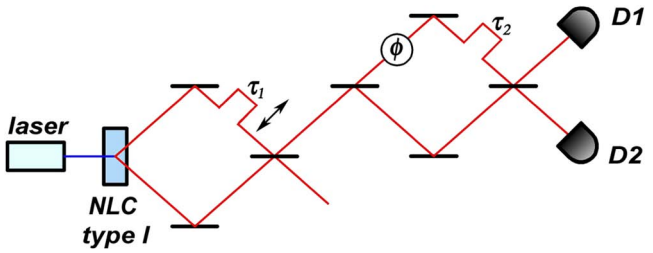

FIG. 1 (color online). Schematic diagram of the optical setup. The SPDC source produces pairs of frequency-anticorrelated photons combining on a beam splitter in a HOM interferometer configuration. Photons exiting one HOM port are fed into a MZ interferometer. Coincidence events are registered between two single-photon detectors at the output ports of the MZ interferometer. A dispersive sample in one arm of the MZ interferometer generates a phase delay (ϕ).

coincidences between two photon-counting detectors, $D1$ and $D2$, at the output ports of the MZ interferometer as a function of τ_1. The interference profile has two distinct patterns. The central interference pattern depends only on even-order dispersion coefficients, while the peripheral pattern depends only on odd-order terms. This ability to manipulate and evaluate odd-order and even-order dispersion terms independently in a single quantum interferometer opens new perspectives in quantum communication and in precise optical measurement.

Theoretical model.—For detectors D_1 and D_2, much slower than the temporal coherence of the down-converted photons, the coincidence rate in such intensity correlation measurements is [12]

$$R_c(\tau_1, \tau_2) = \int dt_1 \int dt_2 G^{(2)}(t_1, t_2), \tag{1}$$

with $G^{(2)}(t_1, t_2)$ the second-order correlation function $G^{(2)}(t_1, t_2)$:

$$G^{(2)}(t_1, t_2) = |\langle 0|\hat{E}_1^{(+)}(t_1)\hat{E}_2^{(+)}(t_2)|\Psi\rangle|^2. \tag{2}$$

$E_1^{(+)}(t_1)$ and $E_2^{(+)}(t_2)$ are the electrical field operators at the surfaces of detectors D_1 and D_2, respectively.

$$\hat{E}_j^{(+)}(t_j) = \frac{1}{\sqrt{2\pi}} \int d\omega_j e^{-i\omega_j t_j} \hat{b}_j(\omega_j), \tag{3}$$

where $\hat{b}_j(\omega_j)$ is the mode operator at detector j, expressed in terms of the input field operators $\hat{a}_j(\omega_j)$ [12]. The quantum state of light emitted in a frequency-degenerate noncollinear type-I phase-matching SPDC process with a monochromatic pump Ω_p is

$$|\Psi\rangle \propto \int d\omega f(\omega)\hat{a}_1^\dagger(\Omega_0 + \omega)\hat{a}_2^\dagger(\Omega_0 - \omega)|0\rangle, \tag{4}$$

where $f(\omega)$ is a photon wave packet spectral function defined by the phase-matching condition in the nonlinear material, $\Omega_0 = \Omega_p/2$ is a central frequency of each wave packet, $\omega_s = \Omega_0 + \omega$ is the signal photon frequency, and $\omega_i = \Omega_0 - \omega$ is the idler frequency.

The phase shift $\phi(\omega)$ acquired by the broadband optical wave packet as it travels through a dispersive material could be expanded in a Taylor's series [13]:

$$\phi(\omega_{s,i}) = c_0 + c_1(\omega_{s,i} - \Omega_0) + c_2(\omega_{s,i} - \Omega_0)^2 + c_3(\omega_{s,i} - \Omega_0)^3 + \cdots, \tag{5}$$

where the linear term c_1 represents the group delay and the second-order term c_2 is responsible for group delay dispersion. In a conventional white-light interferometer, c_1 is responsible for a temporal shift of the interference pattern envelope, c_2 causes its temporal broadening, while c_3 provides a nonsymmetric deformation of the wave packet envelope. Higher-order terms might be included when a strongly-dispersive material is used or in the case of extremely broadband optical wave packets.

In the optical setup of Fig. 1, the dispersive material providing phase shift $\phi(\omega)$ could be situated in three possible locations. When the sample is placed on an arm of the HOM interferometer, it leads to the well-known even-order dispersion cancellation effect [4]. It may be shown that the presence of a dispersive material between the two interferometers does not affect the coincidence interferogram. We thus concentrate on the most interesting case: we place the dispersive sample of phase shift $\phi(\omega)$ inside the MZ interferometer, with delay τ_2 set to a fixed value, and τ_1 as the variable parameter.

Following the usual formalism [12], one can show that the coincidence rate between the detectors is

$$R_c(\tau_1, \tau_2) = \int d\omega[\Phi_0 - \Phi_\alpha(\omega, \tau_2) - \Phi_\beta(\omega, \tau_2)] \times [f(\omega)f^*(\omega) + f(\omega)f^*(-\omega)e^{-2i\omega\tau_1}], \tag{6}$$

where Φ_0 is a constant,

$$\Phi_\alpha(\omega, \tau_2) = e^{-2i\omega\tau_2}e^{i\phi(\Omega_0-\omega)}e^{-i\phi(\Omega_0+\omega)} + \text{c.c.}, \tag{7}$$

and

$$\Phi_\beta(\omega, \tau_2) = e^{-2i\Omega_0\tau_2}e^{-i\phi(\Omega_0-\omega)}e^{-i\phi(\Omega_0+\omega)} + \text{c.c.} \tag{8}$$

Although not obvious from the form of Eq. (6), $R_c(\tau_1, \tau_2)$ is a real function for any spectrum $f(\omega)$, as can be seen by rewriting Eq. (6) in manifestly real form:

$$R_c(\tau_1, \tau_2) = \int d\omega\{|f(\omega)|^2 + |f(-\omega)|^2 + [e^{-2i\omega\tau_1}f(\omega)f^*(-\omega) + \text{c.c.}]\} \times [\Phi_0 - \Phi_\alpha(\omega) - \Phi_\beta(\omega)]. \tag{9}$$

This fact ensures that the technique demonstrated here applies to all types of broadband frequency-anticorrelated states of light, including those with nonsymmetric spectral profiles produced in chirped periodically-polled nonlinear crystals.

The final coincidence counting rate $R_c(\tau_1, \tau_2)$ of Eq. (6) may also be written as a linear superposition:

$$R_c(\tau_1, \tau_2) = B + R_0(\tau_1) - R_{\text{even}}(\tau_1, \tau_2) - R_{\text{odd}}(\tau_1, \tau_2). \tag{10}$$

The first coefficient B incorporates all terms that are not dependent on the variable delay τ_1, providing a constant after integration. It establishes a baseline level for the quantum interferogram. The following terms,

$$R_0(\tau_1) = 4\int d\omega f(\omega)f^*(-\omega)e^{-2i\omega\tau_1}, \tag{11}$$

$$R_{\text{even}}(\tau_1, \tau_2) = \int d\omega f(\omega)f^*(-\omega) \cdot e^{-2i\omega\tau_1}[e^{-2i\Omega_0\tau_2}e^{-i\phi(\Omega_0-\omega)}e^{-i\phi(\Omega_0+\omega)} + e^{2i\Omega_0\tau_2}e^{i\phi(\Omega_0-\omega)}e^{i\phi(\Omega_0+\omega)}], \tag{12}$$

$$R_{\mathrm{odd}}(\tau_1,\tau_2) = \int d\omega f(\omega) f^*(-\omega) \cdot [e^{-2i\omega(\tau_1+\tau_2)} e^{i\phi(\Omega_0-\omega)} e^{-i\phi(\Omega_0+\omega)} + e^{-2i\omega(\tau_1-\tau_2)} e^{-i\phi(\Omega_0-\omega)} e^{i\phi(\Omega_0+\omega)}] \quad (13)$$

are responsible for the shape of the interference pattern.

The term $R_0(\tau_1)$ represents a peak centered at $\tau_1 = 0$ that is simply a Fourier transform of the down-converted radiation spectrum and is insensitive to the dispersion associated with $\phi(\omega)$. Since $R_{\mathrm{even}}(\tau_1, \tau_2)$ is dependent on the sum $\phi(\Omega_0 - \omega) + \phi(\Omega_0 + \omega)$, it is sensitive only to even-order terms in the expansion Eq. (5). This manifests odd-order dispersion cancellation and generates a dispersion-broadened function centered around $\tau_1 = 0$. The last term $R_{\mathrm{odd}}(\tau_1, \tau_2)$, in contrast, is sensitive only to odd-order dispersion terms in $\phi(\omega)$. This term demonstrates the well-known even-order cancellation. The coefficients $e^{-2i\omega(\tau_1+\tau_2)}$ and $e^{-2i\omega(\tau_1-\tau_2)}$ shift the two dips away from the center of the interference pattern in opposite directions. Such decomposition of quantum interference terms makes it possible to observe odd-order and even-order dispersion cancellation effects in two distinct regions of the coincidence interferogram.

Example.—Our results are illustrated by a numerical example of quantum interference for a 3-mm thick slab of a strongly-dispersive optical material ZnSe, inserted in one arm of the MZ interferometer to provide the phase shift $\phi(\omega)$. In this experiment, we assume the use of frequency-entangled down-converted photons with a 100-nm wide spectrum. As illustrated in Fig. 2, one can identify the narrow peak $R_0(\tau_1)$ in the center, which is insensitive to dispersion, along with the component $R_{\mathrm{even}}(\tau_1, \tau_2)$, which is broadened by even-order dispersion contributions only. This central component of the interferogram illustrates the odd-order dispersion cancellation effect.

Two symmetric side dips $R_{\mathrm{odd}}(\tau_1, \tau_2)$ appear shifted far away from the central peak by the group velocity delay c_1 acquired by entangled photons inside the dispersive material. However, this shift can be controlled by properly adjusting the value of the fixed delay τ_2. Such a simple adjustment moves both dips back closer to the center and makes it convenient for observing both dispersion cancellation features in a single scan of the variable delay line (τ_1) inside the HOM interferometer (see Fig. 2). The appearance of asymmetric fringes on the side of two dips is a clear sign of the third-order dispersion [13].

Discussion.—This result can also be understood physically by analyzing all possible probability amplitudes that lead to measured coincidence events between $D1$ and $D2$. The MZ interferometer input is a pair of spectrally-entangled photons separated by time delay τ_1; if the leading photon has a high frequency, the lagging photon will have a low frequency, and vice versa. We consider first the case when no dispersive element is present, so that the MZ interferometer introduces only a time delay τ_2 between its two arms. We assume that τ_2 is much greater than the photon wave packet width, τ_c. To explain the dependence of the photon coincidence rate on τ_1, as shown in Fig. 2, we consider three processes occurring at the input ports of the last beam splitter in the MZ interferometer: (1) If $|\tau_1| > \tau_c$ and $|\tau_2 - \tau_1| > \tau_c$, then the two photons arriving at the final beam splitter will be distinguishable, so that no quantum interference is exhibited. (2) If $|\tau_1| \approx |\tau_2|$, so that $|\tau_2 - \tau_1| < \tau_c$, then quantum interference can occur when the leading photon takes the long path of the MZ interferometer and the lagging photon takes the short path. The two arrive almost simultaneously (within a time τ_c) at the two ports of the final beam splitter. Then the HOM effect is exhibited at the beam splitter, albeit with only 25% visibility because of the presence of the other possibility that both photons arrive at a single port, leading to a background coincidence rate independent of τ_1. From a different perspective, one may regard this scenario as similar to that obtained in a Franson interferometer [14], for which photon pairs follow long-long or short-short paths. This scenario explains the components of the coincidence interferogram near $\tau_1 = \pm\tau_2$, and in this case the two spectrally-entangled photons entering separate ports of the final beam splitter lead to quantum interference accompanied by even-order dispersion cancellation. (3) Finally, when $|\tau_1| < \tau_c$, then one possibility is that the photons arrive at separate input ports of the final beam splitter. Since these photons are separated by a time $\tau_2 \gg \tau_c$, they are distinguishable and do not contribute to quantum interference. The other possibility is that the pair arrive at the same beam splitter input port. In this case, upon transmission or reflection at the beam splitter there are two alternatives for producing coincidence: transmission of the high-frequency photon and reflection of the low-frequency photon, or vice versa. This explains the compo-

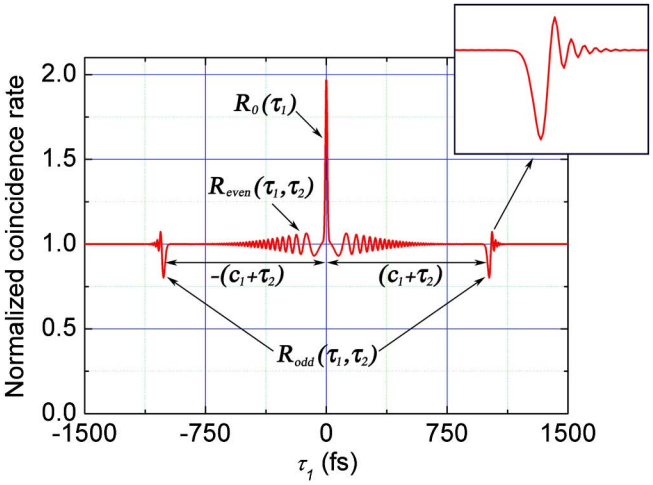

FIG. 2 (color online). The normalized coincidence rate as a function of τ_1 when a 3-mm thick ZnSe sample is placed in the MZ interferometer. The fixed delay $\tau_2 = 26$ ps is used. The insert illustrates the odd-order dispersion contribution.

nent of the coincidence interferogram near $\tau_1 \approx 0$. In this scenario, which involves two spectrally-entangled photons entering a single port of a beam splitter, quantum interference is accompanied by odd-order dispersion cancellation. We thus see that the quantum interference effects exhibited in scenarios (2) and (3) are accompanied by dispersion cancellation—although in opposite manners in the two cases.

In conclusion, we have demonstrated a new effect in which even- and odd-order dispersion cancellations appear in different regions of a single interferogram. This is achieved via frequency-anticorrelated photons in a new quantum interferometer formed by a variable delay HOM interferometer followed by a single-input, fixed-delay Mach-Zehnder interferometer. The possibility of independently evaluating even- and odd-order dispersion coefficients of a medium has potential for applications in quantum communication and in quantum metrology of complex dispersive photonics structures. In particular, the ability to accurately characterize higher-order dispersion coefficients is of great interest in the study of flattened-dispersion optical fibers [15,16] and in dispersion engineering with metamaterials [17]. The demonstrated potential of even-order dispersion cancellation has stimulated the search for classical analogues [8,9]. We expect that the scheme presented here would also trigger the similar development of nonlinear optical techniques mimicking this quantum effect. Finally, note that our apparatus may be extended by adding a second Mach-Zehnder to the unused HOM output port, allowing the investigation of new four-photon interference effects.

We would like to thank Andrey Antipov from SUNY Buffalo for assistance with numerical simulations. This work was supported by a U. S. Army Research Office (ARO) Multidisciplinary University Research Initiative (MURI) grant; by the Bernard M. Gordon Center for Subsurface Sensing and Imaging Systems (CenSSIS), an NSF Engineering Research Center; by the Intelligence Advanced Research Projects Activity (IARPA) and ARO through Grant No. W911NF-07-1-0629.

*Corresponding author.
alexserg@bu.edu

[1] J. D. Franson, Phys. Rev. A **45**, 3126 (1992).
[2] A. M. Steinberg, P. G. Kwiat, and R. Y. Chiao, Phys. Rev. A **45**, 6659 (1992).
[3] C. K. Hong, Z. Y. Ou, and L. Mandel, Phys. Rev. Lett. **59**, 2044 (1987).
[4] A. F. Abouraddy *et al.*, Phys. Rev. A **65**, 053817 (2002).
[5] A. M. Steinberg, P. G. Kwiat, and R. Y. Chiao, Phys. Rev. Lett. **68**, 2421 (1992).
[6] V. Giovannetti, S. Lloyd, and L. Maccone, Nature (London) **412**, 417 (2001).
[7] M. B. Nasr, B. E. A. Saleh, A. V. Sergienko, and M. C. Teich, Phys. Rev. Lett. **91**, 083601 (2003).
[8] B. I. Erkmen and J. H. Shapiro, Phys. Rev. A **74**, 041601 (R) (2006).
[9] K. J. Resch *et al.*, Opt. Express **15**, 8797 (2007).
[10] R. Kaltenbaek, J. Lavoie, D. Biggenstaff, and K. J. Resch, Nature Phys. **4**, 864 (2008).
[11] R. A. Campos, B. E. A. Saleh, and M. C. Teich, Phys. Rev. A **42**, 4127 (1990).
[12] M. H. Rubin, D. N. Klyshko, Y. H. Shih, and A. V. Sergienko, Phys. Rev. A **50**, 5122 (1994).
[13] J.-C. Diels and W. Rudolph, *Ultrashort Laser Pulse Phenomena* (Elsevier Inc. Academic Press, London, 2006).
[14] J. D. Franson, Phys. Rev. Lett. **62**, 2205 (1989).
[15] A. Ferrando, E. Silvestre, P. Andrées, J. Miret, and M. Andrés, Opt. Express **9**, 687 (2001).
[16] W. Reeves, J. Knight, P. S. Russell, and P. Roberts, Opt. Express **10**, 609 (2002).
[17] G. V. Eleftheriades and K. G. Balmain, *Negative-Refraction Metamaterials* (Wiley-IEEE Press, New York, 2005).

Spatial-dispersion cancellation in quantum interferometry

D. S. Simon[1] and A. V. Sergienko[1,2]
[1]*Department of Electrical and Computer Engineering, Boston University, 8 Saint Mary's Street, Boston, Maassachusetts 02215, USA*
[2]*Department of Physics, Boston University, 590 Commonwealth Avenue, Boston, Massachusetts 02215, USA*
(Received 17 August 2009; published 10 November 2009)

We investigate cancellation of spatial aberrations induced by an object placed in a quantum coincidence interferometer with type-II parametric down conversion as a light source. We analyze in detail the physical mechanism by which the cancellation occurs and show that the aberration cancels only when the object resides in one particular plane within the apparatus. In addition, we show that for a special case of the apparatus it is possible to produce simultaneous cancellation of *both* even-order and odd-order aberrations in this plane.

DOI: 10.1103/PhysRevA.80.053813 PACS number(s): 42.50.St, 42.15.Fr, 42.50.Dv, 42.30.Kq

I. INTRODUCTION AND BACKGROUND

A. Introduction

Aberration or spatial dispersion occurs when light passing through or reflecting off of an object gains unwanted phase shifts that vary in the transverse spatial direction (orthogonal to the optical axis). These phase shifts are "unwanted" in the sense that they differ from those obtained from Gaussian optics and cause distortions of the outgoing wavefronts. Mathematically, we can represent the aberrations by pure imaginary exponentials $e^{i\phi(\mathbf{x})}$, where $\mathbf{x}$ is the transverse distance. Often $\phi(\mathbf{x})$ may be expanded into a power series in $|\mathbf{x}|$ and separated into even and odd orders,

$$\phi(\mathbf{x}) = \phi_{even}(\mathbf{x}) + \phi_{odd}(\mathbf{x}), \tag{1}$$

$$\phi_{even}(\mathbf{x}) = \sum_j a_{2j} r^{2j} P_{2j}(\theta), \tag{2}$$

$$\phi_{even}(\mathbf{x}) = \sum_j a_{2j+1} r^{2j+1} P_{2j}(\theta). \tag{3}$$

Here, $r=|\mathbf{x}|$, while $P_{2j}(\theta)$ and $P_{2j+1}(\theta)$ are polynomials in $\sin\theta$ and/or $\cos\theta$. Usually, the expansion is expressed in terms of Seidel or Zernike polynomials [1–3], but for our purposes the details of the expansion are not important. The important point here is simply that the even-order terms are symmetric under reflection, $\phi_{even}(\mathbf{x})=\phi_{even}(-\mathbf{x})$, while the odd terms are antisymmetric, $\phi_{odd}(\mathbf{x})=-\phi_{odd}(-\mathbf{x})$.

In Refs. [4,5], a particular type of interferometric device was described, and it was shown that if an object was placed in either arm of this device, then all even-order phase shifts introduced by the object will cancel in a temporal correlation experiment. The effect is very similar to the even-order frequency-dispersion cancellation first described in Refs. [6,7]. As a light source, the aberration-cancellation experiment used photon pairs produced via spontaneous parametric down conversion (SPDC). The cancellation effect depended on the entanglement of the transverse spatial momenta in the resulting entangled-photon pairs.

In this paper we re-examine the setup of Refs. [4,5] with two purposes in mind. After reviewing the apparatus and the even-order aberration-cancellation effect in the next subsection, we first show (in Sec. II) that for a special case of the apparatus we can in fact cancel *all* aberration, both even order and odd order. This cancellation only occurs when the sample is placed in one particular plane and opens up the possibility of cancelling sample-induced aberration in dynamic light scattering [8,9], fluorescence correlation spectroscopy [10], or other temporal correlation-based experiments. Our second purpose (carried out in Sec. III) is to analyze in more detail the results for the coincidence rate in order to better understand the physical mechanisms involved in aberration cancellation. In Sec. IV we discuss the conclusions that can be drawn from these results.

Note that, because we are motivated by the desire to cancel aberrations, we will use the phrase "aberration cancellation" for convenience throughout this paper, but in fact we mean the cancellation of *all* phase shifts arising in a given plane not just the subset that differ from the predictions of Gaussian optics. In other words, "aberration cancellation" here means that only the intensity of the light is affected by the object, not the phase. So, for example, the placement in the object plane of an ideal lens, whose operation depends on second-order phase shifts, should have no focusing power at this point; it will be as if the lens is not there.

B. Even-order aberration cancellation

Consider the setup shown in Fig. 1. In the main part of the apparatus, the two branches each consist of a Fourier transform system containing lenses of focal length f and a sample providing a modulation $G_j(\mathbf{y})$ of the beam, where $j=1,2$ labels the branch and $\mathbf{y}$ is the transverse distance from the optic axis. The G_j represent objects or samples whose properties we wish to analyze, and the goal is to cancel optical aberrations introduced by the samples. The case where there is a sample only in branch 1 is included by simply setting $G_2=1$, but we will keep the more general two-sample case; we will see later that the extra generality pays off by allowing useful additional effects. A controllable time delay τ is inserted in one arm of the interferometer. Since we will be referring to it often, we give a name to the plane containing the samples, denoting this plane by Π. The Π plane is simultaneously the back focal plane of the first lens and the front focal plane of the second. The two lenses together form a $4f$ Fourier transform system. We will examine in a later section what happens when the sample is moved out of the Π plane. Throughout this paper, we assume that the sample is of neg-

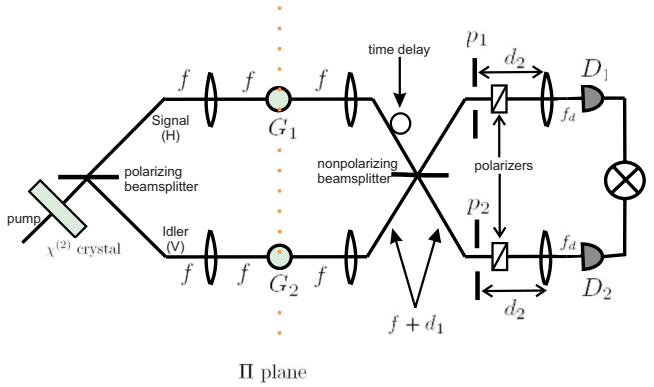

FIG. 1. (Color online) Schematic view of aberration-cancellation setup. (Distances and angles not necessarily drawn in correct proportions.) The horizontally polarized signal travels in the upper branch and experiences modulation G_1, while the vertically polarized idler experiences modulation G_2 in the lower branch. G_1 and G_2 are both located in the plane Π, halfway between the lenses of focal length f. The beam splitter mixes the beams before they reach the detectors D_1 and D_2, which are connected by a coincidence circuit.

ligible thickness compared to all of the other distances involved in the apparatus. We will refer to the photon in the upper branch (branch 1) as the signal and the photon in branch 2 as the idler. The polarizing beam splitter sends the horizontally polarized photon into the upper (signal) branch and the vertically polarized photon into the lower (idler) branch.

Photons are fed into the system by a continuous-wave laser which pumps a $\chi^{(2)}$ nonlinear crystal, leading to collinear type-II parametric down conversion. The frequencies of the two photons are $\Omega_0 \pm \nu$, while the transverse momenta are $\pm\mathbf{q}$. For simplicity, assume the frequency bandwidth is narrow compared to Ω_0. The two photons have total wave numbers $\frac{\Omega_0 \pm \nu}{c}$, which will be approximated by $k=\frac{\Omega_0}{c}$ where appropriate. The down-conversion spectrum is given by

$$\Phi(\mathbf{q},\nu) = \mathrm{sinc}\left[\frac{L\Delta(\mathbf{q},\nu)}{2}\right] e^{i[L\Delta(\mathbf{q},\nu)]/2}. \tag{4}$$

Here, L is the thickness of the nonlinear crystal and for type-II down conversion we have

$$\Delta(\mathbf{q},\nu) = -\nu D + M\hat{\mathbf{e}}_2 \cdot \mathbf{q} + \frac{2|\mathbf{q}|^2}{k_{pump}}. \tag{5}$$

D is the difference between the group velocities of the ordinary and extraordinary waves in the crystal, and M is the spatial walk off in the direction $\hat{\mathbf{e}}_2$ perpendicular to the interferometer plane. The last term in Δ is due to diffraction as the wave propagates through the crystal.

The parametric down-conversion process may be described by a Hamiltonian of the form

$$\hat{H} = i\hbar\chi \hat{a}_s^\dagger \hat{a}_i^\dagger + \mathrm{H.c.}, \tag{6}$$

where $\hat{a}_s$ and $\hat{a}_i$ are annihilation operators for the signal and idler photons. The constant χ includes the amplitude of the classical pump field. Applying the time evolution operator $e^{-i\hat{H}t/\hbar}$ to the vacuum state, we find that the wave function entering the apparatus from the crystal can be written as

$$|\Psi(t)\rangle = (1-|\eta|^2/2)|0\rangle + \eta|\Psi_2\rangle + \eta^2|\Psi_4\rangle + \cdots, \tag{7}$$

where $\eta=\chi t$, and $|\Psi_{2n}\rangle$ represents a term with n photons in the signal mode and n in the idler mode. For parametric down conversion we operate in the regime where $|\eta| \ll 1$ so that terms higher than $|\Psi_2\rangle$ may be neglected. In addition, the vacuum term may be ignored since it will not contribute to coincidence detection. Thus, effectively our wave function is given by

$$|\Psi\rangle \approx |\Psi_2\rangle = \int dq d\nu \Phi(\mathbf{q},\nu)\hat{a}_s^\dagger(\mathbf{q},\Omega_0+\nu)\hat{a}_i^\dagger(-\mathbf{q},\Omega_0-\nu)|0\rangle. \tag{8}$$

Note that G_1 and G_2 could be produced by two separate objects at two separate points in space, in which case we would need to use a polarizing beam splitter (PBS) to separate the incoming beams. Alternatively, G_1 and G_2 could both be produced by a single object which acts differently on the two polarization states, in which case we could dispense with the PBS.

In the detection stage, two bucket detectors D_1 and D_2 are connected in coincidence. We add adjustable irises with aperture functions $p_1(\mathbf{x}_1)$ and $p_2(\mathbf{x}_2)$ in front of the detectors. We will end up taking these apertures to be of infinite width but initially we leave them in for reasons to be explained below. A lens of focal length f_d is placed one focal length in front of each detector. The distances from the Fourier plane of the main part of the apparatus to the aperture and from the aperture to the lens are d_1 and d_2. In order to erase path information for the photons reaching each detector, a polarizer at 45° to the polarization directions of both incoming beams is placed in each path. The two polarizers are oriented orthogonal to each other.

The full transfer function for each branch is [5]

$$H_{j\alpha}(\mathbf{x}_\alpha,\mathbf{q}_j,\omega) = G_j\left(\frac{f}{k}\mathbf{q}_j\right) H_{D_\alpha}(\mathbf{x}_\alpha,\mathbf{q}_j,\omega), \tag{9}$$

where the transfer function of the detection stage is

$$H_{D_\alpha}(\mathbf{x}_\alpha,\mathbf{q}_j,\omega) = e^{ik(d_1+d_2+f_D)} e^{-(ik/2f_D)[(d_2/f_D)-1]\mathbf{x}_\alpha^2} e^{-i(d_1/2k)\mathbf{q}_j^2} \times \tilde{\mathcal{P}}_\alpha\left(\frac{k}{f_D}\mathbf{x}_\alpha - \mathbf{q}_j\right). \tag{10}$$

$\tilde{\mathcal{P}}_\alpha$ is the Fourier transform of the aperture function,

$$\tilde{\mathcal{P}}_\alpha\left(\frac{k}{f_D}\mathbf{x}_\alpha - \mathbf{q}_j\right) = \int d^2x' p_\alpha(\mathbf{x}') e^{-i[(k/f_D)\mathbf{x}_\alpha - \mathbf{q}_j]\cdot\mathbf{x}'}, \tag{11}$$

with $\alpha=\{1,2\}$ labeling the detector and $j=\{s,i\}$ labeling the signal or idler branch. In these expressions, k is the longitudinal wave number, $k=\sqrt{(\omega/c)^2-q^2} \approx \frac{\omega}{c}$ for $|\mathbf{q}| \ll k$.

The nonpolarizing beam splitter mixes the incident beams, so each detector sees a superposition of the signal and idler beams. The positive-frequency part of the field entering detector α is given by

$$E_\alpha^{(+)}(\mathbf{x}_\alpha,t_\alpha)=\int dqd\omega e^{-i\omega t_\alpha}[H_{s\alpha}(\mathbf{x}_\alpha,\mathbf{q}_s,\omega)\hat{a}_s(\mathbf{q}_s,\omega)+H_{i\alpha}(\mathbf{x}_\alpha,\mathbf{q}_i,\omega)\hat{a}_i(\mathbf{q}_i,\omega)]. \tag{12}$$

Using this field, we can compute the amplitude for coincidence detection:

$$\begin{aligned}A(\mathbf{x}_1,\mathbf{x}_2,t_1,t_2)&=\langle 0|E_1^{(+)}(\mathbf{x}_1,t_1)E_2^{(+)}(\mathbf{x}_2,t_2)|\Psi\rangle\\&=\int d^2qd\nu\Phi(\mathbf{q},\nu)\\&\times[e^{-i(\Omega_o+\nu)t_1}e^{-i(\Omega_o-\nu)t_2}H_{s1}(\mathbf{x}_1,\mathbf{q},\nu)\\&\times H_{i2}(\mathbf{x}_2,-\mathbf{q},-\nu)+e^{-i(\Omega_o-\nu)t_1}e^{-i(\Omega_o+\nu)t_2}\\&\times H_{i1}(\mathbf{x}_1,-\mathbf{q},-\nu)H_{s2}(\mathbf{x}_2,\mathbf{q},\nu)],\end{aligned} \tag{13}$$

where $H_{j\alpha}(\mathbf{x}_\alpha,\mathbf{q}_j,\Omega_0\pm\nu)$ have been abbreviated by $H_{j\alpha}(\mathbf{x}_\alpha,\mathbf{q}_j,\pm\nu)$.

The coincidence rate as a function of time delay τ is

$$R(\tau)=\int d^2x_1d^2x_2dt_1dt_2|A(\mathbf{x}_1,\mathbf{x}_2,t_1,t_2)|^2. \tag{14}$$

As was shown in [11], $R(\tau)$ will generically be of the form

$$R(\tau)=R_0\left[1-\Lambda\left(1-\frac{2\tau}{DL}\right)W(\tau)\right]. \tag{15}$$

where $\Lambda(x)$ is the triangular function:

$$\Lambda(x)=\begin{cases}1-|x|, & |x|\le 1\\ 0, & |x|>1\end{cases}. \tag{16}$$

The τ-independent background term R_0 and τ-dependent modulation term $W(\tau)$ were calculated in [5] to be:

$$\begin{aligned}R_0=\int d^2qd^2q'\ \mathrm{sinc}[ML\mathbf{e}_2\cdot(\mathbf{q}-\mathbf{q}')]G_1^*\left(\frac{f\mathbf{q}}{k}\right)G_2^*\left(-\frac{f\mathbf{q}}{k}\right)\\\times G_1\left(\frac{f\mathbf{q}'}{k}\right)G_2\left(-\frac{f\mathbf{q}'}{k}\right)\widetilde{\mathcal{P}}_1(\mathbf{q}-\mathbf{q}')\\\times\widetilde{\mathcal{P}}_2(-\mathbf{q}+\mathbf{q}')e^{-(iML/2)\mathbf{e}_2\cdot(\mathbf{q}-\mathbf{q}')}e^{2i(d_1/k_{pump})(\mathbf{q}^2-\mathbf{q}'^2)},\end{aligned} \tag{17}$$

$$\begin{aligned}W(\tau)=\frac{1}{R_0}\int d^2qd^2q'\ \mathrm{sinc}\left[MLe_2\cdot(\mathbf{q}+\mathbf{q}')\Lambda\left(1-\frac{2\tau}{DL}\right)\right]\\\times G_1^*\left(\frac{f\mathbf{q}}{k}\right)G_2^*\left(-\frac{f\mathbf{q}}{k}\right)G_1\left(\frac{f\mathbf{q}'}{k}\right)G_2\left(-\frac{f\mathbf{q}'}{k}\right)\\\times\widetilde{\mathcal{P}}_1(\mathbf{q}+\mathbf{q}')\widetilde{\mathcal{P}}_2(-\mathbf{q}-\mathbf{q}')e^{-(iM/D)\tau\mathbf{e}_2\cdot(\mathbf{q}-\mathbf{q}')}\\\times e^{2i(d_1/k_{pump})(\mathbf{q}^2-\mathbf{q}'^2)}.\end{aligned} \tag{18}$$

Now let the apertures be large, so that the $\widetilde{\mathcal{P}}_j$ become delta functions, reducing Eqs. (17) and (18) to

$$R_0=\int d^2q\left|G_1\left(\frac{f\mathbf{q}}{k}\right)G_2\left(-\frac{f\mathbf{q}}{k}\right)\right|^2, \tag{19}$$

$$\begin{aligned}W(\tau)=\frac{1}{R_0}\int d^2qe^{-(2iM\tau/D)\mathbf{e}_2\cdot\mathbf{q}}G_1^*\left(\frac{f\mathbf{q}}{k}\right)G_1\left(-\frac{f\mathbf{q}}{k}\right)\\\times G_2^*\left(-\frac{f\mathbf{q}}{k}\right)G_2\left(\frac{f\mathbf{q}}{k}\right).\end{aligned} \tag{20}$$

Suppose that $G_j(\mathbf{x})=t_j(\mathbf{x})e^{i\phi_j(\mathbf{x})}$, where t_j is real and the effects of aberrations are contained in the phase factor ϕ_j. Disregarding the background term for the moment, we see from the presence in Eq. (20) of the factors

$$G_1^*\left(\frac{f\mathbf{q}}{k}\right)G_1\left(-\frac{f\mathbf{q}}{k}\right)=t_1^*\left(\frac{f\mathbf{q}}{k}\right)t_1\left(-\frac{f\mathbf{q}}{k}\right)e^{-i[\phi_1(f\mathbf{q}/k)-\phi_1(-f\mathbf{q}/k)]} \tag{21}$$

that even-order aberration terms arising from sample 1 cancel from the modulation term. The even-order aberrations from sample 2 cancel similarly. This is the even-order cancellation effect of Refs. [4,5].

It should be remarked that the setup of Fig. 1 may be simplified by removing the lenses immediately in front of the detectors. We have left both the lenses and the apertures in the setup because together they lead to the presence of the Fourier-transformed aperture functions $\widetilde{\mathcal{P}}_j$ in Eqs. (17) and (18); the delta functions that arise from the $\widetilde{\mathcal{P}}_j$ when the apertures become large will serve as convenient bookkeeping devices in the following sections as we trace various terms back to their origins. If we choose to simplify the apparatus and remove the lenses, then Eq. (10) will be replaced by

$$\begin{aligned}H_{D_\alpha}(\mathbf{x}_\alpha,\mathbf{q}_j,\omega)=e^{ik(d_1+d)}e^{-id_1\mathbf{q}_j^2/2k}\\\times\int p(\mathbf{x}')e^{(ik/2d)(\mathbf{x}'-\mathbf{x}_\alpha)^2}e^{i\mathbf{q}\cdot\mathbf{x}'}d^2x',\end{aligned} \tag{22}$$

where d is the total aperture-to-detector distance, with corresponding changes in Eqs. (17) and (18). However, in the large-aperture limit this does not affect the coincidence rate, which will still be given by expressions (15), (19), and (20).

II. ALL-ORDER CANCELLATION

A. Aberration cancellation to all orders

Now, consider the background term R_0 in Eq. (19). It depends on G_1 and G_2 only through the squared modulus of each. Thus any phase changes introduced by G_1 or G_2 cancel completely; in particular, the background term R_0 exhibits cancellation of aberrations of *all* orders not just even orders. In the current situation, this R_0 is of no importance, simply being a constant and having no effect on the τ-dependence of the correlation. However, the fact that all orders of aberration can be cancelled in the background term raises the question as to whether it can be arranged for this to happen in the modulation term as well.

It turns out that the answer to this question is positive: it is possible to use this apparatus to cancel *all* aberrations induced by a thin sample, of both even and odd orders. The means for doing so is evident from examining Eq. (20). Sup-

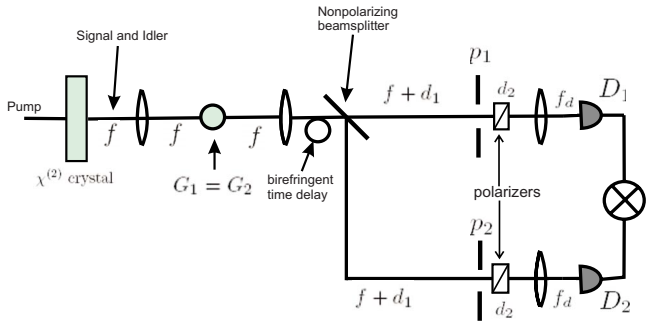

FIG. 2. (Color online) Schematic view of apparatus in Fig. 1, with G_1 set equal to G_2. (Distances and angles not necessarily drawn in correct proportions.) Here G_1 and G_2 are being produced by a single object. The signal and idler are collinear. It is also possible for G_2 and G_2 to be produced by two identical but spatially separate objects interacting with noncollinear signal and idler.

pose that $G_1(\mathbf{x})=G_2(\mathbf{x})$, as shown schematically in Fig. 2. This can happen in one of two ways: either two identical samples may be placed in the two arms or it may be arranged so that the two beams both pass through the same sample; in either case it is necessary for the sample to act in the same manner on both polarization states. The second possibility will usually be of more practical interest, since identical samples will often not be available. For $G_1=G_2$, Eqs. (17) and (18) give

$$R_0 = \int d^2q \left| G_1\left(\frac{f\mathbf{q}}{k}\right) G_1\left(-\frac{f\mathbf{q}}{k}\right)\right|^2, \tag{23}$$

$$W(\tau) = \frac{1}{R_0}\int d^2q e^{-2iM\tau \widehat{\mathbf{e}_2}\cdot\mathbf{q}/D} \left| G_1\left(\frac{f\mathbf{q}}{k}\right) G_1\left(-\frac{f\mathbf{q}}{k}\right)\right|^2. \tag{24}$$

Setting $G_1(\mathbf{x})=t(\mathbf{x})e^{i\phi(\mathbf{x})}$, we see that all phases now cancel from the τ-modulated term W. Thus, *all aberrations induced by the sample, of any order, will completely cancel from the coincidence rate.*

B. Condition for all-ordercancellation

Up to this point, we have assumed that the objects providing the modulation were located in the plane labeled Π in Fig. 1. Now we consider what happens if the modulation objects (the samples) are moved out of the Π plane by some distance $z\neq 0$. Consider a single arm of the apparatus, as shown in Fig. 3. We will take the distance z from Π to be positive if the sample is moved toward the source, and negative if moved toward the detector. Now, the impulse response functions for the first and second lens respectively in each branch of the system will be

$$h_1(\boldsymbol{\xi},\mathbf{y}) = \frac{1}{i\lambda f}\frac{1}{i\lambda(f-z)}\int e^{ik/2\{[\mathbf{y}^2/(f-z)]+(\boldsymbol{\xi}^2/f)\}} e^{ik/2[1/(f-z)]\mathbf{x}'^2} \times e^{-ik\mathbf{x}'\cdot\{[\mathbf{y}/(f-z)]+(\boldsymbol{\xi}/f)\}} d^2x' \tag{25}$$

$$h_2(\mathbf{y},\mathbf{x}) = \frac{1}{i\lambda f}\frac{1}{i\lambda(f+z)}\int e^{ik/2\{[\mathbf{y}^2/(f+z)]+(\mathbf{x}^2/f)\}} e^{ik/2[1/(f+z)]\mathbf{x}''^2} \times e^{-ik\mathbf{x}''\cdot\{[\mathbf{y}/(f+z)]+(\mathbf{x}/f)\}} d^2x'' \tag{26}$$

$\mathbf{y}$, $\mathbf{x}'$, $\mathbf{x}''$, and $\boldsymbol{\xi}$ are the transverse distances at the points shown in Fig. 2. The integrals can be carried out, giving us the result that

$$h_1(\boldsymbol{\xi},\mathbf{y}) = \frac{1}{i\lambda f} e^{(ik/2f)[(z\boldsymbol{\xi}^2/f)-2\boldsymbol{\xi}\cdot\mathbf{y}]}, \tag{27}$$

$$h_2(\mathbf{y},\mathbf{x}) = \frac{1}{i\lambda f} e^{-(ik/2f)[(z\mathbf{x}^2/f)+2\mathbf{x}\cdot\mathbf{y}]} = -h_1^*(-\mathbf{x},\mathbf{y}). \tag{28}$$

So the impulse response for one branch of the apparatus from source to Fourier plane (not including the detection stage) is

$$h_j'(\boldsymbol{\xi},\mathbf{x}) = \int h_1(\boldsymbol{\xi},\mathbf{y}) G_j(\mathbf{y}) h_2(\mathbf{y},\mathbf{x}) d^2y, \tag{29}$$

$$= \frac{e^{(ik/2f^2)z(\boldsymbol{\xi}^2-\mathbf{x}^2)}}{(i\lambda f)^2}\int e^{-(ik/f)(\boldsymbol{\xi}+\mathbf{x})\cdot\mathbf{y}} G_j(\mathbf{y}) d^2y. \tag{30}$$

Fourier transforming to find the transfer function leads to

$$H_j'(\mathbf{x},\mathbf{q},\omega) = \int h(\boldsymbol{\xi},\mathbf{x}) e^{i\mathbf{q}\cdot\boldsymbol{\xi}} d^2\boldsymbol{\xi} \tag{31}$$

$$= \frac{1}{(i\lambda f)^2}\int d^2y G_j(\mathbf{y}) e^{-(ik/f)(\mathbf{x}\cdot\mathbf{y})} e^{-(ik/2f^2)(z\mathbf{x}^2)} \times \int d^2\boldsymbol{\xi} e^{(ikz/2f^2)\boldsymbol{\xi}^2} e^{i\boldsymbol{\xi}(\mathbf{q}-k\mathbf{x}/f)} \tag{32}$$

$$= -\frac{1}{\lambda z} e^{-i\mathbf{q}\cdot\mathbf{x}}\int d^2y G_j\left(\mathbf{y}+\frac{f\mathbf{q}}{k}\right) e^{-(ik/f)(\mathbf{x}\cdot\mathbf{y})} \times e^{(-ik/2z)\mathbf{y}^2} e^{-(ikz/2f^2)\mathbf{x}^2}. \tag{33}$$

Previously, for $z=0$, this transfer function was simply given by

$$H_j'(\mathbf{x},\mathbf{q},\omega) = (\text{constants}) G_j\left(\frac{f\mathbf{q}}{k}\right) e^{-i\mathbf{q}\cdot\mathbf{x}}. \tag{34}$$

Therefore, for $z\neq 0$, we must make the replacement (up to overall constants) (Fig. 3)

$$G\left(\frac{f\mathbf{q}}{k}\right) \to \int d^2y G\left(\mathbf{y}+\frac{f\mathbf{q}}{k}\right) e^{-(ik/f)(\mathbf{x}\cdot\mathbf{y})} e^{(-ikz/2f^2)\mathbf{x}^2}\left(\frac{1}{z} e^{(-ik/2z)\mathbf{y}^2}\right) \tag{35}$$

in all previous results, and Eq. (9) now involves an integral instead of a simple product. (For $z=0$, the factors in the last set of parentheses become proportional to $\delta^{(2)}(\mathbf{y})$, leading back to the previous results.) In particular, in Eqs. (23) and (24), the factor $|G_1(\frac{f\mathbf{q}}{k})|^2$ becomes

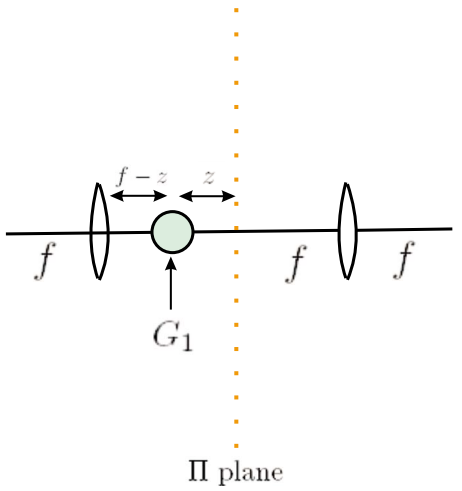

FIG. 3. (Color online) Blown up version of a portion of one branch from apparatus of Fig. 1 (or Fig. 2), with the object moved a distance z out of the central plane, Π.

$$\int d^2y d^2y' G_1\left(\mathbf{y}+\frac{f}{f_D}\mathbf{x}\right)G_1^*\left(\mathbf{y}'+\frac{f}{f_D}\mathbf{x}\right)e^{-(ik/2z)(\mathbf{y}^2-\mathbf{y}'^2)}. \tag{36}$$

Clearly, the phase of G_1 no longer cancels out of this expression since nothing forces $\mathbf{y}$ to equal $\mathbf{y}'$. The arguments of the two factors of G_1 are now unrelated, so that aberration cancellation no longer occurs.

So any cancellation that occurs can hold exactly *only* for phases arising in the Π-plane of the Fourier transform system. The cancellation is approximate in the vicinity of this plane. For samples of finite thickness, the degree of approximate cancellation will diminish as the thickness increases.

Defining $\boldsymbol{\epsilon}=\mathbf{y}-\mathbf{y}'$, the exponential term in Eq. (36) becomes

$$e^{-(ik/2z)(2\boldsymbol{\epsilon}\cdot\mathbf{y}-\boldsymbol{\epsilon}^2)}. \tag{37}$$

Assuming that $G_1^*(\mathbf{y}-\boldsymbol{\epsilon}+\frac{f}{f_d}\mathbf{x})$ is slowly varying in $\boldsymbol{\epsilon}$ compared to the variation of the exponential, we may obtain an estimate of the distance z over which the sample may be moved out of the plane while still maintaining a high degree of aberration cancellation. The aberration cancels when $\boldsymbol{\epsilon}=0$, so we may use the maximum size of $\boldsymbol{\epsilon}$ as a measure of the degree of failure of the aberration cancellation. As $z\to 0$, the rapid oscillations of the exponential term cause the integral of Eq. (36) to go to zero, unless $k|2\boldsymbol{\epsilon}\cdot\mathbf{y}-\boldsymbol{\epsilon}^2|$ also goes to zero at least as fast as $|z|$. So, we must have

$$|2\boldsymbol{\epsilon}\cdot\mathbf{y}-\boldsymbol{\epsilon}^2| \lesssim \left|\frac{z}{k}\right| \sim |z\lambda|. \tag{38}$$

From this, we have

$$|z| \sim \frac{\epsilon_M|\mathbf{y}|}{\lambda}, \tag{39}$$

where ϵ_M is the maximum value of $\boldsymbol{\epsilon}$. Let r_s be the maximum illuminated radius of the sample. Then, by requiring that $|\epsilon_M| \ll r_s$, we have the estimate that

$$|z| \ll \frac{r_s^2}{\lambda}. \tag{40}$$

This is essentially a limit on how far from stationarity we may be and still safely apply a stationary-phase approximation. Actually, we may make this limit a bit more precise. Since two-sample points $\mathbf{y}$ and $\mathbf{y}'$ inside the Airy disk of the lens cannot be distinguished from each other, we may require that $|\epsilon_M| \sim R_{airy}$, where

$$R_{airy} = \frac{1.22f\lambda}{a} \tag{41}$$

is the radius of the Airy disk. By substituting this into Eq. (39), we can thus conclude that, at most, the order of magnitude of $|z|$ may be given by

$$|z| \lesssim \frac{fr_s}{a}. \tag{42}$$

Taking for example the values $r_s \sim 10^{-4}$ m, $a \sim 1$ cm, $f \sim 10$ cm, and $\lambda \sim 10^{-7}$ m, this gives us an upper limit of about 1 mm.

C. Comparison with dispersion cancellation

The idea of aberration cancellation via entangled-photon interferometry arose in analogy to the similar dispersion-cancellation effect [6,7]. It is known that even-order and odd-order dispersion effects may be separated so that either even-order terms or odd-order terms may be cancelled [12] but that it is impossible to simultaneously cancel both sets of terms together. Thus, it is a surprise that in the case of aberrations such a simultaneous cancellation should be possible.

The fact that aberration cancellation only occurs in a single plane sheds some light on the difference between aberration cancellation and dispersion cancellation. Aberrations are caused by phase differences between different points in a plane *transverse to* the propagation direction of the light, while dispersion comes about as a result of phase differences accumulating *along* the propagation direction. We have managed to cancel all orders of aberration produced by *a single transverse plane*. But since dispersive effects accumulate longitudinally, we cannot arrange their cancellation in all of the infinite number of transverse planes the photon travels through; thus, although even-order and odd-order dispersion may each occur separately, simultaneous all-order dispersion cancellation will not occur.

A more physical explanation can be given for the inability in principle to cancel all orders of dispersion. Suppose that the index of refraction is expanded about some frequency ω_0,

$$n(\omega) = n_0 + n_1(\omega-\omega_0) + n_2(\omega-\omega_0)^2 + \cdots. \tag{43}$$

The phase and group velocities are

$$v_p = \frac{c}{n(\omega)}, \tag{44}$$

$$v_g = \left(\frac{dk}{d\omega}\right)^{-1} = c\left[n(\omega) + \omega\frac{dn(\omega)}{d\omega}\right]^{-1}$$
$$= c[n_0 + 2n_1(\omega-\omega_0) + 3n_2(\omega-\omega_0)^2 + \cdots]^{-1}. \quad (45)$$

If both the odd-order and even-order dispersion coefficients vanish simultaneously (including the zeroth-order term), then $n(\omega)$ and $\frac{dn}{d\omega}$ both vanish. In consequence, the phase and group velocities both diverge. This is in contradiction to special relativity, which requires a finite group velocity. In contrast, no similar obstacle exists to prevent the spatially distributed phase shift $\phi(\mathbf{x})$ from vanishing, so there is no fundamental principle preventing all-order aberration cancellation.

One further point to note is that the dispersive and aberrative cases considered here are not entirely analogous, in the sense that one is not simply obtained from the other by interchanging time and space. In the aberration case, the phase is a function of the transverse position $\mathbf{x}$ in the physical coordinate space. In contrast, for the dispersive case the phase is due to a *frequency*-dependent index of refraction; i.e., the source of the effect is in the *Fourier transform space*, not in the (temporal) coordinate space. However, in both cases the cancellation occurs in the Fourier space. Thus, for aberration cancellation an optical Fourier transform system is required to move from the coordinate space (where the source of aberration is) to the Fourier space (where the cancellation occurs). For the dispersive case, the source of the dispersion already operates in the Fourier space so it is not necessary to introduce an extra Fourier transform via the optical system.

III. PHYSICAL INTERPRETATION

We now wish to develop a better understanding of how aberration cancellation occurs in the polarization-based coincidence interferometer that we are using to illustrate this effect. Let $\mathbf{q}$ and $\mathbf{q}'$ be the ingoing and outgoing momenta in the upper branch at the beam splitter. The ingoing and outgoing momenta for the lower branch will be $-\mathbf{q}$ and $-\mathbf{q}'$, as in Figs. 4 and 5 below.

Note first of all that the coincidence detection amplitude in transverse momentum space may be written in the form $A(\mathbf{q})=A_r(\mathbf{q})+A_t(\mathbf{q})$, where A_t represents the amplitude for both photons to be transmitted at the beam splitter and A_r is the amplitude for both to be reflected. The counting rate involves the integrated and squared amplitude; if the momenta $\mathbf{q}$ and $\mathbf{q}'$ were independent variables, we could write this as

$$\left|\int A(\mathbf{q})d^2q\right|^2 = \int A(\mathbf{q})A^*(\mathbf{q}')d^2qd^2q', \quad (46)$$

which has terms $A_r(\mathbf{q})A_t(\mathbf{q}')^*+A_t(\mathbf{q})A_r^*(\mathbf{q}')$ involving interference between reflection and transmission (see Fig. 4), as well as noninterference terms $A_r(\mathbf{q})A_r(\mathbf{q}')^*+A_t(\mathbf{q})A_t^*(\mathbf{q}')$ (Fig. 5). However, $\mathbf{q}$ and $\mathbf{q}'$ are not independent variables; momentum conservation and the fact that the photons are produced from down conversion together force the requirement $\mathbf{q}'=\pm\mathbf{q}$. These constraints are explicitly enforced in the current context by the factors of $\tilde{\mathcal{P}}_j$ in Eqs. (17) and (18), which become delta functions in the large-aperture limit. The delta functions sew together the amplitudes A_r and A_t as shown in the figures.

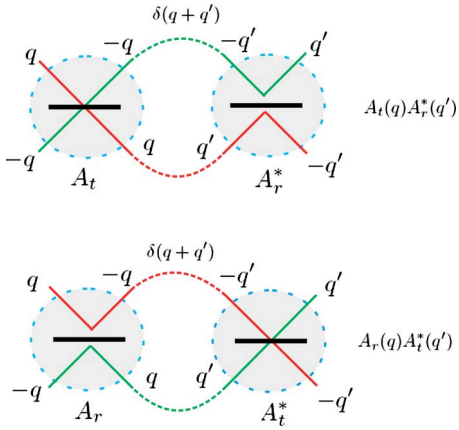

FIG. 4. (Color online) Schematic representation of interference terms. In the squared amplitude $\int dqdq'A(q)A^*(q')$, the part of the amplitude in which both photons undergo reflection at the beam splitter (A_r) interferes with the portion in which both photons are transmitted at the beam splitter (A_t). For these terms, $q=-q'$, due to the delta function that connects the amplitudes.

Suppose again that $G_j(\mathbf{x})=t_j(\mathbf{x})e^{i\phi_j(\mathbf{x})}$. Since we are unconcerned with effects related to amplitude modulation we henceforth set $t_j(\mathbf{x})=1$. Examining Eqs. (17) and (18), we then note that even-order and odd-order aberration cancellation arise from different sources. Even-order cancellation arises from the combination of the following ingredients:

(A1) the Fourier transforming property of the lens in the focal plane. This converts the transverse momentum entanglement into spatial entanglement in the Π plane.

(A2) The condition $\mathbf{q}=-\mathbf{q}'$ satisfied by the nonbackground half of the terms (those that comprise W). These

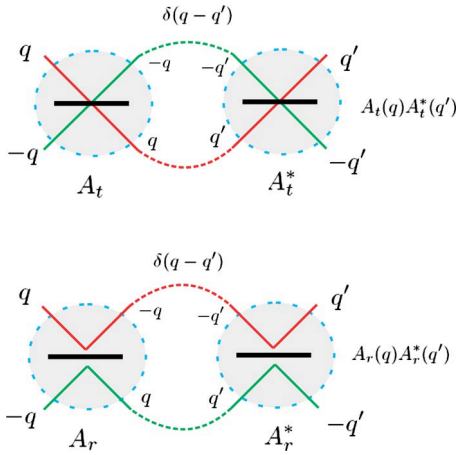

FIG. 5. (Color online) Schematic representation of noninterference terms. In the top part of the figure the transmission portion of the amplitude A_t interacts only with itself, while in the bottom part the same is true of the reflection amplitude A_r. For these terms, $q=q'$

terms arise from the interference part of the squared amplitude, as in Fig. 4.

(A3) The $G_j(\frac{f\mathbf{q}}{k})G_j^*(\frac{f\mathbf{q}'}{k})$ structure that arises from taking the absolute square of the amplitude to find counting rates in quantum mechanics ($j=1,2$). Combined with the momentum constraint of A2, this becomes $G_j(\frac{f\mathbf{q}}{k})G_j^*(-\frac{f\mathbf{q}}{k})=e^{i[\phi_j(\mathbf{q})-\phi_j(-\mathbf{q})]}$.

In contrast, odd-order cancellation occurs when the following combination of ingredients is present:

(B1) the Fourier transforming action of the lens, as in A1;

(B2) for every photon of transverse momentum $\mathbf{q}$ there is a photon of $-\mathbf{q}$ present due to down conversion; and

(B3) $G_1=G_2$ so that the product $G_1(\frac{fq}{k})G_2(-\frac{f\mathbf{q}}{k})$ becomes $G_1(\frac{f\mathbf{q}}{k})G_1(-\frac{f\mathbf{q}}{k})=e^{i[\phi_1(\mathbf{q})+\phi_1(-\mathbf{q})]}$. (Note that the cancellation is taking place between different terms of Eq. (20) than were involved in the cancellation of A3.)

In order to have all-order cancellation, there are two possibilities. Either both of the above sets of conditions may be satisfied simultaneously, or else a third set of conditions may be satisfied:

(C1) same as A1 and B1;

(C2) the condition $\mathbf{q}=\mathbf{q}'$ must be satisfied, as in the background term R_0; this occurs in the noninterference terms of Fig. 5; and

(C3) similar to A3, the $G_j(\frac{f\mathbf{q}}{k})G_j^*(\frac{f\mathbf{q}'}{k})$ structure arises from the quantum-mechanical absolute squaring of the amplitude. But now, coupled with C2, we have $G_j(\frac{f\mathbf{q}}{k})G_j^*(\frac{f\mathbf{q}}{k})=e^{i[\phi_j(\mathbf{q})-\phi_j(\mathbf{q})]}=1$, giving cancellation of all orders.

In A3 and C3 the phase from a single arm of the interferometer cancels with itself, whereas B3 is a cancellation between the two different (but identical in this case) arms. Cases A and B both involve interference between the amplitudes A_r and A_t (shown schematically in Fig. 4), while case C comes from the noninterference terms of Fig. 5 and so will occur even if only one of the two amplitudes A_r and A_t is present.

IV. CONCLUSIONS

To summarize the main results of this paper, for the apparatus of Fig. 1 we have found that:

(i) even-order aberrations induced by the samples G_1 and G_2 cancel;

(ii) if the two beams overlap so that $G_1=G_2$, then *all* orders of aberration cancel; and

(iii) these cancellations only occur if G_1 and G_2 are confined to the $z=0$ plane.

These results open up the possibility of using quantum interferometry to eliminate the effects of sample-induced aberration in experiments using temporal correlation-based methods such as dynamical light scattering or fluorescence correlation spectroscopy. Through the continued study of aberration cancellation and dispersion cancellation, it is hoped that a better understanding of the effects of objects or materials placed in an optical system, and better methods of controlling those effects, will gradually emerge. The results reported here are one more step along that path.

The effects described in this paper make essential use of the spatial entanglement (or equivalently the transverse momentum entanglement) between the photons in the down-conversion pair. In contrast, the frequency entanglement played no essential role. Similarly, the anticorrelation of the polarizations was used primarily to control the paths of the photons and then to erase the path information; but these functions could be accomplished by other means. So only the spatial entanglement was essential. On the other hand, it is the frequency entanglement that is essential for dispersion cancellation. A question for future investigation is whether use of the simultaneous entanglement of frequency, momentum, and polarization variables (so-called *hyperentanglement*) may allow control over further optical effects of materials.

ACKNOWLEDGMENTS

This work was supported by a U. S. Army Research Office (ARO) Multidisciplinary University Research Initiative (MURI) Grant; by the Bernard M. Gordon Center for Subsurface Sensing and Imaging Systems (CenSSIS), an NSF Engineering Research Center; by the Intelligence Advanced Research Projects Activity (IARPA) and ARO through Grant No. W911NF-07-1-0629.

[1] M. Born and E. Wolf, *Principles of Optics*, 7th ed. (Cambridge University Press, New York, 1999).

[2] H. A. Buchdahl, *Optical Aberration Coefficients* (Dover Publications, New York, 1968).

[3] J. C. Wyant and K. Creath, *Basic Wave-Front Aberration Theory for Optical Metrology*, in Applied Optics and Optical Engineering (Academic Press, New York, 1992), Vol. XI.

[4] C. Bonato, A. V. Sergienko, B. E. A. Saleh, S. Bonora, and P. Villoresi, Phys. Rev. Lett. **101**, 233603 (2008).

[5] C. Bonato, D. S. Simon, P. Villoresi, and A. V. Sergienko, Phys. Rev. A **79**, 062304 (2009).

[6] J. D. Franson, Phys. Rev. A **45**, 3126 (1992).

[7] A. M. Steinberg, P. G. Kwiat, and R. Y. Chiao, Phys. Rev. Lett. **68**, 2421 (1992).

[8] B. J. Berne and R. Pecora, *Dynamic Light Scattering; with Applications to Chemistry, biology, and Physics* (Wiley, New York, 1976).

[9] *Dynamic Light Scattering: Applications to Photon Correlation Spectroscopy*, edited by R. Pecora (Plenum Press, New York, 1985).

[10] S. Maiti, U. Haupts, and W. W. Webb, Proc. Natl. Acad. Sci. U.S.A. **94**, 11753 (1997).

[11] M. H. Rubin, D. N. Klyshko, Y. H. Shih, and A. V. Sergienko, Phys. Rev. A **50**, 5122 (1994).

[12] O. Minaeva, C. Bonato, B. E. A. Saleh, D. S. Simon, and A. V. Sergienko, Phys. Rev. Lett. **102**, 100504 (2009).

Correlated-Photon Imaging with Aberration Cancellation

D.S. Simon[1] and A.V. Sergienko[1,2]

[1]*Dept. of Electrical and Computer Engineering, Boston University, 8 Saint Mary's St., Boston, MA 02215*

[2]*Dept. of Physics, Boston University, 590 Commonwealth Ave., Boston, MA 02215*

We discuss an apparatus that is capable of producing correlated-photon images that are free of object-induced aberration. We show that both quantum-entangled and classically correlated light sources are capable of producing the desired spatial-aberration cancellation.

PACS numbers: 42.30.Va,42.15.Fr,42.30.Kq

I. INTRODUCTION

Correlated-photon imaging, also known as "ghost" imaging, in which coincidence measurements are used to form images via photons that never interacted with the object being viewed, has been a topic of great interest since its discovery using entangled photon pairs [1]. It has since been found that most aspects of ghost imaging can be simulated using spatially-correlated classical light [2, 3], including thermal and speckle sources [4, 5, 6, 7, 8, 9].

Separately, it has been demonstrated that the entangled photon pairs produced in spontaneous parametric downconversion (SPDC) may also be used to cancel some of the effects of frequency dispersion [10, 11, 12] or spatial dispersion (aberration) [13, 14, 15].

In [15], it was pointed out that it is possible to construct a device such that if an object is placed in a particular plane then all phase shifts induced by that object, including all orders of aberration induced by it, will cancel. The goal here is to make use of that observation for imaging. We show that this may be achieved by a simple variation of the traditional ghost imaging apparatus of figure 1. We then show that, although an entangled source was required for the temporal correlation experiments discussed in [13, 14, 15], only a classical source with transverse spatial correlation is required for imaging.

The outline of the paper is as follows. In section II, we review ghost imaging and aberration cancellation. In section III we discuss aberration-cancelled ghost imaging with an entangled light source, followed by a similar discussion with a classical source in section IV. We discuss an important technical point about the need for lenses in front of the detectors in section V, with conclusions in section VI.

II. CORRELATED-PHOTON IMAGING AND ABERRATION CANCELLATION

A. Correlated-photon imaging

Correlated-photon or "ghost" imaging [1] is done with an apparatus like the one depicted schematically in figure 1. In the original version, the correlated photon source is a $\chi^{(2)}$ nonlinear crystal pumped by a laser, leading to spontaneous parametric downconversion. Entangled photon pairs with anticorrelated momentum components $\mathbf{q}$ and $-\mathbf{q}$ transverse to the propagation direction travel along the two arms of the apparatus. The object to be viewed is placed in arm 2 (the upper branch), followed by a large bucket detector, D_2. The detector's area is integrated over, so D_2 can not record any information on the position or momentum of the photon that reached the object; all this detector is able to tell us is whether the photon reached the detector unimpeded, or whether its passage was blocked by an object. In the other branch of the apparatus there is no object, and all of the photons reach a CCD camera or array of pointlike detectors without hindrance. A coincidence circuit is used to record a count every time a photon detection occurs simultaneously (within the coincidence time window) at each detector. By plotting the coincidence rate as a function of position $\mathbf{x}_1$ in detector 1, we build up an image of the object. This is true even though photons that actually encountered the object in branch 2 left no record of the object's position, and the photons in branch 1 that do carry position information never encounter the object.

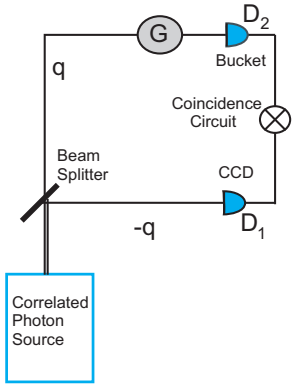

FIG. 1: *Schematic depiction of correlated-photon imaging setup. The photons in the two arms have anticorrelated transverse momenta* $\pm\mathbf{q}$.

The crucial ingredient is the spatial correlation of the downconverted photon pair. The question arose as to whether the entanglement of the photons was necessary,

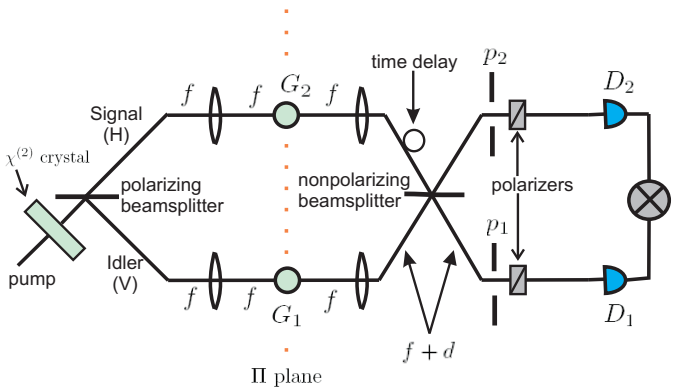

FIG. 2: *Schematic of interferometer with even-order aberration-cancellation. Large bucket detectors D_1 and D_2 are integrated over.*

or if a classical source with anticorrelated transverse momenta could mimic the effect. It was found [2, 3] that this was indeed possible. The correlated light source in this case consists of a beam steering modulator (a rotating mirror, for example) which directs a classical light beam through a range of $\mathbf{q}$ vectors, illuminating different spots on the object. The beamsplitter then turns the single beam of transverse momentum $\mathbf{q}$ into a pair of beams with momenta $\mathbf{q}$ and $-\mathbf{q}$. The results were similar to those with the entangled source, but with half the visibility. It was later shown that thermal and speckle sources may also lead to ghost imaging ([4, 5, 6, 7, 8, 9]).

B. Aberration Cancellation in Quantum Interferometry

Consider the setup shown in figure 2 [13, 14, 15]. Each branch contains a 4f Fourier transform system with lenses of focal length f and a thin sample that provides modulation $G_j(\mathbf{y})$ of the beam, where $j = 1, 2$ labels the branch, and $\mathbf{y}$ is the position in the plane transverse to the axis. The goal is to cancel sample-induced optical aberrations (position-dependent phase shifts produced by the G_j). The case where there is a sample only in one branch may be included by simply setting $G = 1$ in the other branch. The plane containing the samples, which we denote by the letter Π is simultaneously the back focal plane of the first lens and the front focal plane of the second. Time delay τ is inserted in one branch. The light may be either transmitted through each sample, or reflected off of it.

In the detection stage, two large bucket detectors D_1 and D_2, connected in coincidence, record the arrival of photons, but not their positions. Apertures described by aperture functions $p_1(\mathbf{x}_1)$ and $p_2(\mathbf{x}_2)$ are followed by crossed polarizers at 45° to each beam's polarization, before arriving at the detectors.

A continuous wave laser pumps a $\chi^{(2)}$ nonlinear crystal, leading to type II parametric downconversion. The frequencies of the two photons are $\Omega_0 \pm \nu$, with transverse momenta $\pm\mathbf{q}$. For simplicity, assume the frequency bandwidth is narrow compared to Ω_0. The two photons have total wavenumbers $\frac{\Omega_0 \pm \nu}{c} \approx \frac{\Omega_0}{c}$. The downconversion spectrum is

$$\Phi(\mathbf{q}, \nu) = sinc\left[\frac{L\Delta(\mathbf{q}, \nu)}{2}\right] e^{i\frac{L\Delta(\mathbf{q},\nu)}{2}}, \tag{1}$$

where L is the thickness of the crystal, and

$$\Delta(\mathbf{q}, \nu) = -\nu D + M\hat{\mathbf{e}}_2 \cdot \mathbf{q} + \frac{2|\mathbf{q}|^2}{k_{pump}}. \tag{2}$$

D is the difference between the group velocities of the ordinary and extraordinary waves in the crystal, and M is the spatial walk-off in the direction $\hat{\mathbf{e}}_2$ perpendicular to the interferometer plane. The last term in Δ is due to diffraction as the wave propagates through the crystal. Ignoring the vacuum term and terms of higher photon number, the wavefunction entering the apparatus is approximately the biphoton wavefunction of the downconverted pair, given by

$$|\Psi\rangle = \int d^2q\, d\nu\, \Phi(\mathbf{q}, \nu)\hat{a}_s^\dagger(\mathbf{q}, \Omega_0 + \nu)\hat{a}_i^\dagger(-\mathbf{q}, \Omega_0 - \nu)|0\rangle, \tag{3}$$

where $\hat{a}_s$ and $\hat{a}_i$ are annihilation operators for the signal and idler photons. For collinear pairs, horizontally polarized photons are directed into the upper branch and vertically polarized photons into the lower branch by means of a polarizing beamsplitter. Alternatively, noncollinear pairs could be used with polarizers selecting horizontal (H) polarization in the upper branch and vertical (V) in the lower one. In either case, we will refer to the H photon in the upper branch (branch 2) as the signal and the V photon in branch 1 as the idler.

The coincidence rate is of the generic form [16]

$$R(\tau) = R_0\left[1 - \Lambda\left(1 - \frac{2\tau}{DL}\right)W(\tau)\right], \tag{4}$$

where $\Lambda(x)$ is the triangular function:

$$\Lambda(x) = \begin{cases} 1 - |x|, & |x| \le 1 \\ 0, & |x| > 1 \end{cases} \tag{5}$$

For large apertures, $p_1(\mathbf{x}_1) = p_2(\mathbf{x}_2) \approx 1$; so, as shown in [14], the background and τ-modulation terms are

$$R_0 = \int d^2q \left|G_1\left(\frac{f\mathbf{q}}{k}\right) G_2\left(-\frac{f\mathbf{q}}{k}\right)\right|^2 \tag{6}$$

$$W(\tau) = \frac{1}{R_0}\int d^2q e^{-\frac{2iM\tau}{D}\mathbf{e}_2\cdot\mathbf{q}} \times G_1^*\left(\frac{f\mathbf{q}}{k}\right) G_1\left(-\frac{f\mathbf{q}}{k}\right) G_2^*\left(-\frac{f\mathbf{q}}{k}\right) G_2\left(\frac{f\mathbf{q}}{k}\right), \tag{7}$$

where k is the longitudinal wavenumber.

We are concerned here with the phases introduced by the G_j, not with their effect on amplitude, so we will

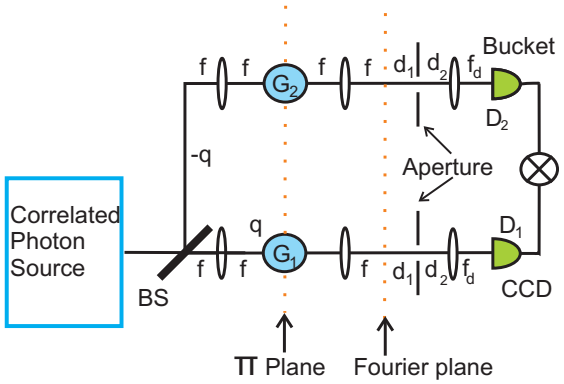

FIG. 3: *Schematic of correlated-photon imaging setup with aberration-cancellation. All orders of aberration cancel.*

assume that the G_j are pure phase objects, $G_j(\mathbf{x}) = e^{i\phi_j(\mathbf{x})}$, with aberration effects contained in the phase factor ϕ_j. The presence in equation (8) of the factors $G_1^*\left(\frac{f\mathbf{q}}{k}\right) G_1\left(-\frac{f\mathbf{q}}{k}\right) = e^{-i[\phi_1(\frac{f\mathbf{q}}{k})-\phi_1(-\frac{f\mathbf{q}}{k})]}$ shows that even-order aberrations arising from sample 1 cancel from the modulation term. The even-order aberrations from sample 2 cancel in a similar manner. This is the even-order cancellation effect demonstrated in [13] and [14]. As pointed out in [15], if $G_1 = G_2$, then both even- and odd-orders cancel simultaneously. These cancellations are exact only for aberrations induced by passage through thin objects in the plane Π, or by reflection from a single surface at the same location.

In the term R_0, both even-order and odd-order aberrations occur even when $G_1 \neq G_2$. For time correlation experiments, this is an unimportant background term; however it is this term that is the foundation of the imaging apparatus described below, since by removing the beamsplitter, the modulation term $W(\tau)$ will be absent.

The physical mechanism of the various possible cancellations are discussed in more detail in [15].

III. ABERRATION-CANCELLED IMAGING WITH ENTANGLED SOURCE

Now we wish to combine aberration cancellation with ghost imaging, in the hybrid device of fig. 3. In this section, we assume that the light source is parametric downconversion from a nonlinear crystal. This new apparatus differs from that of fig. 2 in several respects. First, we have removed the time delay and polarization filters, which are not necessary for imaging purposes. Second, the beam splitter before the detectors has been removed. As described in [15], even-order-only cancellation effects occur due to interference between reflection and transmission amplitudes, while non-interference terms exhibit all-order interference. The beamsplitter needed to produce the interference effects desired in [13, 14, 15] is not needed for the imaging desired here. Without it there will be no interference, so we expect to find all-order cancellation. Finally, one bucket detector (D_1) is replaced by a moveable pointlike detector, or a CCD camera. Whether the remaining beamsplitter is polarizing or not is unimportant. After making these changes and allowing for an arbitrary source of correlated (quantum or classical) light, we arrive at an apparatus that looks very much like the ghost imaging setup of figure 1.

The coincidence rate at location $\mathbf{x}_1$ of D_1 is

$$R(\mathbf{x}_1) = \int d^2x_2 dt_1 dt_2 |A(\mathbf{x}_1, \mathbf{x}_2, t_1, t_2)|^2, \qquad (8)$$

where the transition amplitude is

$$A(\mathbf{x}_1, \mathbf{x}_2, t_1, t_2) = \langle 0|E_1^{(+)}(\mathbf{x}_1, t_1) E_2^{(+)}(\mathbf{x}_2, t_2)|\Psi\rangle. \qquad (9)$$

Taking the two detection apertures described by p_1 and p_2 to be large, we can compute the coincidence rate to be

$$R(\mathbf{x}_1) = \{[B(\mathbf{x}_1) + B(-\mathbf{x}_1)] + [C(\mathbf{x}_1) + C^*(\mathbf{x}_1)]\} \times \left| G_1\left(\frac{f}{f_D}\mathbf{x}_1\right) G_2\left(-\frac{f}{f_D}\mathbf{x}_1\right)\right|^2, \qquad (10)$$

where

$$B(\mathbf{x}_1) = \int d\nu \left|\Phi\left(\frac{k\mathbf{x}_1}{f_D}, \nu\right)\right|^2, \qquad (11)$$

$$C(\mathbf{x}_1) = \int d\nu\, \Phi\left(\frac{k\mathbf{x}_1}{f_D}, \nu\right) \Phi^*\left(-\frac{k\mathbf{x}_1}{f_D}, -\nu\right). \qquad (12)$$

Using eq. (1), these integrals may be evaluated; they turn out to be x_1-independent constants. Sweeping all overall constants into a single constant $\mathcal{R}_0$, we find:

$$R(\mathbf{x}_1) = \mathcal{R}_0 \left| G_1\left(\frac{f}{f_D}\mathbf{x}_1\right) G_2\left(-\frac{f}{f_D}\mathbf{x}_1\right)\right|^2. \qquad (13)$$

We see that only the modulus-squared of each G_j enters into $R(\mathbf{x})$, so that the aberration introduced by each object cancels to all orders. If $G_2 = 1$, then we have an ordinary (non-ghost) image of G_1. On the other hand, if $G_1 = 1$ then we have an inverted ghost image of G_2. In either case, the image is magnified by a factor of $\frac{f}{f_D}$.

IV. ABERRATION-CANCELLED IMAGING WITH CLASSICAL SOURCE

We now replace the downconversion source of the previous section by a classical source of anticorrelated photons, as in [2]. Light entering a beam splitter with transverse momentum $\mathbf{q}$ leads to outgoing beams with anticorrelated momenta $\mathbf{q}$ and $-\mathbf{q}$. If the beam steering modulator produces momentum spectrum $f(\mathbf{q})$, the input state for pairs of photons having the same $\mathbf{q}$ before the beamsplitter will be $\sim \int d^2q F(\mathbf{q}) \hat{a}_p^\dagger(\mathbf{q}) \hat{a}_p^\dagger(\mathbf{q})|0\rangle$, where $\hat{a}_p^\dagger$ is the creation operator for pump photons and $F(\mathbf{q}) \equiv f^2(\mathbf{q})$.

We assume for simplicity that $F(\mathbf{q})$ is an even function, $F(\mathbf{q}) = F(-\mathbf{q})$. Denoting creation operators in the two outgoing branches by $\hat{a}_1^\dagger$ and $\hat{a}_2^\dagger$, the incoming photon pair will produce a state after the beamsplitter given by:

$$\begin{aligned} |\Psi\rangle &= \frac{1}{2}\int d^2qF(\mathbf{q})\left[\hat{a}_1^\dagger(\mathbf{q}) + \hat{a}_2^\dagger(-\mathbf{q})\right]\cdot\left[\hat{a}_1^\dagger(\mathbf{q}) + \hat{a}_2^\dagger(-\mathbf{q})\right]|0\rangle \\ &= \int d^2qF(\mathbf{q})\left[\hat{a}_1^\dagger(\mathbf{q})\hat{a}_2^\dagger(-\mathbf{q}) + \text{additional terms}\right]|0\rangle, \quad (14) \end{aligned}$$

where the "additional terms" do not contribute to coincidence detection. The detection amplitude of eq. (9) is then proportional to

$$\int d^2qF(\mathbf{q})e^{i\mathbf{q}\cdot(\mathbf{x}_1-\mathbf{x}_2)}H_1(\mathbf{q},\mathbf{x}_1)H_2(-\mathbf{q},\mathbf{x}_2), \quad (15)$$

where H_j is the transfer function for branch j. Integrating over D_2, we then have the coincidence rate:

$$R(\mathbf{x}_1) = \left|F\left(\frac{k}{f_D}\mathbf{x}_1\right)G_1\left(\frac{f}{f_D}\mathbf{x}_1\right)G_2\left(-\frac{f}{f_D}\mathbf{x}_1\right)\right|^2. \quad (16)$$

This is similar to the result for the entangled-source apparatus, except modulated by the factor $F\left(\frac{k}{f_D}\mathbf{x}_1\right)$ which is determined by the details of the beam steering modulator. Similarly, for thermal or speckle sources, this factor will arises from the transverse momentum spectrum of the source.

V. ROLE OF THE DETECTION LENS

Consider now the lenses immediately before the detectors in figure 3. With no such detection lens present, the transfer function for branch j would be

$$H_j(\mathbf{q}_j,\mathbf{x}_j) = G_j\left(\frac{f\mathbf{q}_j}{k}\right)e^{i\mathbf{q}\cdot\mathbf{x_j}}, \quad (17)$$

from which we see that the information from each $\mathbf{q}$ value is spread over all $\mathbf{x}$ values. But *with* the lens, eq. (17) becomes

$$H_j(\mathbf{q}_j,\mathbf{x}_j) = G_j\left(\frac{f\mathbf{q}_j}{k}\right)e^{-\frac{ik{\mathbf{x}_j}^2}{2f_D}\left(\frac{d_2}{f_D}-1\right)}e^{-\frac{id_1{\mathbf{q}_j}^2}{2k}}\delta\left(\frac{k\mathbf{x}_j}{f_D}-\mathbf{q_j}\right), \quad (18)$$

so that each $\mathbf{q}$ value is localized at a single point in the detector plane via the delta function. Since each $\mathbf{q}$ value is also matched to a sample point, the localization in the second case defines a correspondence between points in the sample plane and points in the detection plane, allowing reconstruction of an image by the pointlike detector D_1. This can be explicitly verified by computing the coincidence rate with or without the final lenses, i.e. using either eq. (17) or eq. (18). Doing this, we find that without the lens in branch 1 the coincidence rate becomes independent of $\mathbf{x}_1$, making imaging impossible. In contrast, removing the lens in branch 2 has no effect. This makes intuitive sense: since we integrate over $\mathbf{x}_2$ anyway, it does not matter whether the momentum information in this branch is localized or spread over the entire detector.

Thus we arrive at an important technical point: the lens in branch 1 is essential for imaging, whereas the lens before the bucket detector may be removed without harm.

The need for a lens before D_1 may be viewed as follows. The 4f system in either branch transfers modulation G_j from the transverse coordinate space ($\mathbf{x}$) to the Fourier space ($\mathbf{q}$), which is where the aberration cancellation actually takes place (see [15]). The lens in front of D_1 is then needed to transfer the modulation back to coordinate space for imaging.

VI. CONCLUSIONS

In conclusion we have proposed a means of producing ghost imaging of a reflecting surface or thin translucent object with cancellation of object-induced aberrations. The method involves a relatively simple apparatus and can be done with either entangled photon pairs or with a classically-correlated light source. This aberration-cancellation effect has potential for producing improved image quality in a number of applications in biomedical research and other fields.

Acknowledgments

This work was supported by a U. S. Army Research Office (ARO) Multidisciplinary University Research Initiative (MURI) Grant; by the Bernard M. Gordon Center for Subsurface Sensing and Imaging Systems (CenSSIS), an NSF Engineering Research Center; by the Intelligence Advanced Research Projects Activity (IARPA) and ARO through Grant No. W911NF-07-1-0629.

The authors would like to thank Dr. Lee Goldstein and Dr. Robert Webb for some very useful discussions and advice.

[1] T.B. Pittman, Y.H. Shih, D.V. Strekalov, A.V. Sergienko, *Phys. Rev. A* **52** R3429 (1995).
[2] R.S. Bennink, S.J. Bentley, R.W. Boyd, *Phys. Rev. Lett.* **89**, 113601 (2002)
[3] R.S. Bennink, et. al., *Phys. Rev. Lett.* **92**, 033601 (2004)
[4] A. Gatti, E. Brambilla, M. Bache, L.A. Lugiato, *Phys. Rev. A* **70**, 013802 (2004).
[5] Y.J. Cai, S.Y. Zhu, *Phys. Rev. E* **71**, 056607 (2005).
[6] A. Valencia, G. Scarcelli, M. D'Angelo, Y.H. Shih, *Phys. Rev. Lett.* **94**, 063601 (2005).
[7] G. Scarcelli, V. Berardi, Y.H. Shih, *Phys. Rev. Lett.* **96**, 063602 (2006).
[8] F. Ferri *et al.*, *Phys. Rev. Lett.* **94**, 183602 (2005).
[9] D. Zhang, *Opt. Lett.*, **30**, 2354 (2005).
[10] J.D. Franson, *Phys. Rev. A* **45** 3126 (1992).
[11] A.M. Steinberg, P.G. Kwiat, R.Y. Chiao, *Phys. Rev. Lett.* **68** 2421 (1992).
[12] O. Minaeva, C. Bonato, B.E.A. Saleh, D.S. Simon, A.V. Sergienko, *Phys. Rev. Lett.* **102** 100504 (2009).
[13] C. Bonato, A.V. Sergienko, B.E.A. Saleh, S. Bonora, P. Villoresi, *Phys. Rev. Lett.* **101** 233603 (2008).
[14] C. Bonato, D.S. Simon, P. Villoresi, A.V. Sergienko,

Phys. Rev. A **79** 062304 (2009).
[15] D.S. Simon, A.V. Sergienko, to appear in *Phys. Rev. A* (2009).
[16] M.H. Rubin, D.N. Klyshko, Y.H. Shih, A.V. Sergienko, *Phys. Rev. A* **50** 5122 (1994).